NAA-SR-2470
COPY

AN IN-PILE LOOP STUDY OF THE PERFORMANCE OF POLYPHENYL REACTOR COOLANTS

AEC Research and Development Report

ATOMICS INTERNATIONAL
A DIVISION OF NORTH AMERICAN AVIATION, INC.

NAA-SR-2470
REACTORS-POWER
143 PAGES

AN IN-PILE LOOP STUDY OF THE PERFORMANCE OF POLYPHENYL REACTOR COOLANTS

BY
WILLIAM N. BLEY

ATOMICS INTERNATIONAL
A DIVISION OF NORTH AMERICAN AVIATION, INC.
P.O. BOX 309 CANOGA PARK, CALIFORNIA

CONTRACT: AT(11-1)-GEN-8 (ORIGINALLY AT(04-3)-88)
ISSUED: SEPTEMBER 15, 1958

DISTRIBUTION

This report has been distributed according to the category "Reactors - Power" as given in "Standard Distribution Lists for Unclassified Scientific and Technical Reports" TID-4500 (13th Ed., Rev.), February 15, 1958. A total of 620 copies was printed.

Al, Mg, mild steel, stainless steel, and Zr corrosion specimens were exposed in the in-pile section, and all the specimens except Mg and Zr were considered acceptable for use in a reactor. Mg and Zr were found unsatisfactory due to their tendency to become oxidized or hydrided.

ACKNOWLEDGMENT

The results reported in this paper were obtained during work performed by the Atomics International Division of North American Aviation, Inc. under Contract Number AT(04-3)-88 for the United States Atomic Energy Commission.

The advice and assistance offered by Dr. C. A. Trilling, project engineer of the OMRE, and D. W. Bareis, supervisor of the Process Development Unit during the entire program, was of great value.

Many other individuals contributed to the successful completion of this program. D. A. Huber, S. Loeb, W. J. Cudahy, M. L. Silberberg, and G. C. Cox were active in the analysis and reduction of the data, preparation of portions of the report, construction and design of the experimental equipment, and the operation of the experiment. S. Nakazato, J. Guon, and N. J. Grisanti did much of the preliminary work on the aims of the program and the design of the experimental equipment. T. H. Christensen, L. T. Cartee, F. O. Streck, R. E. Snouffer, and J. E. Mills constructed, assembled, operated the equipment, and collected the experimental data.

The assistance and cooperation of R. E. Fearnow, Project Engineer, and F. L. McMillan, Chief Project Engineer, of the Atomic Energy Division of the Phillips Petroleum Company, in installing the experimental equipment at the Materials Testing Reactor is also gratefully acknowledged.

ABSTRACT

An in-pile loop experiment was performed to evaluate several promising polyphenyl materials for use as reactor moderator coolants.

Isopropyl diphenyl, diphenyl, a mixture of Santowax O and Santowax M, and Santowax R were circulated in an in-pile loop containing a uranium heater, at bulk fluid temperatures of 500 to 700°F and at fluid velocities of 10 to 20 ft/sec over the heat transfer surfaces. Heat fluxes ranged from 120,000 - 200,000 Btu/hr-ft^2. Peak reactor fluxes surrounding the in-pile assembly were 5×10^{13} thermal neutrons/cm^2-sec, 1.2×10^{12} fast neutrons/cm^2-sec, and 0.6 watt/gm gamma heating.

No significant differences between the materials irradiated were apparent insofar as radiation stability, heat transfer properties, and corrosion were concerned.

Radiation decomposition rates were slightly greater than those measured in previous work. However, the decomposition rates were not unreasonable. Coolant activation and corrosion were negligible. Heat transfer characteristics were not adversely affected by physical property changes or high radiation fields.

TABLE OF CONTENTS

	Page No.
I. Introduction	11
II. Equipment	13
A. In-Pile Section	13
B. Test Heater	19
C. Circulation System	22
D. Instrumentation	25
E. Sampling	29
III. Testing Program	30
A. Procedure and Requirements	30
B. Operating Conditions	31
IV. Results and Discussion	34
A. Coolant Decomposition	34
1. Decomposition Rates	36
2. Pyrolytic Effects	45
3. Estimated Accuracy in Determination of G_{HBR}	45
4. Radiolytic Gas Generation	47
5. Radiolytic Gas Composition	49
B. Heat Transfer	54
1. The Effect of Coolant Decomposition and Radiation on Heat Transfer	54
2. Hot Cell Examination of the Uranium Heaters	79
C. Corrosion of Structural Metals in Irradiated Polyphenyls	82
D. Coolant Activation and Physical Properties	83
1. Coolant Activation	83
2. Physical Properties	88
E. Equipment Examination	99
Appendices	109
I. Radiation Decomposition Calculations	111
A. General	111
B. High Boiler Residue Generation Rate	112
C. Radiation Energy Absorption in the Coolant	112

TABLE OF CONTENTS (Continued)

Page No.

Appendices (Continued)

II. Test Heater Heat Transfer Analysis 125

III. Uranium Heater Heat Transfer Analysis 133

IV. Nomenclature 137

References 142

LIST OF TABLES

I. Composition of Materials Irradiated 12

II. System Volumes 27

III. Nominal Operating Conditions 32

IV. Molecular Weight of Residue During Extended Diphenyl Irradiation 35

V. Summary of Individual Decomposition Rates for all Materials . 38

VI. Gas and Liquid Phase Gas Sample Analysis (single cycle irradiations) 49

VIIA. Gas and Liquid Phase Gas Sample Analysis - Extended Diphenyl Irradiation - MTR Cycle 82 51

VIIB. Gas and Liquid Phase Gas Sample Analysis - Extended Diphenyl Irradiation - MTR Cycle 83 52

VIIC. Gas and Liquid Phase Gas Sample Analysis - Extended Diphenyl Irradiation - MTR Cycle 84 53

VIII. Test Heater Heat Transfer Coefficients - Isopropyl Diphenyl - MTR Cycle 77 57

IX. Test Heater Heat Transfer Coefficients - Diphenyl - MTR Cycle 78 58

X. Test Heater Heat Transfer Coefficients - Santowax R- MTR Cycle 79 59

XI. Test Heater Heat Transfer Coefficients - Santowax O - Santowax M - MTR Cycle 81 60

XIIA. Test Heater Heat Transfer Coefficients - Extended Diphenyl Irradiation - MTR Cycle 82 61

LIST OF TABLES (Continued)

XIIB. Test Heater Heat Transfer Coefficients - Extended Diphenyl Irradiation - MTR Cycles 83 and 84. 62

XIII. Uranium Heater Heat Transfer Coefficients - Isopropyl Diphenyl - MTR Cycle 77 70

XIV. Uranium Heater Heat Transfer Coefficients - Diphenyl - MTR Cycle 78 71

XV. Uranium Heater Heat Transfer Coefficients - Santowax R - MTR Cycle 79 73

XVI. Uranium Heater Heat Transfer Coefficients - Santowax O - Santowax M - MTR Cycle 81 74

XVIIA. Uranium Heater Heat Transfer Coefficients - Extended Diphenyl Irradiation - MTR Cycle 82 75

XVIIB. Uranium Heater Heat Transfer Coefficients - Extended Diphenyl Irradiation - MTR Cycles 83 and 84 76

XVIII. Corrosion Test Results on Materials Exposed to Irradiated Polyphenyls 84

XIX. Individual Reactor Flux Contributions for all Materials 116

XX. Typical Calculation for G_{HBR} - Santowax O - Santowax M . . . 123

LIST OF FIGURES

1a. Isometric Sketch 14

1b. Schematic Flow Diagram 15

2. In-Pile Section 16

3. Uranium Heater 18

4. Test Heater (Drawing) 20

5. Test Heater (Photograph) 21

6. Console Piping 23

7. Console at MTR 24

8. Instrumentation Panels 28

9. Decomposition Rates of Polyphenyl Materials 37

10. Decomposition Rates for Isopropyl Diphenyl 40

11. Decomposition Rates for Diphenyl 41

LIST OF FIGURES (Continued)

		Page No.
12.	Decomposition Rates for Santowax R	42
13.	Decomposition Rates for Santowax O - Santowax M	43
14.	Decomposition Rates for Extended Diphenyl Irradiation	44
15.	Pyrolysis of Polyphenyls	46
16.	Radiolytic Gas Composition in the Gas Phase vs High Boiler Residue Content - Extended Diphenyl Irradiation	55
17.	Heat Transfer vs HBR Content for Isopropyl Diphenyl Irradiation - MTR Cycle 77	64
18.	Heat Transfer vs HBR Content for Diphenyl Irradiation - MTR Cycle 78	65
19.	Heat Transfer vs HBR Content for Santowax R Irradiation - MTR Cycle 79	66
20.	Heat Transfer vs HBR Content for Santowax O - Santowax M Irradiation - MTR Cycle 81	67
21.	Heat Transfer vs HBR Content for Extended Diphenyl Irradiation - MTR Cycles 82, 83, and 84	68
22.	In-Pile Heat Transfer Surface of Uranium Heater Exposed to Irradiated Santowax R	81
23.	Typical Gamma Spectra of Irradiated and Unirradiated Diphenyl	86
24.	Density of Irradiated Isopropyl Diphenyl	89
25.	Density of Irradiated Santowax O	90
26.	Density of Irradiated Santowax R	91
27.	Density of Irradiated Diphenyl	92
28.	Viscosity of Irradiated Isopropyl Diphenyl	93
29.	Viscosity of Irradiated Diphenyl	94
30.	Viscosity of Irradiated Santowax R	95
31.	Viscosity of Irradiated Santowax O - Santowax M	96
32.	Specific Heat of Polyphenyls	97
33.	Estimated Thermal Conductivity of Polyphenyls	98
34.	Melting Points of Irradiated Polyphenyls	100
35.	Pump Rotor	102

LIST OF FIGURES (Continued)

		Page No.
36.	Pump Impeller Housing	103
37.	Pump Bearings	104
38.	Surge Tank Sight Glass	105
39.	Valve Stem Assemblies	106
40.	Rotameter Float Assembly	107
41.	High Boiler Residue Buildup vs Time	113
42.	High Boiler Residue Produced vs Time	114
43.	Typical Flux Traverse Over In-Pile Section	115
44.	Temperature Profile - Test Heater	126

I. INTRODUCTION

Previous work with Van de Graaf and mixed in-pile irradiations of several polyphenyl materials[1, 2, 3, 4, 5] indicated their suitability as reactor moderator-coolants.

The Organic Moderated Reactor Experiment (OMRE) was designed, constructed, and is now operating at the National Reactor Testing Station in Idaho. The purpose of the OMRE is to demonstrate the concept of a reactor which is moderated and cooled by a suitable organic material.

While earlier experiments[1, 2, 3, 4, 5] indicated the applicability of the polyphenyls for use as reactor coolant-moderators insofar as radiation and thermal stability were concerned, the wide range of melting points, vapor pressures, and costs exhibited by the polyphenyls and their derivatives, make these additional variables important considerations in the selection of a suitable coolant for the OMRE and future organic moderated reactors.

Prior work was incomplete or inadequate to predict reactor heat transfer with polyphenyls containing high concentrations of their decomposition products. Heat fluxes, bulk temperatures, and high boiler residue concentrations were too low to be of practical value to extrapolate to the heat transfer characteristics to be expected in a reactor. Decomposition rates of polyphenyls could only be estimated under exposure to mixed reactor fluxes. Consequently, an in-pile loop was designed and operated at the Materials Testing Reactor to provide information useful in the operation of the OMRE. Reactor conditions were duplicated as much as possible so that extrapolation to reactor operation would be at a minimum.

Decomposition rates, heat transfer rates, fouling characteristics, physical properties, induced activity, and corrosion rates were the parameters studied for isopropyl diphenyl, diphenyl, Santowax R, and a 2 to 1 mixture of Santowax O and Santowax M (Santowax O - Santowax M). Table I presents the composition of the materials irradiated.

TABLE I

COMPOSITION OF MATERIALS IRRADIATED

Polyphenyl	Composition, Weight Percent			
	Diphenyl	Ortho-,	Meta-,	Para-terphenyl
Diphenyl	99.5	-	-	-
Santowax R	0.3	11.7	60.0	28.1
Santowax O — Santowax M	trace	65.2	32.3	2.5
Isopropyl diphenyl	55.4 weight percent meta-isopropyl diphenyl 44.6 weight percent para-isopropyl diphenyl			

II. EQUIPMENT

A sketch of the in-pile loop piping and method of installation is shown in Fig. 1a. Fig. 1b is a schematic flow diagram of the system. The loop was assembled in two sections which were connected at the expansion bellows and the electrical and instrument head. The in-pile section was replaced for each material irradiated, while the valve and pump console was permanently installed on the top face of the Materials Testing Reactor (MTR) and served as the pumping and control station for all the separate irradiations. Each in-pile section including the loop lines was replaced in its entirety. The uranium heaters, the thermocouples, the gamma monitors, and heating circuits were thus renewed for each irradiation. In this manner, the specific effects and performance of each material under irradiation could be evaluated.

The in-pile section was installed vertically in the A-13 position of the MTR. This position was in a high-flux region of the beryllium reflector zone. The average perturbed flux conditions at the uranium heater with the reactor operating at 40 Mw were as follows:

Fast neutron flux	1.2×10^{12} n/cm^2-sec
Thermal neutron flux	2×10^{13} n/cm^2-sec
Gamma flux	0.6 watt/gm

These values changed somewhat from cycle to cycle and from fuel loading to fuel loading. The reactor fluxes decreased as each irradiation progressed and also decreased over the in-pile section in each direction from the reactor midplane.

A. IN-PILE SECTION

The in-pile section of the loop, shown in Fig. 2, is that part which was located within the high flux region of the reactor. It consisted of an outer aluminum shell, a reservoir to contain the organic fluid, and the in-pile, uranium-fueled heater.

The outer aluminum shell had the same external dimensions as an MTR beryllium reflector "A" piece. The aluminum shell was 3 inches square by 53 inches long, including the tubing brace at the top. A 2-inch, carbon-steel pipe, capped at each end, was centered within the square shell and served as a pressure-tight, in-pile reservoir for the fluid to be tested.

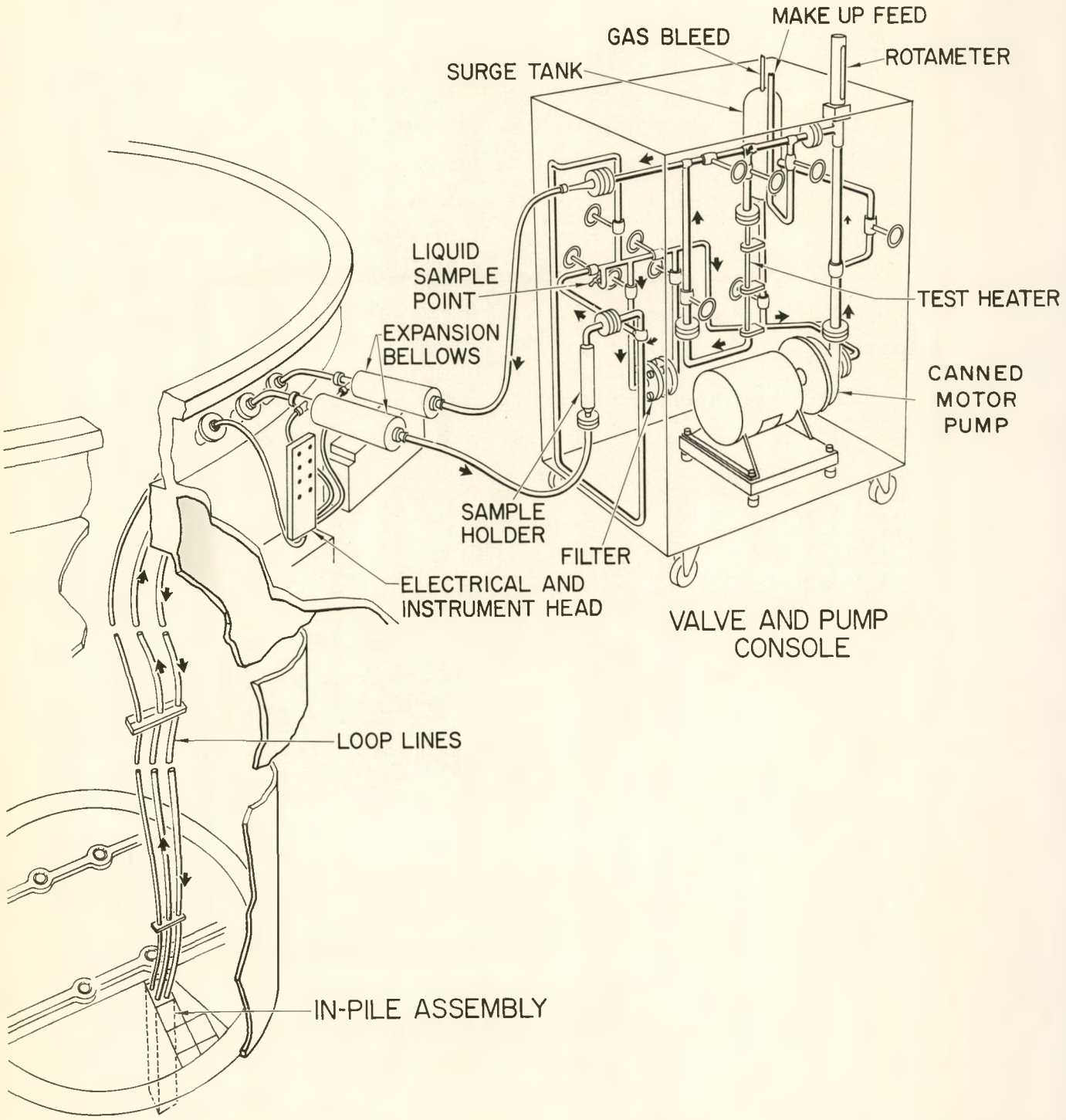

Fig. 1a. Isometric Sketch

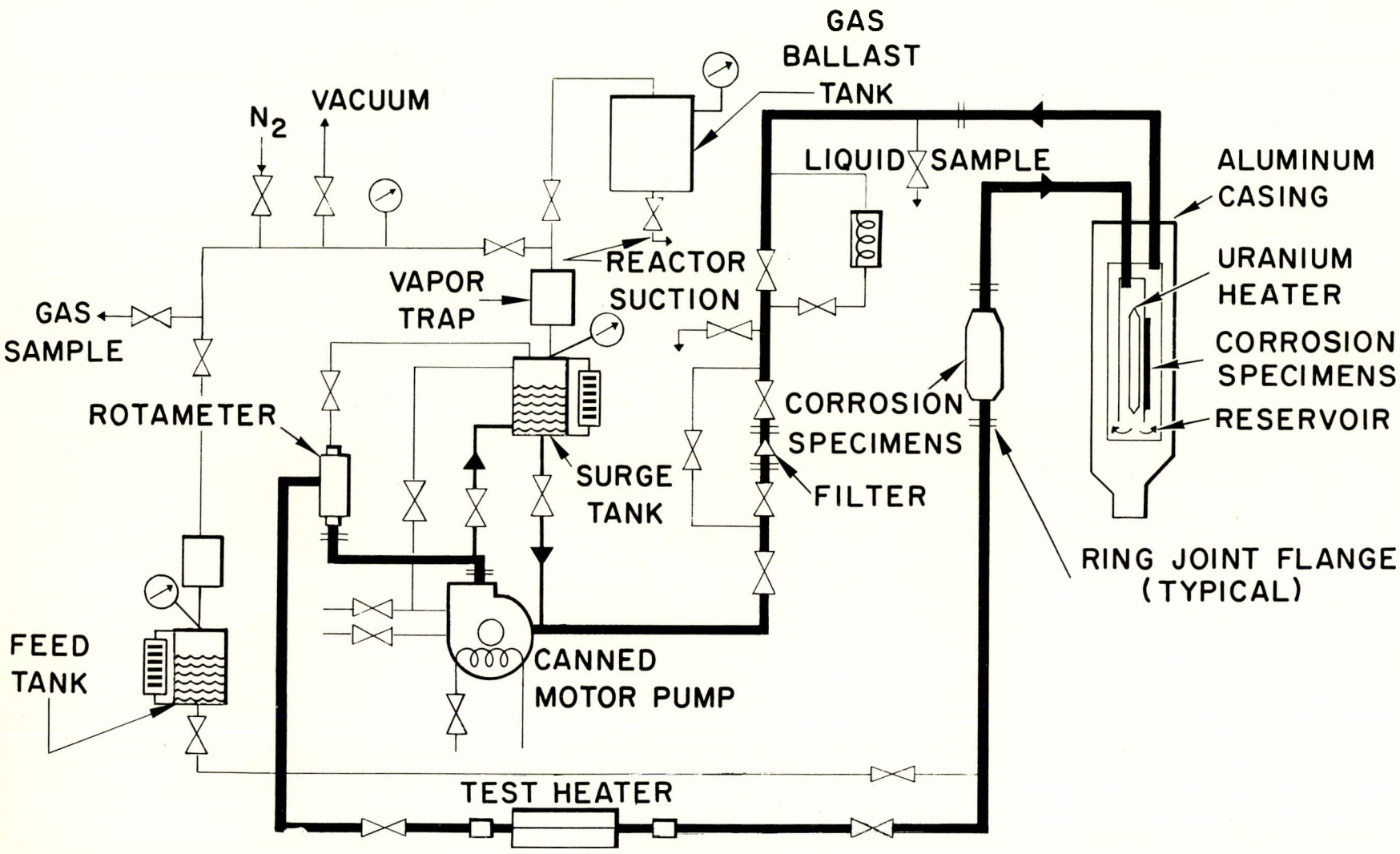

Fig. 1b. Schematic Flow Diagram

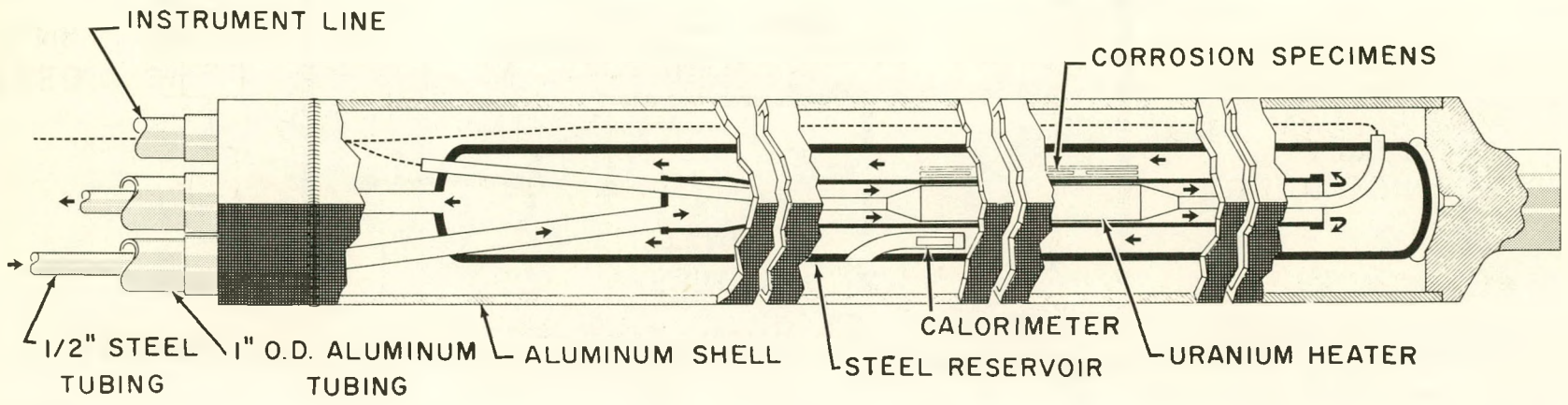

Fig. 2. In-Pile Section

The uranium heater was located within the reservoir as shown in Fig. 2. The heater itself is shown in Fig. 3. The active section consisted of a 5-inch long assembly of hollow uranium slugs, each containing 2.78 wt. -% U^{235} The nominal weight of the uranium assembly was 135 grams with an outer diameter of 0.398 inch and an inner diameter of 0.218 inch. (The heater for the isopropyl diphenyl irradiation contained only 97.28 grams of uranium. The outer diameter of these uranium slugs was 0.357 inch.) The uranium assembly was enclosed in a stainless-steel tube having an outer diameter of 0.625 inch and an inner diameter of 0.459 inch. The annular space between the uranium and the stainless steel was filled with NaK to provide a heat conduction medium for removal of the fission heat generated by the uranium. This entire assembly was enclosed in a steel tube. The annular space between the uranium heater assembly and the steel tube carried the polyphenyl on its downward pass through the in-pile section.

A close-fitting, 3/16-inch O. D. tube extended through the hollow uranium slugs. The annular space between the tube and the uranium was filled with NaK. Core thermocouples, located within this tube, measured the maximum uranium temperature. Additional thermocouples were installed in the outer stainless steel tube by drilling longitudinal holes in the wall of the tube and silver soldering the thermocouple junction as close to the surface of the sheath as possible. A typical thermocouple installation is shown in the cutaway view presented in Fig. 3. Chromel-alumel thermocouple wires swaged in MgO inside stainless-steel sheaths were used for all the in-pile thermocouple measurements. Glass-insulated Chromel-alumel wire was used for the gamma calorimeters. The core thermocouple sheaths had an outside diameter of 0.060 inch. The sheath diameter of the wall thermocouples was 0.040 inch.

Flow through the in-pile section was downward through the annulus between the uranium sheath and the enclosing steel tube, then upward through the larger annulus between the heater-enclosing tube and the reservoir wall.

Neutron and gamma fluxes were monitored in the in-pile section of the loop. Integrated thermal neutron flux was measured by four cobalt-aluminum wires which extended the length of the in-pile section, one running down each corner of the outer aluminum shell. In these wires, Co^{59} absorbed neutrons and became Co^{60}. The thermal flux is a function of the number of atoms of Co^{60} formed and

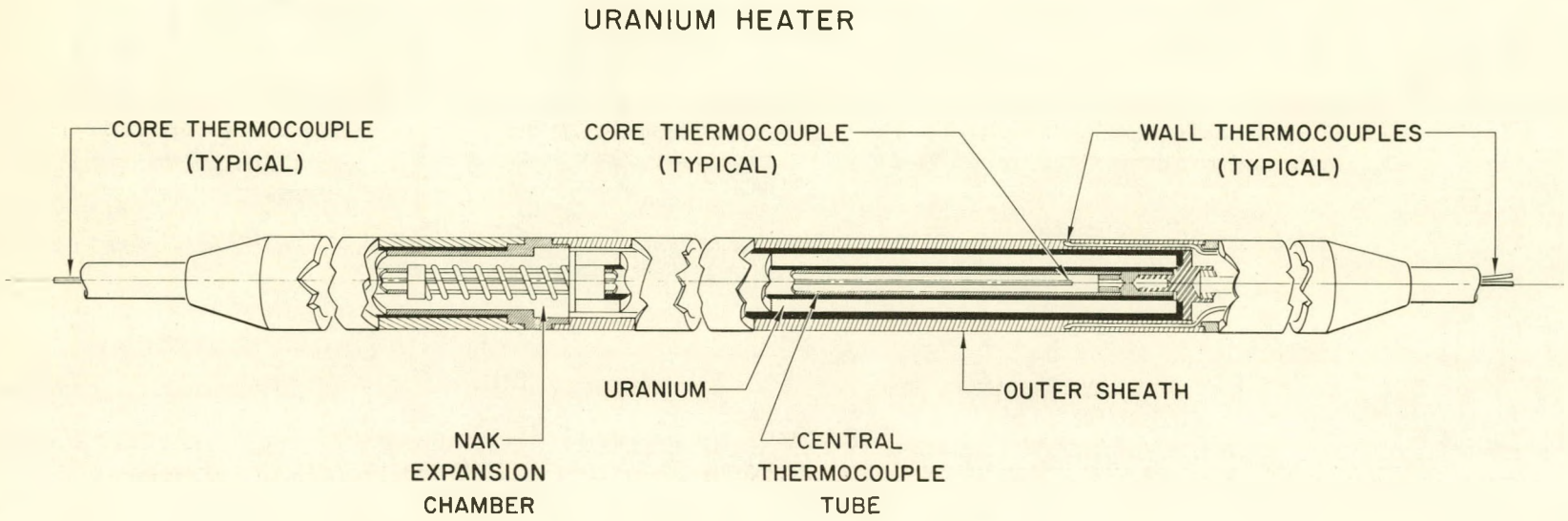

Fig. 3. Uranium Heater

of the reactor power during the cycle. Four pure nickel wires, also extending down the corners of the outer aluminum shell, monitored the integrated fast neutron flux. In these monitors, Co^{58} was formed through a neutron-proton reaction with the nickel.

The gamma flux was measured by three "gamma calorimeters," which are shown in Fig. 2. The gamma calorimeter consisted of a mild-steel rod located within the reservoir in the polyphenyl flow path. The rod was insulated so that only the lower end was cooled by the hydrocarbon. Heat was generated within the rod by gamma heating and the (n, γ) reaction with thermal neutrons. The temperature difference from one end of the rod to the other is a function of the rate of heating and of the temperature of the surroundings and is, therefore, a measure of the gamma flux and the thermal neutron flux. Temperatures along the rod were measured by appropriately located thermocouples.

Corrosion specimens were installed in specially designed holders which were welded to the central steel tube in the in-pile section. The specimens were exposed to high-temperature hydrocarbon at the peak reactor fluxes present at the reactor midplane. Control specimens were installed in the line between the valve and pump console and the expansion bellows. Figures 1a and 2 show the location of the specimens.

B. TEST HEATER

The test heater, shown in Fig. 4, was designed for the same linear fluid velocity and heat flux as the in-pile heater. It consisted of a 10-inch-long stainless steel tube having a 3/8-inch outside diameter and a 0.012-inch wall thickness. The polyphenyl flowed through this tube. Three electrical terminals were silver-soldered to the tube, one at the center and one at each end, giving two active heating lengths of 5 inches each. By passing a large alternating current (up to 1000 amperes at 8 volts) through the center terminal (Figs. 4 and 5), and through each half of the heater tube to the ground terminals, heating of the tube was accomplished through its own resistance to the large electrical current.

The heater tube was surrounded by a trace-heated pipe referred to as an "adiabatic furnace." The furnace was maintained at the same temperature as the outer wall of the heater tube to minimize heat losses from the tube to the surroundings.

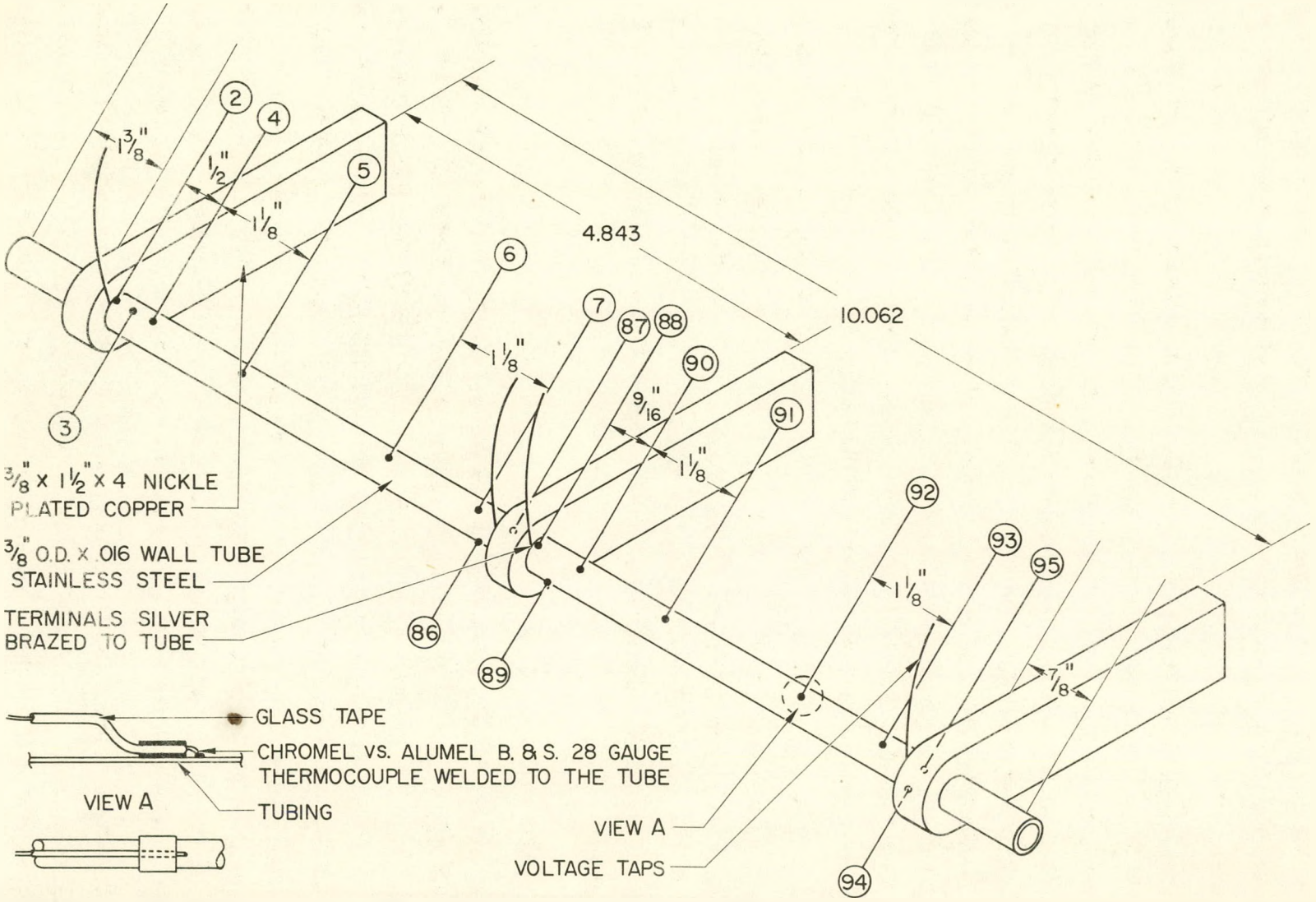

Fig. 4. Test Heater (Drawing)

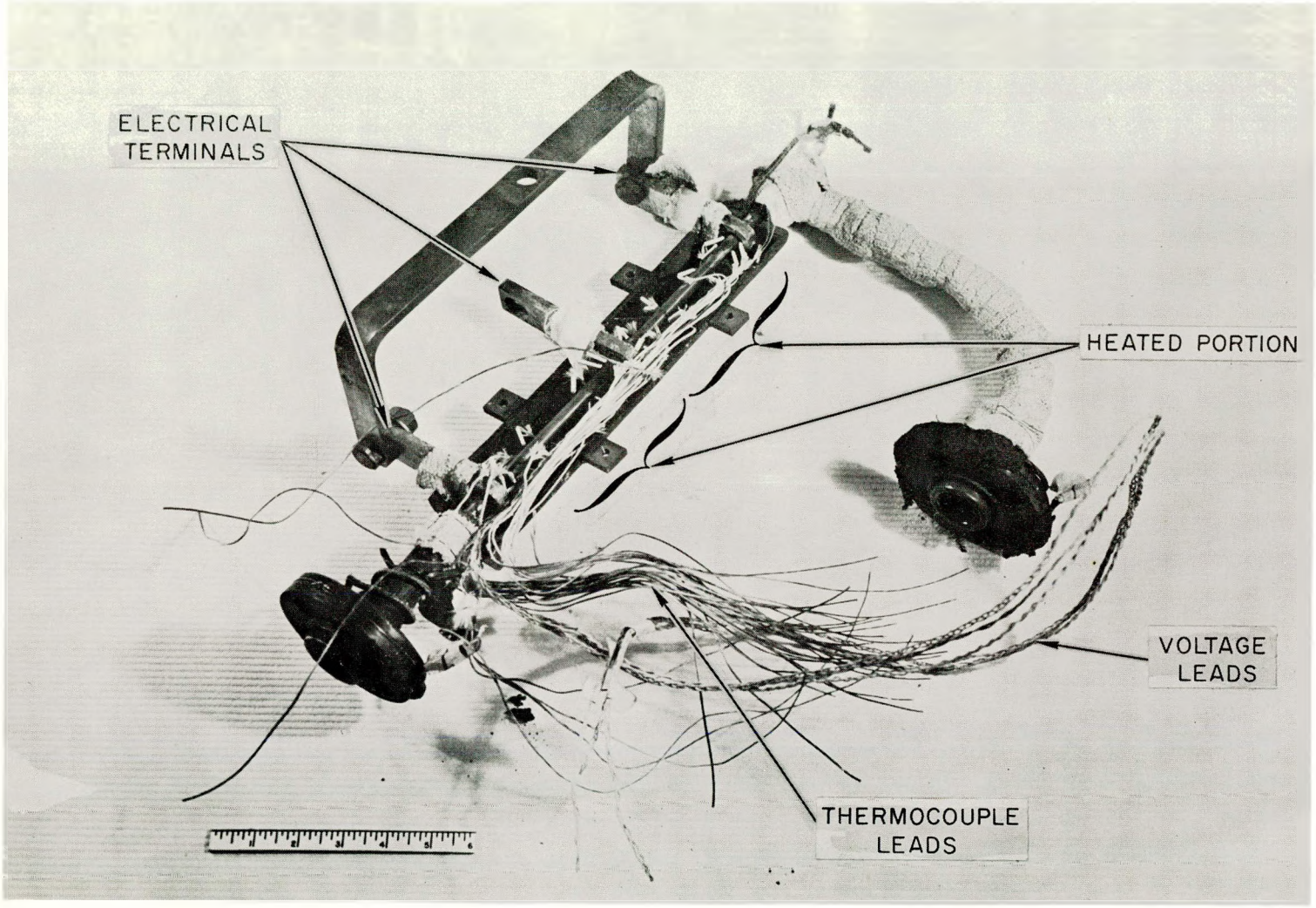

Fig. 5. Test Heater

Thermocouples were appropriately located, as shown in Fig. 4, to obtain heater-tube wall temperatures and inlet and outlet bulk polyphenyl temperatures.

C. CIRCULATION SYSTEM

The in-pile loop is shown schematically in Fig. 1a. The components, other than the in-pile section, are shown mounted in the valve console in Figs. 6 and 7.

The polyphenyl was circulated through the system by a canned motor pump. A by-pass stream of polyphenyl was circulated through the pump motor housing to lubricate the Graphitar bearings and cool the motor windings. Mainstream cooling was accomplished by passing the polyphenyl through a double-pipe heat exchanger where a mixture of Dowtherm A and Xylene was used as the coolant. The bubble point of the secondary coolant was set at approximately 310°F in order to prevent freezing of the polyphenyl.

A surge tank was connected into the system to permit expansion and contraction of the polyphenyl and to provide for system pressurization. A side stream from the discharge side of the pump maintained circulation through the surge tank into the main stream to ensure that the polyphenyl was uniformly irradiated and that decomposition gases collected in the surge tank. A feed tank, for adding polyphenyl to the system, was connected into the piping at the discharge side of the pump. The feed tank could be pressurized with nitrogen to introduce makeup material. Vapor traps were installed in the pressurizing lines to each tank to prevent polyphenyl vapors from entering or plugging the gas lines.

A filter was installed in the system to remove particulate matter from the circulating stream and prevent coolant activation from this source. A sintered bronze filter element was used which retains all particles larger than 100 microns.

Mild or low carbon steel was used throughout for construction of all the system tanks and piping. Components of the system which were constructed of stainless steel were the bellows-seal valves, the pump, the test heater, the uranium heater, and the rotameter.

All process piping was welded and bellows seal valves were used to preclude problems associated with leakage from the comparatively small circulating system. Where welding was not possible, such as at the filter, external heater, and the connections between the console and in-pile sections, metal ring joint flanges

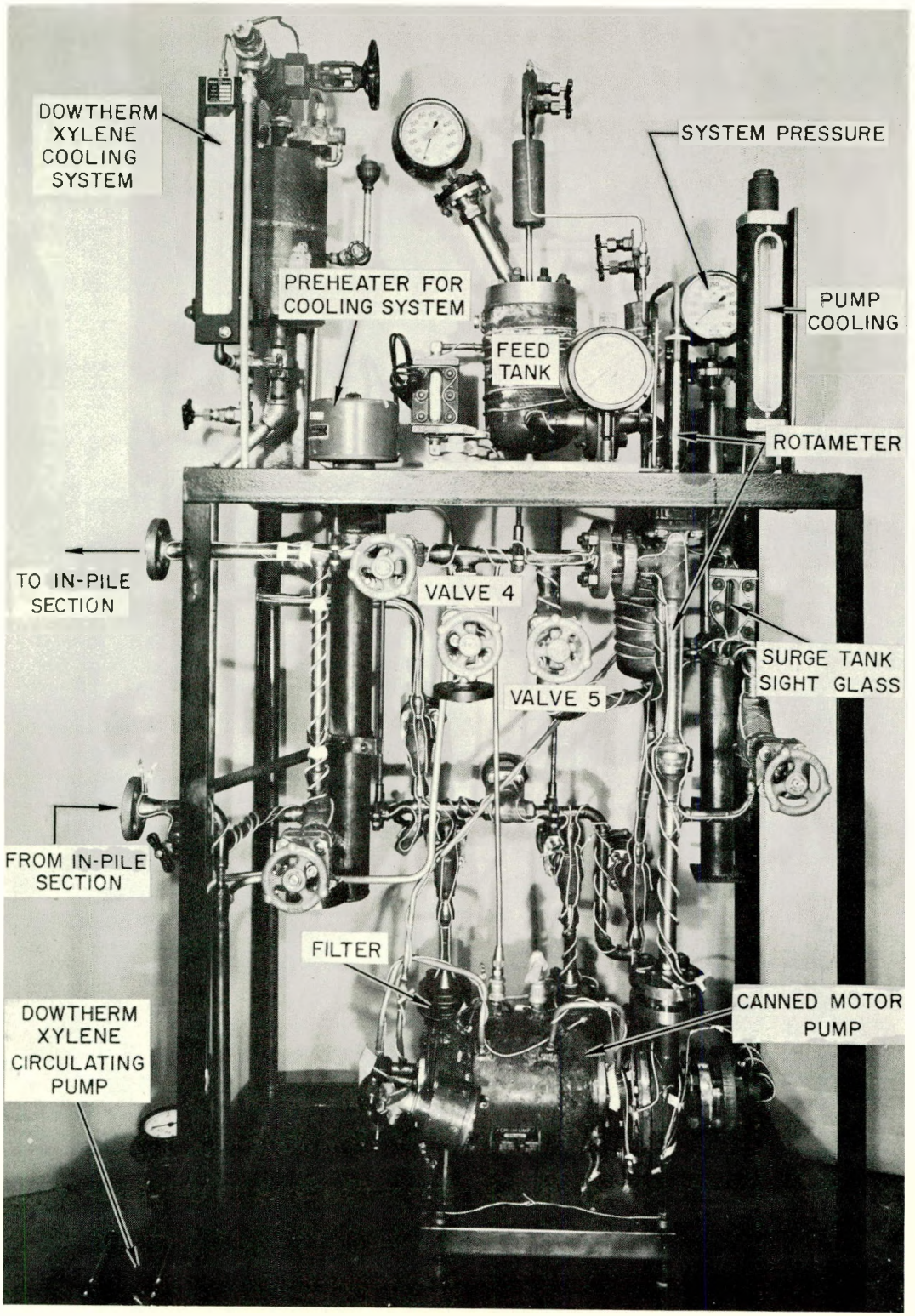

Fig. 6. Console Piping

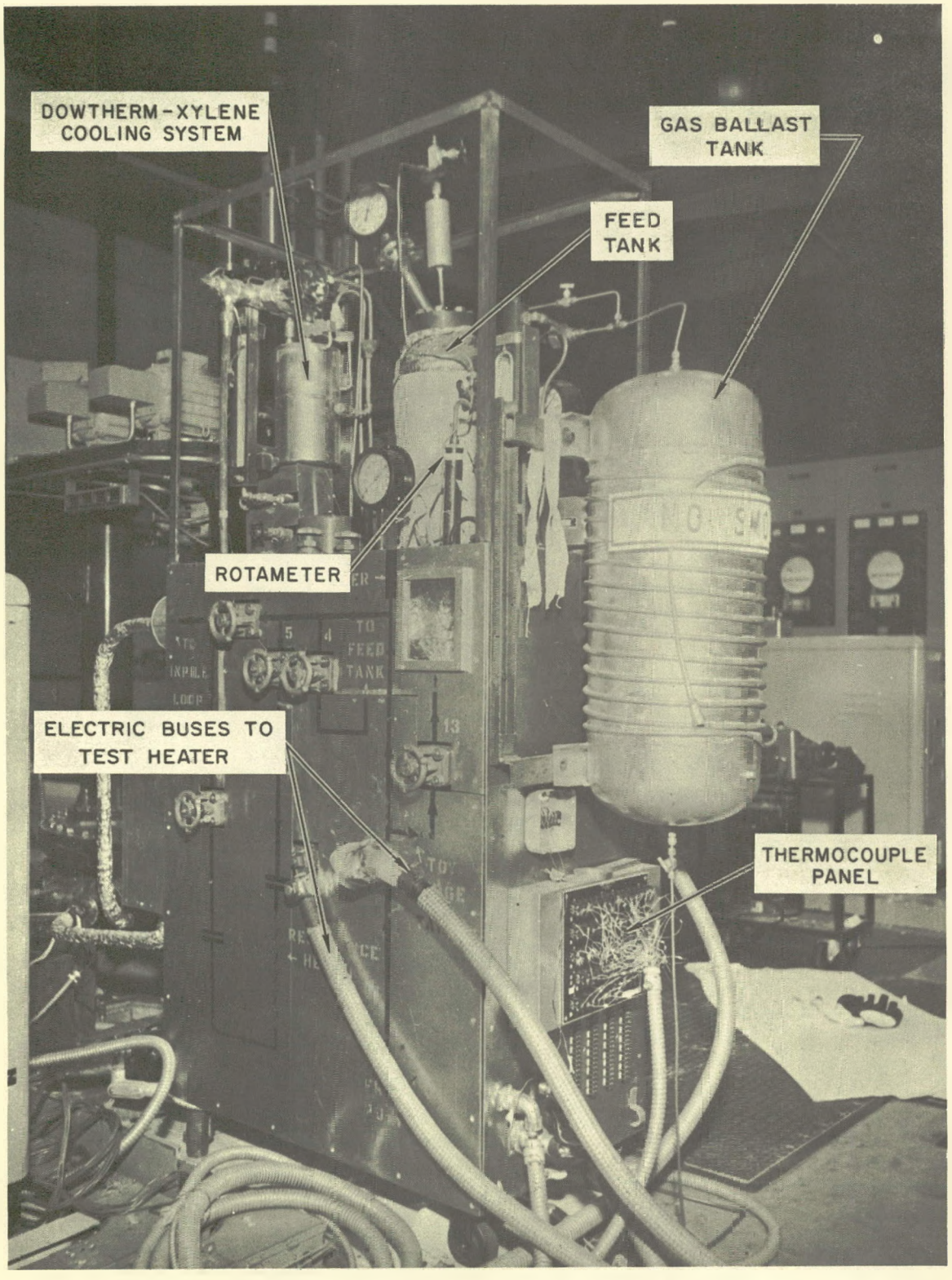

Fig. 7. Console at MTR

were used. The filter and external heater could be isolated by valve manipulation for removal and replacement during operation. All piping was trace-heated and insulated to provide for preheating to temperatures above the melting point of the polyphenyl.

The tubes connecting the valve and pump console with the in-pile section were immersed in the reactor circulating water for the greater part of their length. These tubes, referred to as loop lines, were enclosed in outer tubing of 52S aluminum. The annulus between the inner and outer tubing contained nichrome trace-heating wire and thermal insulation. This annulus and the space within the in-pile section between the outer aluminum shell and the reservoir were pressurized with nitrogen as a precaution against inleakage of reactor water in case a leak in the aluminum box or loop lines should have developed. The in-pile thermocouples and heater wires were carried from the in-pile section out of the reactor by a third aluminum tube, designated as the "instrument line."

An expansion bellows and a gas-tight junction box served to terminate the aluminum envelope around the loop lines, in-pile reservoir, and the thermocouple and electrical leads. Electrical leads to the heating wires on the upper portions of the loop lines were conveyed to the sealed junction box via Swagelok "tees" located between the reactor and the expansion bellows (Fig. 1a).

D. INSTRUMENTATION

Temperature measurements were made on all portions of the loop which could be expected to be "cold spots." Chromel-alumel thermocouples were used throughout. Swaged chromel-alumel wires in MgO and stainless steel sheathing were used to measure all the bulk coolant and uranium temperatures in the in-pile section, with the sheathed portion extending to a point just outside the reactor tank. The gamma calorimeter thermocouples were fabricated from 28 gauge chromel-alumel wire, which was sheathed in ceramic tubes to afford protection against insulation failure under radiation.

Calibration of the thermocouples in the in-pile section and the external heater was accomplished by an isothermal reading of all the thermocouples before the reactor was brought to power. Since temperature differences between the thermocouples were values used for the heat transfer determination, this method of calibration was considered to be adequate. Multipoint selector switches permitted

the temperature of any thermocouple to be read on a precision potentiometer which used an ice bath for a reference temperature. All heat-transfer-data temperatures were taken with the potentiometer. In addition, the uranium and bulk temperatures were continually monitored on multipoint recorders.

Two uranium thermocouples, one in the wall and one in the core, were connected into the reactor scram system to give protection from excessive uranium temperatures and loss of flow which results in high uranium temperatures. The two uranium temperatures were continuously recorded separately by two strip chart instruments. Figure 8 shows the panel layout of the instrumentation.

Pressure measurements, flow measurement, and level measurements of the circulating polyphenyl were accomplished at the valve console. Diaphragm type chemical gauges filled with "Dowtherm A" transmitting fluid were used to measure system pressure at the surge tank and feed tank. An additional bourdon type gauge was installed beyond the vapor traps to measure pressurizing gas pressures and sampling pressures for gas sampling. Flow measurement was made with a direct-reading metal tube rotameter with magnetic extension and follower. A small bleed line connected the top of the rotameter with the surge tank to remove any gas which collected in the top of the extension tube. Calibration of the rotameter was made with alcohol, which has a density very close to that of the materials circulated at temperature. Meter characteristics and density corrections were then used to correct the meter reading for density and temperature to obtain the volumetric flow rate through the system.

Standard high-pressure, high-temperature sight glasses were used on the feed tank and surge tank to monitor system levels. The entire system volume was determined by parts and as an assembly by fluid addition as a function of level in the surge tank sight glass. The feed tank was likewise calibrated. Table II presents the volume of various portions of the circulating system.

Precise electrical measurements of the voltage and current to the external resistance heater were accomplished by voltage taps at the point of connection between the lugs and the tube and by a calibrated shunt ammeter on one of the standard 800,000 circular mil copper cables supplying the current to the heater. The step-down transformer had an isolated secondary winding to prevent shorts to ground from the current buses.

TABLE II

SYSTEM VOLUMES

Valve and Pump Console	cm^3	ft^3
Surge tank level		
1 inch	5026	0.1770
3 inches	5444	0.1920
Loop Lines and Connecting Piping Including Corrosion Sample Holder	1430	0.0504
In-Pile Reservoir	1600	0.0565
Total Volume of System		
Surge tank level		
1 inch	8056	0.2840
3 inches	8474	0.2990

Ratio: In-Pile Volume to Out-of-Pile Volume

1 inch in surge tank = 0.198

3 inches in surge tank = 0.189

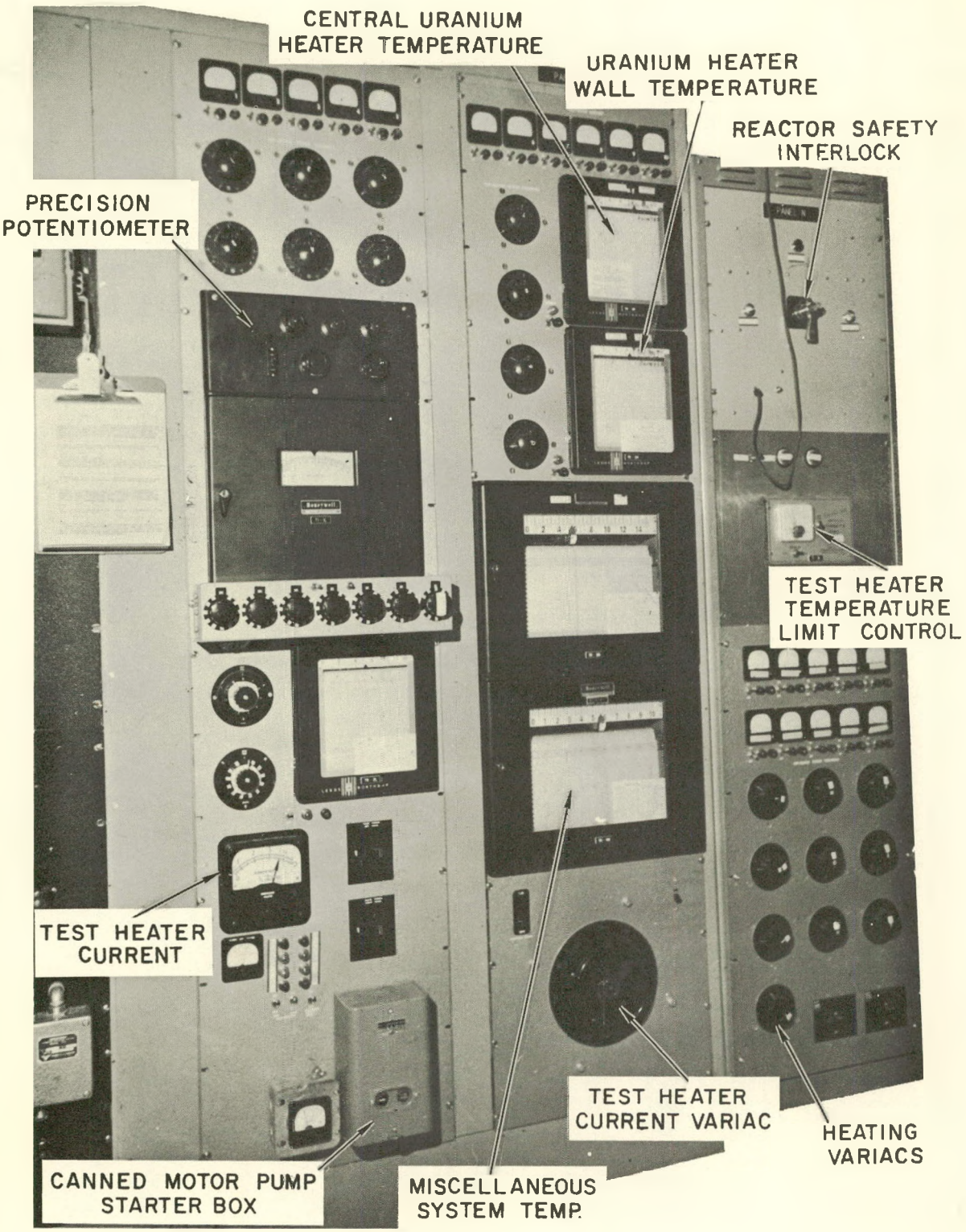

Fig. 8. Instrumentation Panels

A safety interlock prevented energizing of the step-down transformer until after the main circulating pump starter coil had been energized. A high-temperature unit switch was also provided to shut off the power to the external heater if high tube wall temperatures occurred.

E. SAMPLING

Provision was made to withdraw samples directly from the circulating stream and from the gas space in the surge tank. All samples were collected in sealed carbon-steel bombs constructed from pipe with valves welded at both ends.

Sampling of the circulating liquid was accomplished by attaching the bomb to the sample valve, evacuating the bomb with both bomb valves open, then closing the outermost valve and opening the sample valve. The location of the sample valve inside the console provided a means of preheating the sample bomb, since ambient temperatures in the console with all panels closed were over 200°F. In addition, heat conducted from the circulating fluid via the sampling valve and the sampling tube, coupled with the high temperatures of the sampled fluid, minimized problems associated with freezing and assured homogeneous samples.

Sixty-gram liquid samples provided high-boiler residue (HBR)* buildup data and samples for physical property analysis. High-boiler residue determination was by a semi-micro distillation technique at 5 microns pressure in a small bore tube immersed in a silicone oil bath. Bath temperature was 165°C for the isopropyl diphenyl and diphenyl materials and 240°C for the terphenyls. Approximately 0.5 gram of irradiated material was placed in the distillation tube and distilled for 1-1/2 hours at bath temperature to drive off the volatile materials. Previous laboratory work with single and multi-plate stills indicated good agreement between the semi-micro technique and the macro-scale distillations.

Liquid samples of 50 gm and 300 gm size were withdrawn for dissolved gas extraction and removal of HBR from the system to maintain desired HBR concentration in the circulating hydrocarbon.

Gas solubility samples were boiled under vacuum and the gas was extracted and collected with a Toepler Pump.

Gas samples were taken in conjunction with gas solubility samples. The gases were sealed in glass bulbs and analyzed by spectroscopy techniques.

---

* High-boiler residue is defined as all material in the coolant less volatile than para-terphenyl.

III. TESTING PROGRAM

A. PROCEDURE AND REQUIREMENTS

Four polyphenyl materials which were considered as the most promising moderator-coolants were tested for one cycle at the Materials Testing Reactor (MTR) in Idaho. These materials were, in the order of their testing, isopropyl diphenyl, diphenyl, Santowax R, and a low-melting, synthesized mixture of Santowax O - Santowax M. Upon completion of the four single-cycle irradiations, diphenyl was irradiated for three consecutive MTR cycles in order to evaluate long term effects, if any.

An MTR cycle was a three week period which was essentially divided into two portions. The first portion was devoted to refueling and installation of new experiments. The second portion was the actual operating time of the reactor and was generally 12 to 14 days long.

Operation of the reactor was at its maximum power of 40 megawatts for most of the operating period. In general, over 98 percent of all the dosage on the experiment was under maximum flux and power conditions. The accumulated reactor power in megawatt-hours $(Mwh)_o$ was used as an exposure scale in all irradiations. Single-cycle exposures were sufficient to increase the HBR content of the moderator-coolant tested to approximately 30 percent.

The program was designed to test the materials under nearly identical conditions in order that any advantages a material might have over another insofar as its performance as a reactor coolant-moderator was concerned would become apparent. The following aspects of the performance of each coolant were to be evaluated:

1) Radiation decomposition rates
2) Heat transfer properties as affected by changing HBR concentrations and possible deposits of decomposed materials on heat transfer surfaces both in a radiation field and out of a radiation field
3) Coolant activation
4) Corrosion

5) Physical property and moderating ability changes due to irradiation

6) Characteristics of a coolant containing high concentrations of the decomposition products.

The portions of the system consisting of the in-pile section, the loop lines, and the external corrosion sample holder were replaced for each of the four single-cycle irradiations and for the three-cycle irradiation. In this manner, the subsequent hot-cell and corrosion examinations could be made on the basis of the specific effects from each material tested. The neutron flux monitors were removed during hot-cell examinations and gave a measure of the integrated fast and slow neutron fluxes for each irradiation.

B. OPERATING CONDITIONS

Operating conditions were maintained at nearly constant values of maximum bulk temperatures and at a velocity of 13.5 fps at the test heater and uranium heater throughout each cycle. Bulk temperatures were dictated by a maximum heater surface temperature of 800°F from OMRE design criteria[6, 7] and the general fact that above 800°F the pyrolytic damage to most organic materials may become excessive. Consequently, bulk temperatures varied as the heat transfer coefficients changed and heat fluxes changed. Table III presents the operating conditions during each irradiation.

Heat transfer measurements were carried out on the test heater and the uranium heater after each approximate 5 percent increase in the HBR concentration. Fluid velocities were varied from 10 fps to 20 fps at bulk temperatures of 500°, 600°, and 650°F. Differences between the coefficients measured at the surface of the uranium heater and those measured at the surface of the test heater would then be an indication of a radiation effect or fouling of the in-pile heat transfer surface.

Fluid samples were withdrawn after each approximate 5 percent change in HBR concentration. Fifty-gram samples were withdrawn during the buildup period for physical property measurements and for determination of the HBR concentration change. In the case of the 3-cycle diphenyl irradiation, 300-gram samples were withdrawn in order to maintain the polymer concentration at 35 - 40 percent by replacement with fresh undamaged diphenyl. With the exception of the isopropyl diphenyl

TABLE III

NOMINAL OPERATING CONDITIONS

Material Irradiated*	MTR Cycle	Bulk Fluid Temperature	System Pressure§	High Boiler Residue Concentration	Loop Operating Time	Reactor Operating Time	Accumulated Reactor Power	Heat Flux		Wall Temp. Maximum		Fluid Velocity at Surface of Heaters
								Uranium Heater†	Test Heater	Uranium Heater	Test Heater	
		(°F)	(psig)	(wt.-%)	(Days)	(Days)	$(Mwh)_o$	$(q/A \times 10^{-3})$ Btu/hr-ft^2		(°F)	(°F)	(ft/sec)
Isopropyl Diphenyl	77	520 to 600	300 to 350	0 to 27.6	18.3	11.3	11,364	130 to 160	140.0	700	780	13.5
Diphenyl	78	640 to 670	300 to 310	0 to 35.0	18.2	15.9	12,952	160 to 180	175.0	780	800	13.5
Santowax R	79	540 to 600	110	0 to 29.0	17.7	13.5	12,666	140 to 160	180.0	750	800	13.5
Santowax O plus Santowax M	81	560 to 675	200 to 300	0 to 32.7	19.8	13.9	12,855	160 to 180	130 to 200	750	800	13.5
	82	620 to 650	230 to 300	0 to 33.3	17.0	15.1	14,330	160 to 200	180	750	800	13.5
Diphenyl	83	500 to 520	230 to 300	29.0 to 36.1	21.0	14.8	14,082	130 to 180	170	650	800	13.5
	84	610 to 620	230 to 300	33.0 to 39.8	21.0	13.2	11,926	160 to 190	175	710	800	13.5
Totals for Extended Diphenyl Irradiation (MTR cycles 82, 83, and 84)					59.0	43.1	40,338					

* Composition of the coolants are presented in Table I.
† Based on Thermal Neutron Flux.
§ The system was initially pressurized with nitrogen. Thereafter pressure was maintained by bleed off of decomposition gases. See section on Radiolytic Gas

irradiation, periodic additions were required to make up for leakage from the main pump flange. However, the leakage could be accurately determined by difference and the loss of HBR computed and accounted for.

At the completion of each irradiation, the loop lines were severed and sealed and the in-pile assembly was discharged via the reactor discharge chute to the storage canal. The assemblies were removed from the canal with a shielded coffin to the hot cell for visual examination of the heaters, weighing and cleansing of the corrosion specimens, and collection of the flux monitor wires.

IV. RESULTS AND DISCUSSION

A. COOLANT DECOMPOSITION

The amount of material produced of a lower volatility than para-terphenyl was used as an index to the rate of coolant decomposition. This material was defined as high boiler residue (HBR) and was separated from the irradiated coolant by distillation. It was assumed that the primary mechanism of decomposition was a condensation reaction of the diphenyl molecule to quatrephenyl and of a terphenyl molecule to hexaphenyl. Both quatrephenyl and hexaphenyl have a very low volatility, hence an analytical distillation technique for determination of the decomposition products was considered adequate. In addition, if a condensation reaction was the prime source of decomposition products, then hydrogen could be expected to be the most prevalent gas evolved from radiolysis of the polyphenyls. Data presented in Tables IV, VI, and VII substantiate to some degree the assumptions made on the natures of the decomposition products and the major reaction occurring. While Table IV presents the average molecular weight of the residue measured during the extended diphenyl irradiation, it also shows that the molecular weight changed with continued exposure to radiation. Consequently, the decomposition rate was computed on a weight basis. The decomposition gases generated did not amount to a major weight fraction of the decomposition products formed.

Previous investigators have used viscosity change[2] and the amount of residue formed of a given molecular weight[4] with reactor exposure time at a given reactor flux, or the amount of energy absorbed in the coolant, to index the amount of radiation damage occurring. The molecular weight of the residue formed using the second index was assumed to be 460.* Conversion of that index (G_p) to the one employed in this report can be made by multiplying G_p as follows:

$$G_{HBR} = 378\, G_p \ ,$$

where

$$G_p = \frac{molecules\ of\ 460\ Mw\ formed}{100\ ev\ absorbed\ in\ the\ coolant}$$

* The molecular weight is assumed to be that of hexaphenyl when $G_{(polymer)} \equiv (G_p)$ is used.

TABLE IV

MOLECULAR WEIGHT OF RESIDUE
DURING EXTENDED DIPHENYL IRRADIATION

Sample**	% of Sample	%H	Atom C/H	Molecular Weight	M.P., °C
NAA 2078-14 *Distillate	63.5	6.58	1.19	155	52 to 61
†High Boiler Residue	36.5	5.86	1.34	350	88 to 92
§Sublimate	32.8	5.92	1.35	238	56 to 61
Sublimation Residue	3.7	5.13	1.54	870	243 to 260
NAA 2084-46 *Distillate	58.0	6.61	1.18	153	53 to 61
†High Boiler Residue	42.0	5.60	1.31	457	88 to 96
§Sublimate	36.5	6.03	1.35	388	60 to 63
Sublimation Residue	5.5	5.18	1.54	1300	256 to 268

* The distillate is that portion of the coolant more volatile than para-terphenyl. Para-terphenyl is included in this fraction.

† The High Boiler Residue (HBR) is the same fraction used elsewhere in the report and is that portion less volatile than para-terphenyl.

§ The sublimate is the volatile portion of the HBR while the less volatile material in the HBR is Sublimation Residue.

**Sample number NAA-2078-14 was the sample withdrawn near the end of of the single cycle diphenyl irradiation (MTR cycle 78). Sample number NAA-2084-46 was the sample withdrawn near the end of the extended diphenyl irradiation (MTR cycles 82, 83, and 84).

and

$$G_{HBR} = \frac{lbs\ of\ HBR\ formed}{Mwh\ absorbed\ in\ the\ coolant}$$

The index of decomposition used is called G_{HBR} and has the units

$$\frac{(lbs\ of\ HBR\ formed)}{(Mwh\ of\ energy\ absorbed\ in\ the\ coolant)}$$

It is abbreviated to $\frac{lbs\ of\ HBR}{(Mwh)_a}$ and appears in this manner in the report. Material balances on the system combined with periodic sampling were used to determine the rate of production of HBR. Calorimeters, which are discussed in the equipment section, were used to determine the gamma flux at three positions along the in-pile section. Pure nickel and cobalt-aluminum flux wires were used to measure the fast neutron and thermal neutron fluxes along the in-pile section. The method for computation and interpretation of the HBR generation rate and energy absorption rate at the in-pile assembly is presented in detail in Appendix I. In this appendix, a plot of a flux traverse over the in-pile assembly is shown in Fig. 41; Table XIX lists the energy absorbed from the individual reactor fluxes for all the irradiations conducted. Eighteen percent of the energy absorbed in the coolant resulted from the moderation of fast and epithermal neutrons. The remaining 82 percent resulted from the Compton scattering of the gamma photons. (This assumes that the gamma photons have an energy greater than 1.0 Mev)

1. Decomposition Rates

Decomposition of an organic coolant in a reactor can be expected to occur from two mechanisms, pyrolytic and radiolytic damage. In general, pyrolysis of polyphenyls is negligible at temperatures below 800°F. Figure 15 in Section IV-A, 2 is a presentation of the available data on the pyrolysis of some polyphenyl materials. The pyrolysis data are presented between lines representing maximum and minimum rates reported. In the radiation zone, the two mechanisms can be expected to occur simultaneously. However, since the combined rate is the item of interest, G_{HBR} is measured as the total of both pyrolysis and radiolysis occurring under the temperature and radiation conditions which were present at the in-pile section. Figure 9 is a plot of G_{HBR} for all the single cycle irradiations and the first cycle of the extended diphenyl irradiation. Table V presents all the values of G_{HBR} for all cycles. A summary of the materials irradiated and the length of reactor exposure is given on the following page.

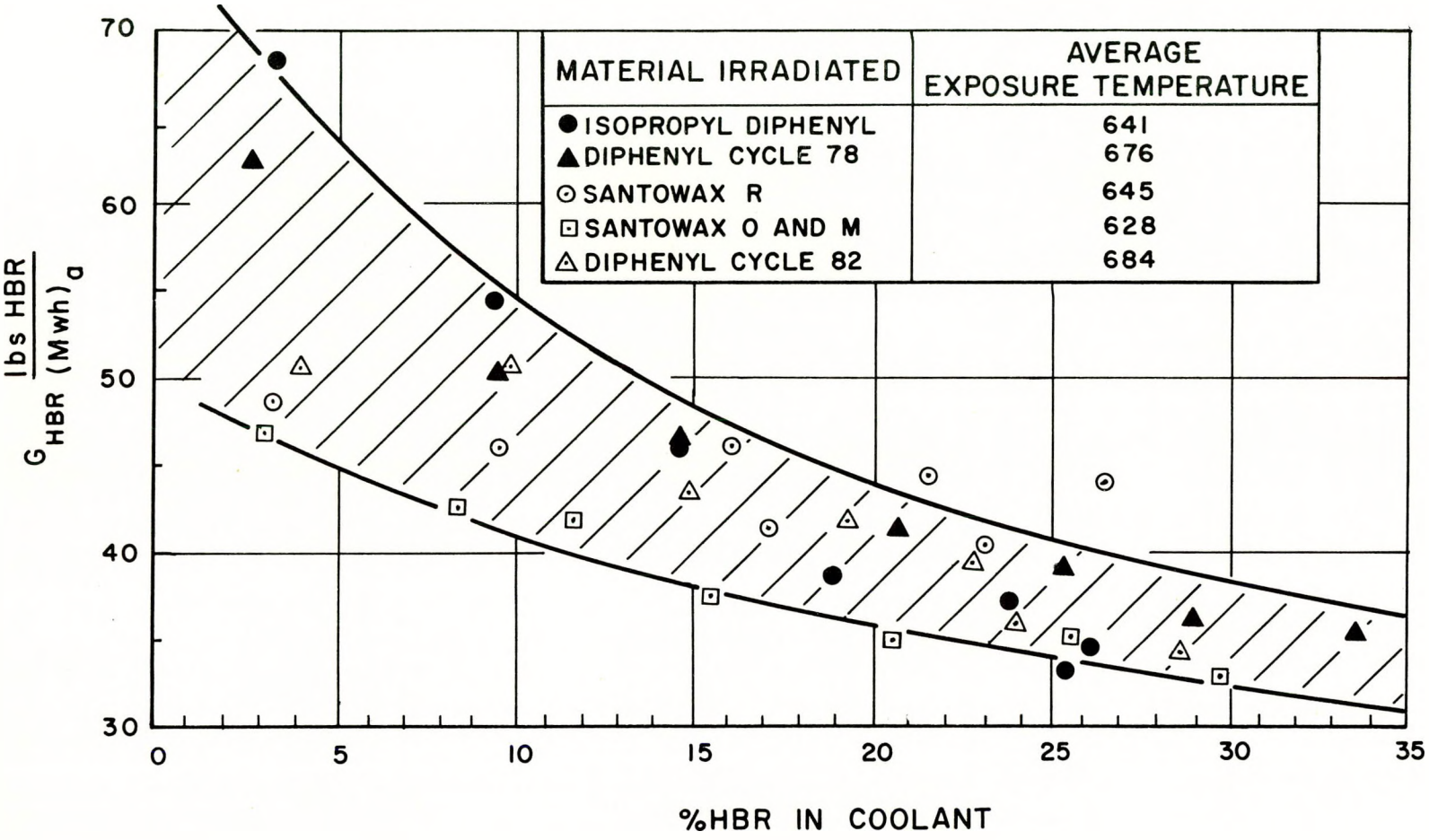

Fig. 9. Decomposition Rates of Polyphenyl Materials

TABLE V

SUMMARY OF INDIVIDUAL DECOMPOSITION RATES FOR ALL MATERIALS

Material Irradiated	MTR Cycle	Period of Irradiation (days)	Reservoir* Av. Temp. (°F)	Average Density (lbs/ft^3)	Average %HBR	G_{HBR} ($lbs\ HBR/(Mwh)_a$)	G_p (molecules/100ev)
IPD	77	10/18-10/21	600	48.1	3.4	68.4	0.181
IPD	77	10/22-10/23	630	48.0	9.5	54.4	0.144
IPD	77	10/24-10/25	670	47.6	14.7	46.1	0.122
IPD	77	10/26-10/27	625	48.6	19.0	38.9	0.103
IPD	77	10/28-10/29	630	48.7	23.8	37.4	0.099
IPD	77	10/30-10/31	675	47.8	26.2	34.8	0.092
IPD	77	11/ 1-11/3	660	48.1	25.5	33.3	0.088
Average Exposure Temperature			641				
DIP	78	11/10-11/11	655	47.4	2.8	62.4	0.165
DIP	78	11/12-11/13	645	48.7	8.7	50.6	0.134
DIP	78	11/14-11/15	660	49.0	14.8	46.9	0.124
DIP	78	11/16-11/17	680	49.1	20.8	41.6	0.110
DIP	78	11/18-11/20	685	49.2	25.3	39.3	0.104
DIP	78	11/21-11/22	690	49.4	29.0	36.7	0.097
DIP	78	11/23-11/25	700	49.4	33.4	35.9	0.095
Average Exposure Temperature			676				
SWR	79	12/ 1-12/3	550	56.5	3.3	48.4	0.128
SWR	79	12/ 4-12/5	650	54.6	9.8	46.1	0.122
SWR	79	12/ 6-12/7	700	53.6	16.1	46.1	0.122
SWR	79	12/ 8-12/9	700	54.1	21.6	44.6	0.118
SWR	79	12/10-12/11	700	54.1	26.5	44.2	0.117
SWR	79	12/12-12/13	615	55.9	17.2	41.6	0.110
SWR	79	12/14-12/16	620	56.0	23.2	40.8	0.108
Average Exposure Temperature			645				
SOM	81	1/11-1/13	670	52.0	3.1	47.0	0.124
SOM	81	1/14-1/15	670	52.5	7.4	42.8	0.113
SOM	81	1/16-1/17	620	54.4	11.7	42.0	0.111
SOM	81	1/18-1/20	605	55.3	15.6	37.6	0.099
SOM	81	1/21-1/22	590	56.0	20.3	35.5	0.093
SOM	81	1/23-1/24	640	54.9	25.4	35.4	0.094
SOM	81	1/25-1/28	620	55.7	29.6	33.1	0.087
Average Exposure Temperature			628				
Extended Diphenyl Irradiation: DIP-3	82	2/ 1-2/3	690	46.3	4.0	51.0	0.135
DIP-3	82	2/ 4-2/5	705	46.6	9.8	51.0	0.135
DIP-3	82	2/ 6-2/7	695	48.0	14.9	43.8	0.116
DIP-3	82	2/ 8-2/10	695	48.4	19.3	42.0	0.111
DIP-3	82	2/11-2/12	695	48.9	22.8	39.7	0.105
DIP-3	82	2/13-2/14	685	49.1	24.0	36.3	0.096
DIP-3	82	2/15-2/18	670	50.1	28.7	34.8	0.092
Average Exposure Temperature			684				
DIP-3	83	2/23-2/25	655	51.0	31.7	31.4	0.083
DIP-3	83	2/26-2/28	640	51.4	33.3	29.8	0.079
DIP-3	83	3/ 1-3/2	590	53.0	32.7	26.4	0.070
DIP-3	83	3/ 3-3/4	595	52.9	33.3	24.2	0.064
DIP-3	83	3/ 5-3/6	600	52.7	34.0	23.4	0.062
DIP-3	83	3/ 7-3/8	590	53.0	35.1	21.2	0.056
DIP-3	83	3/ 9-3/10	575	53.5	34.4	19.3	0.051
Average Exposure Temperature			597				
DIP-3	84	3/15-3/17	620	52.0	34.1	15.9	0.042
DIP-3	84	33/18-3/19	650	51.4	37.3	25.3	0.067
DIP-3	84	3/20-3/22	655	51.4	36.3	30.6	0.081
DIP-3	84	3/23-3/25	650	51.1	35.1	27.6	0.073
DIP-3	84	3/26-3/27	665	51.1	38.4	20.0	0.053
DIP-3	84	3/28-3/31	660	51.1	38.3	14.3	0.038
Average Exposure Temperature			651				

*The reservoir temperatures shown are higher than the operating temperatures shown on Table 2 and are probably due to the additional sensible heat transfer from the outer pipe and the long residence time in the reservoir.

Material Irradiated	MTR Cycle No.	Reactor Exposure $(Mwh)_o^*$
Isopropyl Diphenyl	77	11364
Diphenyl	78	12952
Santowax R	79	12666
Santowax O - Santowax M	81	12855
Diphenyl (Extended Irradiation)	82	14330
	83	14082
	84	11926
Total for Extended Diphenyl Irradiation		40338

Individual values of G_{HBR} and the operating conditions under which they were determined are presented in Table V. Figures 10 through 14 present single cycle data from Table V plotted on semi-log scales. Semi-log plots were used to show that an exponential decrease in G_{HBR} was noted and that G_{HBR} was dependent upon the amount of undamaged material in the coolant.

No temperature effect could be noted when bulk temperatures were varied by plus or minus 50°F from an average bulk temperature in the in-pile reservoir of approximately 650°F. Temperature changes of this magnitude occurred quite frequently when heat transfer determinations were made. The changes were of sufficient duration that if G_{HBR} were to increase appreciably with temperature, it would have been detected.

The values of G_{HBR} from all three cycles of the extended diphenyl irradiation (MTR cycles 82, 83, and 84) are presented in Fig. 14, because two separate effects not noted in the single-cycle irradiations occurred. First G_{HBR} decreased with time at constant HBR content during cycle 83. Second, G_{HBR} exhibited a momentary increase when, at the beginning of cycle 84, bulk temperatures were raised after prolonged operation at a lower temperature during the previous cycle.

Uncertainty in the information from the uranium thermocouples required that, for safety reasons, bulk temperatures be maintained approximately 90°F lower at the beginning of cycle 83 than the operating temperatures during cycle 82. The HBR content was maintained by coolant withdrawal and makeup at approximately

---

* The MTR operating time is reported as megawatt-hours of thermal power generated. Since the operating power was nearly constant at 40 megawatts, $(\text{megawatt-hours})_{\text{operating}}$ $(Mwh)_o$ is used as a time scale.

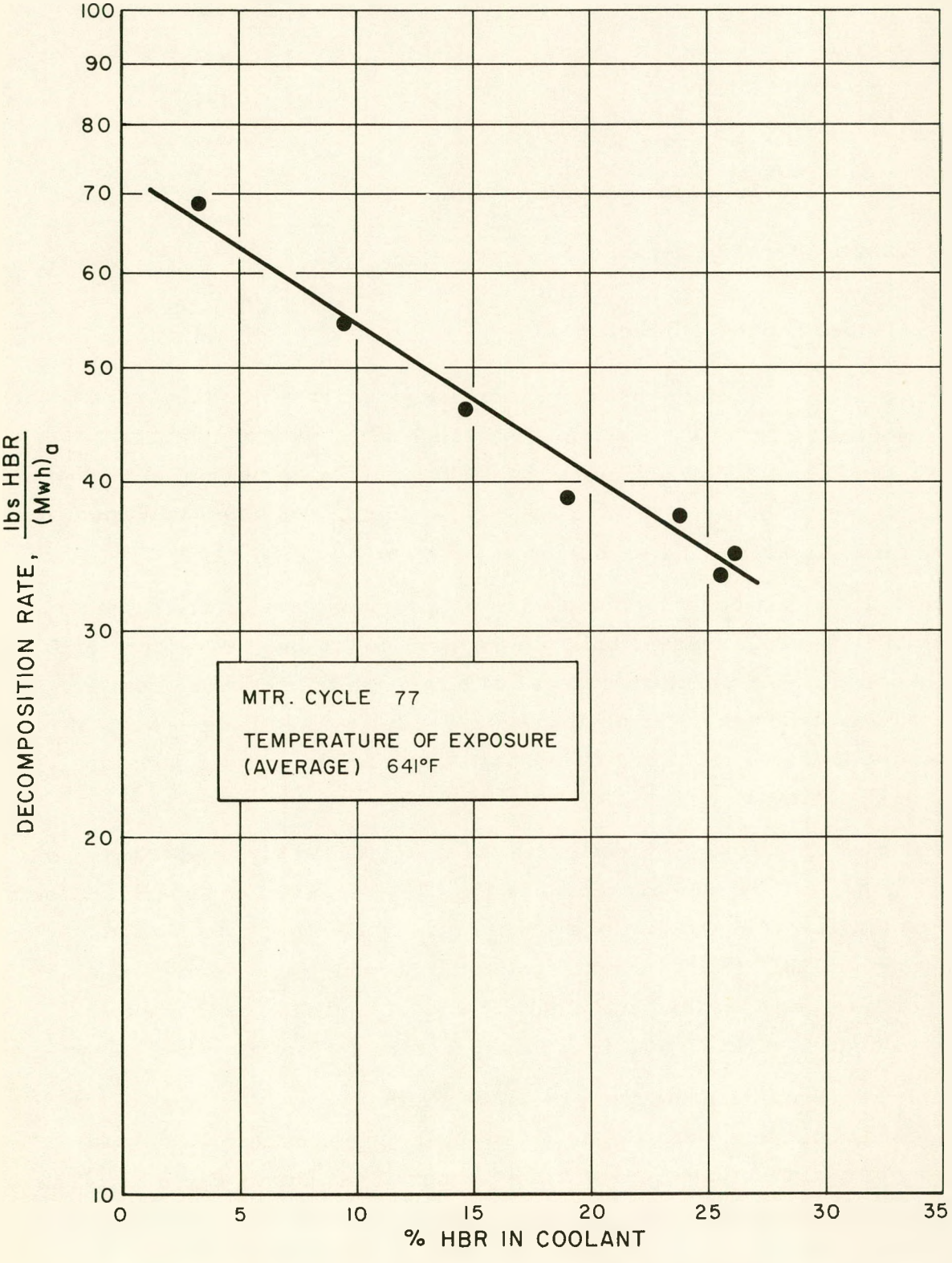

Fig. 10. Decomposition Rates for Isopropyl Diphenyl

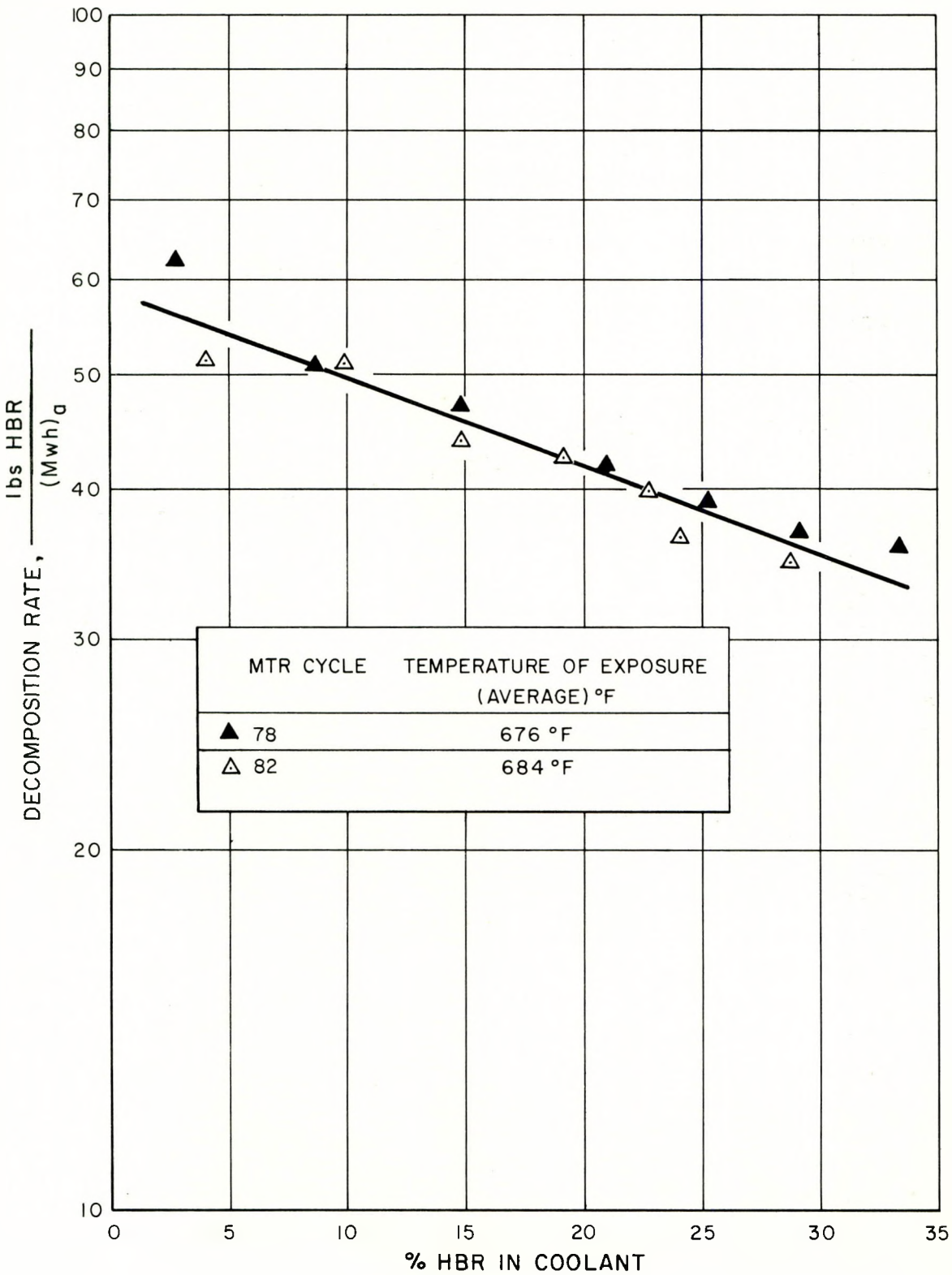

Fig. 11. Decomposition Rates for Diphenyl

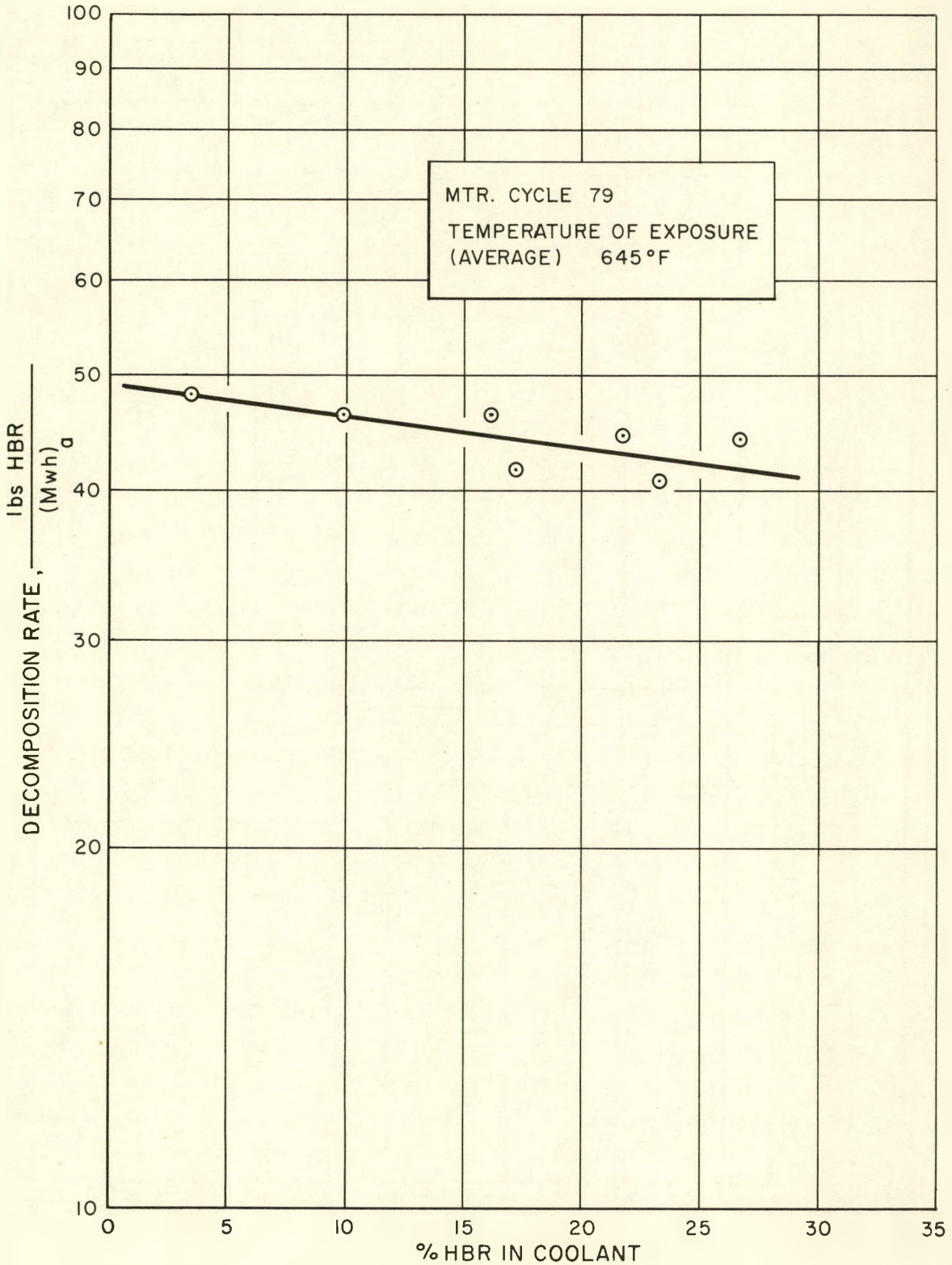

Fig. 12. Decomposition Rates for Santowax R

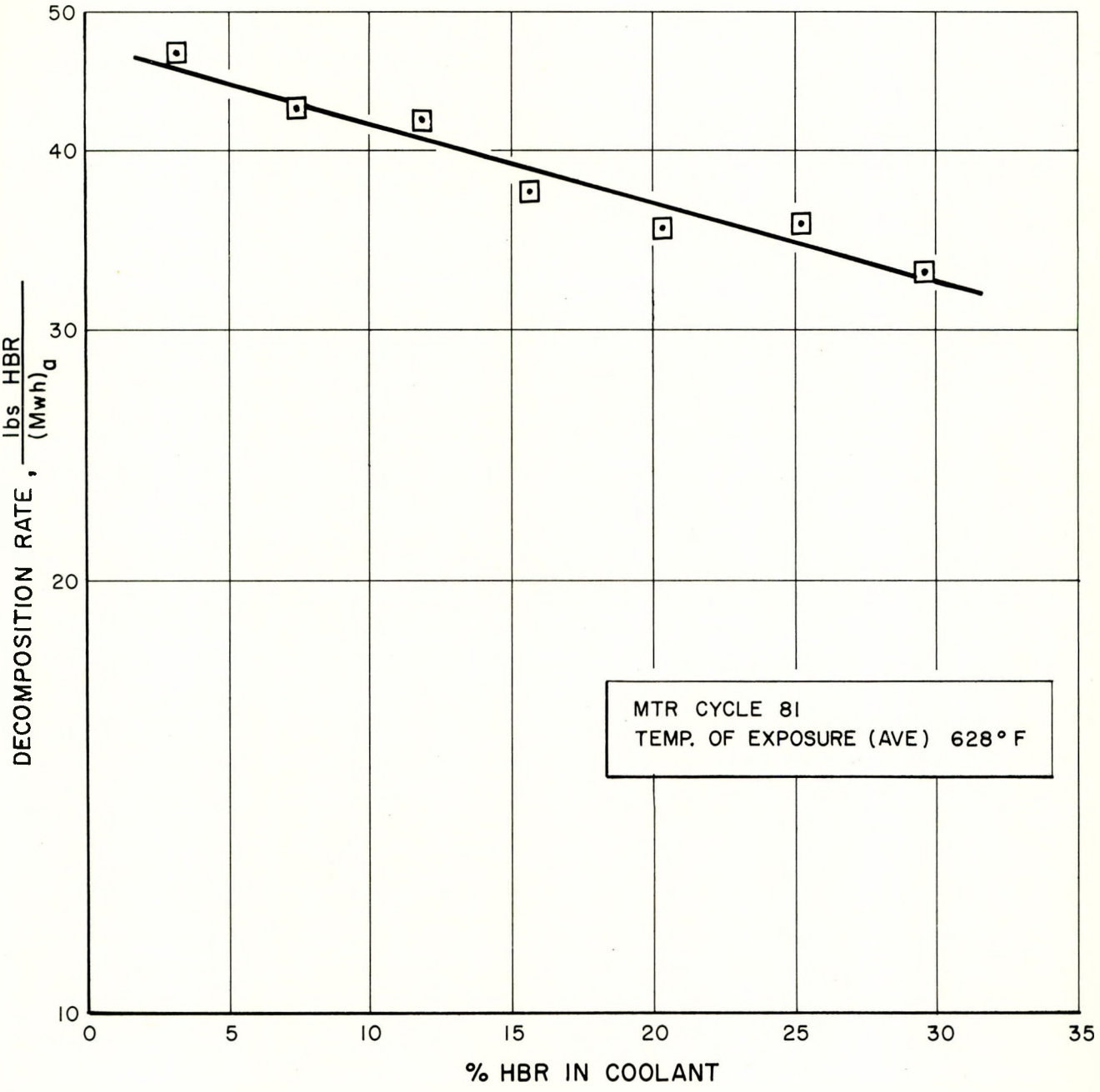

Fig. 13. Decomposition Rates for Santowax O - Santowax M

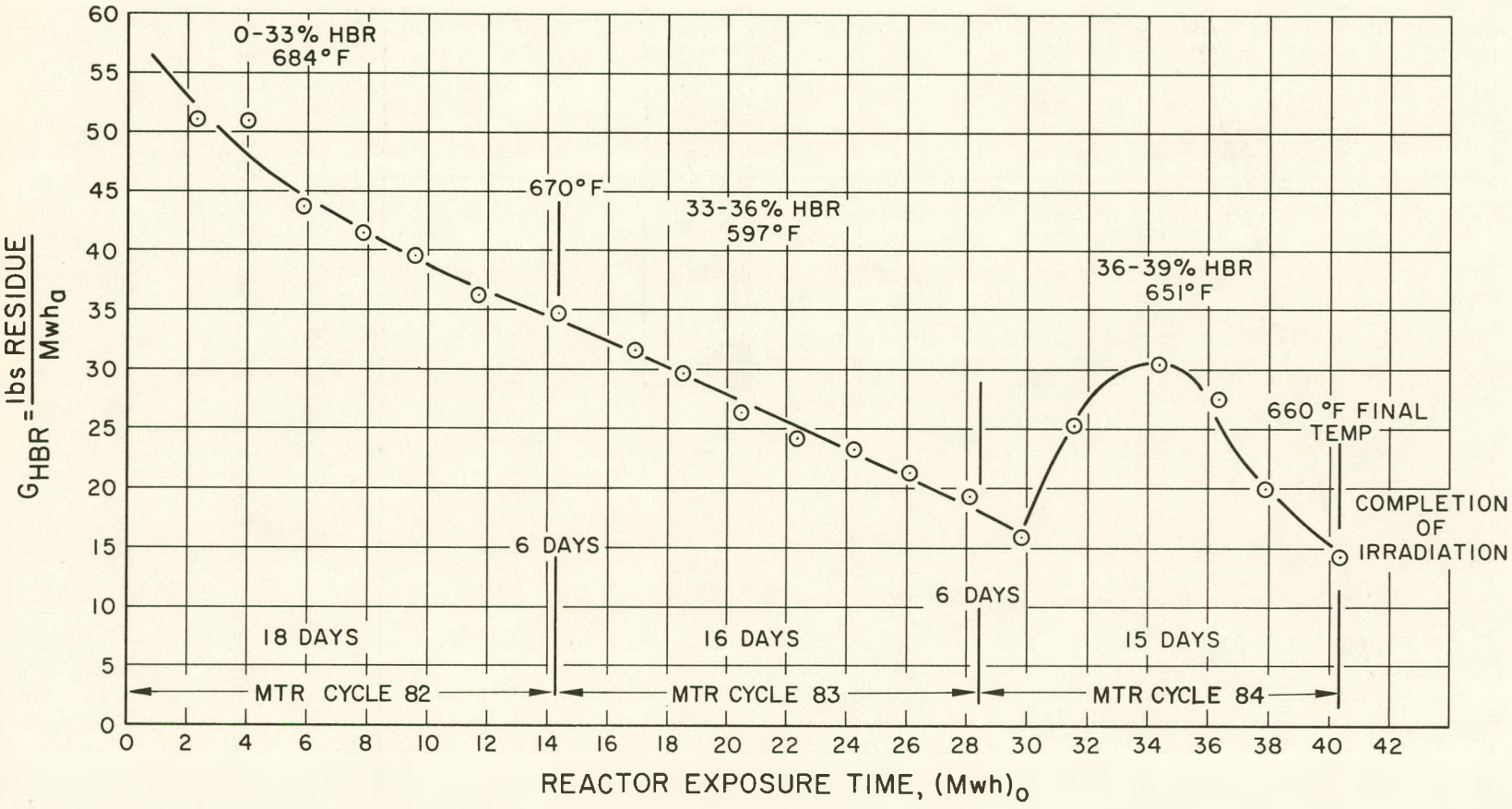

Fig. 14. Decomposition Rates for Extended Diphenyl Irradiation

35 percent HBR by weight. As shown in Table V and plotted in Fig. 14, the value of G_{HBR} decreased with time until a low value of 15.9 $\frac{\text{lbs HBR}}{(\text{Mwh})_o}$ was reached at the end of cycle 83. Commencing with cycle 84, the operating temperatures were raised approximately 50°F. The G_{HBR} rose to a value of 30.6 $\frac{\text{lbs HBR}}{(\text{Mwh})_a}$, which was approximately equal to the value at the end of cycle 82. For the remainder of the third cycle and until the completion of the irradiation, the damage rate continued to decrease as it did during cycle 83. There were no indications that G_{HBR} was approaching as asymptotic value. The values of G_{HBR} are felt to represent a real effect, since the changes were so large.

The increase in G_{HBR} at the beginning of cycle 83 may represent a temperature effect, not previously observed when bulk fluid temperatures were changed by as much as 50°F. However, due to the complexity of the radiolysis mechanisms involved, not enough information is available to explain the decrease in G_{HBR} which occurred during the extended diphenyl irradiation.

2. Pyrolytic Effects

Only 20 percent of the entire system volume was in the reactor flux. The remainder of the material being tested was, however, exposed to the test temperature and therefore could be expected to be undergoing pyrolysis and generating decomposition products. These effects were considered in determining G_{HBR} by using the maximum pyrolytic data as shown in Fig. 15. The amount of HBR generated from this effect was found to comprise less than 1 percent of the total amount of decomposition products formed and was not considered to materially affect the determination of G_{HBR}.

3. Estimated Accuracy in Determination of G_{HBR}

The values of G_{HBR} presented can only be considered in the light of the accuracy of their determination. It is estimated that the probable error in the values presented in Table V and Figs. 10 through 14 is approximately ± 15 percent. The major source of the error can be expected to arise from the inherent uncertainties in determining the reactor fluxes. Accuracy of the MTR thermal neutron flux measurement, utilizing the Co-Al monitor method, is estimated to be ± 20 percent.[8] Assuming a standard thermocouple uncertainty of ± 1 percent in the gamma calorimeter thermocouples, it is estimated that the gamma absorption, after a thermal neutron correction for the (n, γ) reaction has been applied to

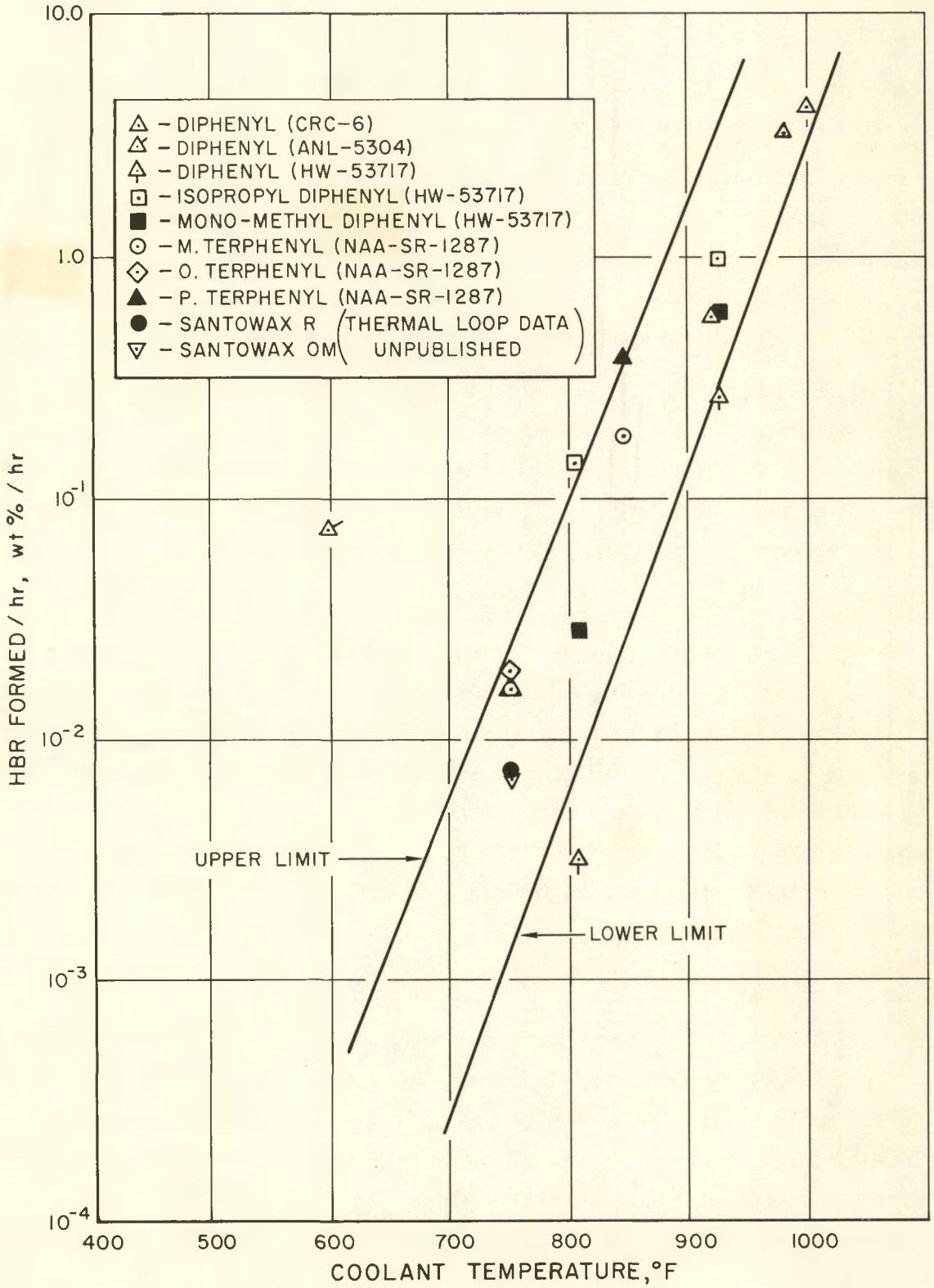

Fig. 15. Pyrolysis of Polyphenyls

the calorimeter, is accurate to ± 13 percent. The largest uncertainty exists in the determination of the fast neutron flux. Essentially the same errors exist in measuring the fast neutron flux as were present in the determination of the thermal flux. However, due to traces of cobalt in the nickel wires, the wide neutron energy ranges considered, and the lack of precise cross section data, it is estimated that the fast neutron fluxes may be in error by as much as ± 50 percent.

The fast flux contributes approximately 12 percent of the total energy absorbed in the coolant, with the gamma flux contributing the remaining 88 percent. Based on these energy fractions and the mass balance for high-boiler residue formed, which is accurate to within ± 5 percent, except for the Santowax R irradiation, it is estimated that the maximum uncertainty in G_{HBR} will not exceed ± 25 percent. However, considering the deviations and the fact that the measurements were done under a variety of conditions with different equipment for each cycle, it is probable the error is nearer to the ± 15 percent already mentioned.

Correlation between the reactor fluxes measured at position A-13 in this experiment and the reported MTR fluxes[9] was approximately ± 15 percent.

During the Santowax R irradiation, a loss-of-flow accident caused the test heater to rupture. A large portion of the coolant was lost as a result of the rupture, and, since the high boiler residue content could only be estimated by difference, the values of G_{HBR} for Santowax R may be subject to larger errors. There are only two points in Fig. 9 which fall out of the two lines outlining all values of G_{HBR} for the single-cycle irradiations. The Santowax R data appear to be somewhat higher than the Santowax O - Santowax M data. It is recommended that the Santowax O - Santowax M decomposition rates be used for terphenyls because of the larger uncertainty in the Santowax R data.

4. Radiolytic Gas Generation

The system was not designed to measure the radiolytic gas generation rates. Initial pressurization was with nitrogen with no nitrogen purge used during operation. Gas was bled off as required to maintain system pressure within the desired limits.

Based on the surge tank volume, and treating the mixed radiolytic gases as perfect gases, it was computed that the gas generation rate during the isopropyl diphenyl irradiation was 0.24 ft^3 (STP) of gas generated per pound of residue formed. This value compares favorably with the BNL in-pile loop data,[10] which was 15 standard cubic centimeters/gram of residue formed.

After the isopropyl diphenyl irradiation, fluid leakage from the main circulating pump flange made determination of the gas generation rates during all the remaining irradiations very difficult. In the case of the isopropyl diphenyl irradiation, gas withdrawal was necessary about twice during an 8-hour period. During the diphenyl and terphenyl irradiations, it was not necessary to bleed off gas unless very large fluid additions were made to the system. The gas generation rate for all the remaining irradiations appeared to be just equal to the amount being lost through gas dissolved in the leakage plus the increase in volume in the surge tank gas space due to the leakage.

Based on the system pressure, and allowing for the radiolytic gases dissolved in the leakage from the system, it is estimated that the gas generation rates for the diphenyl, Santowax R, Santowax O - Santowax M, and the extended diphenyl irradiations were about equal and a factor of ten less than the radiolytic gas generation rate measured during the isopropyl diphenyl irradiation. This value of the gas generation rate for diphenyl and the terphenyls is lower than the rate reported in the BNL in-pile loop work.[11]

5. Radiolytic Gas Composition

Gas samples were withdrawn periodically from the surge tank, sealed in glass bulbs, and analyzed by mass spectroscopy techniques for gas composition. Liquid samples were withdrawn at the same time as the surge tank gas sample, and the dissolved gases extracted by means of a Toepler pump with the liquid sample boiling under vacuum conditions. The dissolved gases were similarly sealed in a glass bulb and analyzed for composition.

The solubility of the gases in the irradiated coolant was roughly determined by measuring the amount of gas extracted.

Tables VI and VII present the gas analysis data and solubility data from representative samples of all four materials irradiated. Hydrogen, methane, ethane, ethene, propane, and propene comprised approximately 96 mol percent of the radiolytic gases found in the gas phase. Other gaseous products containing four to eight carbon atoms per molecule were also detected, but in such small amounts that they may be considered trace quantities. The gases extracted from the liquid contained a larger percentage of the higher molecular weight radiolytic gases produced. Benzene comprised the largest fraction of the lighter ends found

TABLE VI

GAS AND LIQUID PHASE GAS SAMPLE ANALYSES

Material Irradiated	Isopropyl Diphenyl - MTR Cycle 77				Santowax R - MTR Cycle 79			
	Gas Phase	Gas Phase	Gas Phase	Liquid Phase	Gas Phase	Liquid Phase	Gas Phase	Liquid Phase
Sample Number	6G	8G	13G	14G	6G	5G	9G	10G
Loop Exposure - $(Mwh)_o$	4896	6412	11,295	11,308	8164	8152	11,920	11,926
HBR Content - Wt %	18	22	25	25	23	23	22	22
System Conditions - °F	520	520	595	595	620	620	545	545
at Time of Sample - psig	308	330	325	325	117	117	118	118
Gas Solubility - $[ft^3(STP)/lb] \times 10^2$	-	-	-	9.5	-	1.2	-	1.0
Gas Composition - Mol % (Nitrogen Free)								
Hydrogen	58.1	41.8	29.4	4.61	66.0	18.6	77.0	30.0
Methane	21.3	46.0	53.0	39.8	18.3	15.6	8.97	8.38
Ethane	10.1	2.20	4.67	9.88	7.90	15.8	5.65	9.77
Ethene	2.22	0.60	0.64	1.11	2.78	-	2.70	3.86
Acetylene	-	-	-	0.10	-	-	-	0.21
Propane	2.67	6.95	9.48	29.1	1.40	7.30	1.56	4.16
Propene	1.76	1.64	1.09	3.64	0.99	-	0.87	3.64
Cyclopropane	-	-	-	-	-	1.27	-	0.46
Propyne	-	-	-	-	-	0.11	-	-
Vinylacetylene	-	-	-	-	-	-	-	-
N-butane	0.95	0.38	0.32	2.12	0.51	4.40	0.82	4.16
Iso-butane	-	0.19	0.46	2.08	-	0.52	0.08	-
Butenes and/or Cyclobutane	0.72	0.14	0.11	0.97	0.35	4.25	0.40	3.90
N-Pentane	0.36	0.08	0.24	0.66	-	0.75	-	0.79
Iso-pentane	-	-	-	0.49	-	1.10	-	0.50
Pentanes	0.23	0.11	0.18	0.59	-	-	-	-
Pentene	-	-	-	-	-	0.83	0.12	1.17
Cyclopentane	-	-	-	-	-	3.12	-	2.06
Cyclopentene	0.10	-	-	0.07	-	1.76	0.07	1.81
Hexane	-	-	-	0.38	-	0.49	-	0.42
Hexenes	-	-	-	-	-	0.64	-	0.46
3-Me-2-Pentane	-	-	-	0.31	-	-	-	-
Cyclohexane	-	-	-	0.07	-	0.19	-	0.21
Hexyne	-	-	-	0.10	-	0.26	-	0.29
Heptane	-	-	-	-	-	0.04	-	-
Heptenes	-	-	-	-	-	-	-	0.17
Heptyne	-	-	-	-	-	0.15	-	0.17
Benzene	1.53	0.14	0.29	2.88	0.64	21.9	0.59	21.9
Toluene	-	-	0.03	0.14	0.06	0.26	0.07	0.38
Nitrogen - Mol %	69.3	9.40	5.93	0.87	51.4	16.1	59.7	28.2

TABLE VI (Continued)

GAS AND LIQUID PHASE GAS SAMPLE ANALYSIS

Material Irradiated	Santowax O - Santowax M - MTR Cycle 81						
	Gas Phase	Liquid Phase	Gas Phase	Liquid Phase	Gas Phase	Gas Phase	Liquid Phase
Sample Number	5G	6G	7G	9G	10G	12G	13G
Loop Exposure -$(Mwh)_o$	3466	6608	6608	10,430	10,430	12,215	12,229
HBR Content - Wt %	10.0	18.7	18.7	26.5	26.5	31.0	31.0
System Conditions - °F	650	565	565	595	595	580	580
at Time of Sample- psig	280	220	220	200	200	191	191
Gas Solubility - $[ft^3(STP)/lb].10^2$	-	2.2	-	2.5	-	2.4	-
Gas Composition - Mol % (Nitrogen Free)							
Hydrogen	75.6	22.6	70.6	16.0	56.2	45.8	13.1
Methane	13.7	16.6	15.7	21.5	23.7	30.2	21.9
Ethane	5.52	18.5	7.17	23.3	11.0	15.2	25.4
Ethene	1.76	2.34	1.09	2.70	2.34	2.26	1.78
Acetylene	-	-	-	-	-	-	0.32
Propane	1.63	9.82	2.51	12.7	2.75	3.90	12.5
Propene	1.58	4.64	1.01	2.14	1.16	0.93	1.90
N-butane	-	5.75	0.81	7.25	0.72	0.81	6.65
Iso-Butane	-	-	-	0.17	1.45	0.30	0.53
Cyclobutane	-	3.12	-	2.32	-	-	2.65
Butenes	-	-	0.06	-	0.13	0.18	-
Diacetylene	-	-	-	0.01	-	-	0.02
Vinylacetylene	0.10	0.17	-	0.10	-	-	0.10
Butynes	-	0.16	-	0.06	-	-	0.08
n-Pentane	-	0.88	-	1.43	-	-	1.39
Iso-Pentane	-	-	-	-	-	-	-
Cyclopentane	-	1.61	-	2.19	-	-	2.06
Cyclopentene	-	0.95	0.03	0.51	0.10	0.05	0.55
Pentenes	-	0.85	0.12	0.45	0.12	0.09	0.58
Hexanes	-	0.19	-	0.27	-	-	0.32
Hexenes	-	0.23	-	0.24	-	-	0.28
Hexynes	-	0.08	-	0.04	-	-	0.05
Heptynes	-	0.06	-	0.03	-	-	0.05
Benzene	-	11.5	0.14	6.36	0.25	0.09	7.60
Toluene	-	0.10	-	0.05	-	-	0.12
Nitrogen - Mol %	76.9	29.1	64.4	20.2	51.1	41.9	15.9

TABLE VIIA

GAS AND LIQUID PHASE GAS ANALYSIS
EXTENDED DIPHENYL IRRADIATION - MTR CYCLE 82

	Gas Phase	Liquid Phase	Gas Phase	Liquid Phase	Gas Phase	Liquid Phase
Sample Number	2G	3G	7G	6G	12G	11G
Loop Exposure - $(Mwh)_o$	1847	1850	5741	5725	9682	9679
HBR Content - Wt %	6.0	6.0	18.2	18.2	23.2	23.2
System Conditions - °F	625	625	630	630	640	640
at Time of Sample - psig	268	268	278	278	295	295
Gas Solubility - $[ft^3(STP)/lb]\ 10^2$	-	2.7	-	3.5	-	4.2
Gas Composition Nitrogen Free - Mol %						
Hydrogen	85.1	46.7	50.4	17.7	37.1	11.7
Methane	6.00	8.35	26.0	20.5	33.5	25.4
Ethane	3.27	7.92	13.2	20.4	18.0	24.0
Ethene	2.08	4.05	2.34	2.20	1.25	1.90
Acetylene	-	-	-	-	0.17	-
Propane	0.50	2.88	3.79	9.12	5.60	12.8
Propene	0.69	2.86	1.12	4.34	1.25	3.17
N-Butane	-	0.94	0.80	3.98	1.18	5.48
Iso-Butane	-	0.28	0.32	0.98	0.47	1.10
Butenes and/or Cyclobutane	-	1.14	0.45	1.97	0.31	1.80
N-Pentane	-	0.11	-	1.09	-	1.35
Iso-Pentane	-	-	-	-	0.17	-
Pentene	-	0.51	0.10	0.67	0.14	0.45
Cyclopentane	-	0.28	0.03	1.37	-	1.55
Cyclopentene	-	0.66	0.06	0.70	0.05	0.41
Hexane	-	0.30	-	0.33	-	0.25
Hexenes	-	0.38	-	0.60	-	0.51
Hexyne	-	1.97	-	0.15	-	0.10
Heptene	-	-	-	-	-	-
Heptyne	-	0.10	-	0.10	-	0.10
Benzene	0.15	18.06	0.23	12.5	0.24	7.44
Toluene	-	0.15	-	0.20	-	1.02
Nitrogen	79.2	55.9	68.7	37.7	57.5	30.7

TABLE VIIB

GAS AND LIQUID PHASE GAS ANALYSIS

EXTENDED DIPHENYL IRRADIATION - MTR CYCLE 83

	Gas Phase	Liquid Phase	Gas Phase	Liquid Phase	Gas Phase	Liquid Phase
Sample Number	19G	20G	24G	25G	30G	28G
Loop Exposure -$(Mwh)_o$	20,073	20,086	23,883	23,889	27,801	27,780
HBR Content - Wt %	32.6	32.6	35.4	35.4	35.4	35.4
System Conditions - °F	525	525	525	525	510	510
at Time of Sample - psig	274	274	270	270	295	295
Gas Solubility - $[ft^3(STP)/lb]10^2$	-	4.0	-	3.5	-	4.0
Gas Composition Nitrogen Free - Mol %						
Hydrogen	41.2	13.6	52.5	16.2	54.0	17.9
Methane	26.0	17.7	22.2	16.8	23.0	19.9
Ethane	17.0	25.5	12.9	21.3	11.6	21.5
Ethene	2.95	4.96	2.74	4.43	2.98	3.95
Acetylene	-	-	-	-	-	0.23
Propane	6.81	15.1	4.16	11.5	3.13	9.22
Propane	1.05	4.68	1.62	5.41	1.64	4.95
N-Butane	1.81	0.72	1.56	6.09	1.71	6.30
Isobutane	0.49	0.94	0.16	0.85	-	0.17
Butenes and/or Cyclobutane	0.19	2.30	0.22	2.55	0.22	2.40
N-Pentane	0.38	1.60	0.29	1.56	0.30	0.89
Isopentane	0.38	1.05	0.22	0.50	0.22	0.49
Pentene	0.19	0.94	0.29	1.08	0.30	1.03
Cyclopentane	0.30	1.71	0.07	1.43	-	0.85
Cyclopentene	0.11	0.55	0.07	0.62	0.06	0.45
Hexane	-	0.38	-	0.50	-	0.32
Hexenes	0.11	0.60	0.16	0.71	-	0.59
Hexyne	-	0.06	-	1.08	-	1.08
Heptene	-	-	-	-	-	-
Heptyne	-	0.03	-	0.04	-	0.09
Benzene	0.95	6.70	0.67	6.93	0.45	6.83
Toluene	-	-	-	0.13	-	0.13
Nitrogen	62.7	28.9	54.7	24.8	53.3	24.5

TABLE VIIC

GAS AND LIQUID PHASE GAS ANALYSIS

EXTENDED DIPHENYL IRRADIATION - MTR CYCLE 84

	Gas Phase	Liquid Phase	Gas Phase	Liquid Phase	Gas Phase	Liquid Phase
Sample Number	31G	32G	37G	38G	42G	43G
Loop Exposure -$(Mwh)_o$	31,138	31,142	33,998	34,038	37,535	37,555
HBR Content - Wt %	37.9	37.9	37.1	37.1	39.0	39.0
System Conditions - °F	585	585	580	580	600	600
at Time of Sample - psig	273	273	281	281	285	285
Gas Solubility - $[ft^3(STP)/lb]\ 10^2$	-	3.7	-	4.0	-	4.7
Gas Composition Nitrogen Free - Mol %						
Hydrogen	40.4	9.20	30.9	8.51	23.4	5.57
Methane	32.6	23.6	37.0	24.0	41.2	26.0
Ethane	15.7	26.4	19.1	25.4	21.7	28.6
Ethene	1.96	1.75	1.51	2.03	1.45	1.28
Acetylene	-	-	-	-	-	-
Propane	4.47	12.3	5.79	12.5	6.73	14.1
Propene	1.29	3.33	1.09	1.78	1.30	2.35
N-Butane	1.63	7.92	2.00	6.39	2.15	6.76
Isobutane	0.17	-	-	0.56	-	1.08
Butenes and/or Cyclobutane	0.32	1.19	0.48	0.92	0.16	0.91
N-Pentane	0.17	2.42	0.36	2.13	0.23	2.07
Isopentane	-	-	-	-	-	-
Pentene	0.17	0.82	-	-	-	-
Cyclopentane	0.17	1.32	0.18	1.93	-	1.79
Cyclopentene	0.09	0.45	0.07	0.56	0.08	0.42
Hexane	-	0.66	-	0.77	-	0.57
Hexenes	0.17	0.73	0.12	0.75	0.16	0.78
Hexyne	-	0.10	-	0.10	-	-
Heptene	-	0.12	-	0.20	0.08	0.16
Heptyne	-	0.07	-	0.05	-	-
Benzene	0.56	6.69	1.09	10.2	0.91	6.43
Toluene	-	0.16	0.06	0.36	0.06	0.21
Nitrogen	52.9	21.5	47.9	20.0	46.0	16.8

in the liquid. Figure 16 is a plot of the mol percent of hydrogen, methane, ethane plus ethene, and propane plus propene found in the gas phase for the extended diphenyl irradiation. The composition appears to vary as a function of the HBR concentration with the hydrogen content decreasing with increasing HBR content. The proportion of the gases containing one, two, and three carbon atoms appears to increase as the HBR content increases.

Temperature also seems to have a slight effect on gas composition. Lower temperatures appear to increase the proportion of hydrogen present. Gas samples 1 G, 24 G, and 30 G from the extended diphenyl irradiation show this effect. As the temperature was increased during the last cycle, the percentage of hydrogen decreased. Sample 9 G from Santowax R also exhibited a similar effect.

Gas solubilities probably change somewhat during irradiation due to the changes occurring in the coolant. For the purposes of the above comparisons, this effect has not been considered. Ratios of the mol percent in the gas phase to that in the liquid phase do change slightly, indicating that the solubilities of the various constituents also change. The solubility change appears to be small in relation to the change in the gas composition. Hydrogen generation would arise from the formation of a longer chain polyphenyl molecule such as quatrephenyl (from diphenyl) or hexaphenyl (from terphenyls). Higher molecular weight gases would be generated by opening the benzene ring.

Of particular significance is the fact that there was no evidence of the formation of gases containing nitrogen.

No radioactivity was detected when a standard air monitor was used during sampling from the system or when gases were required to be bled off.

B. HEAT TRANSFER

1. The Effect of Coolant Decomposition and Radiation on Heat Transfer

Heat transfer determinations were made with an electrically heated test heater and an in-pile uranium heater at varying conditions of bulk temperature and fluid velocities. The uranium heater and test heater are described in sections II A and II B. Measurements were made under nearly identical heat transfer conditions at the uranium heater and at the test heater. This allowed a comparison of the effect of reactor radiation fields on the heat transfer surface and on the heat

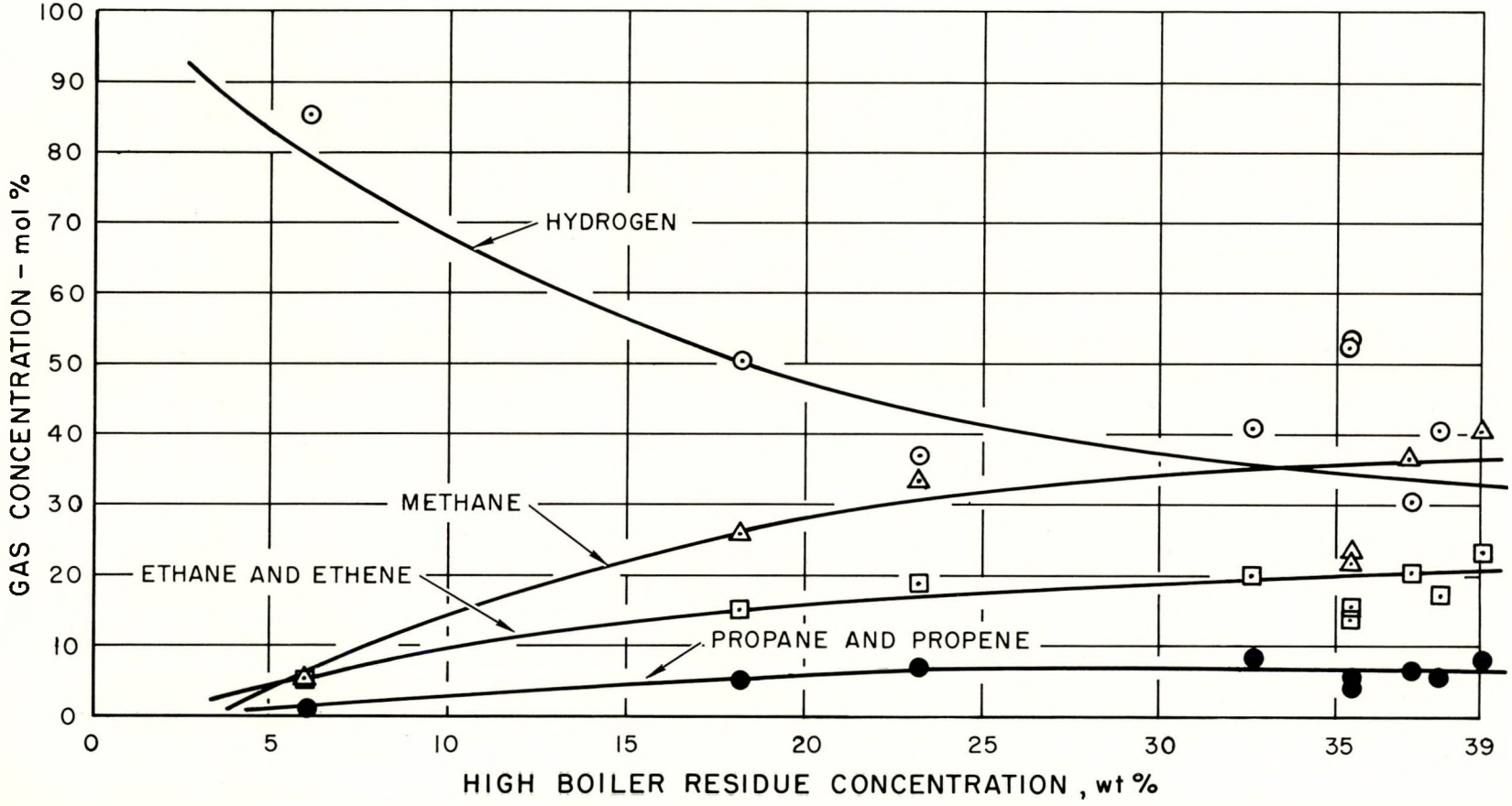

Fig. 16. Radiolytic Gas Composition in the Gas Phase vs Boiler Residue Content - Extended Diphenyl Irradiation

transfer characteristics of the coolant to be made. Since the physical properties of the coolant were the same at each heater during the runs, the effect of high-boiler residue in the coolant on the heat transfer properties would not introduce an additional variable in determining the radiation effect on heat transfer.

The operating conditions under which heat transfer determinations were made were briefly outlined in Section III B. Due to the many important aspects of an organic reactor coolant-moderator to be evaluated for each material, no one effect could be tested under the most desirable conditions. Coolant decomposition and heat transfer were considered to be of almost equal importance insofar as the operation of the experiment was concerned. It was desirable to maintain a high bulk temperature at a maximum uranium heater surface temperature of 800°F during the experiment so that conditions approximating those to be expected in a reactor could be attained. Maximum reactor thermal neutron flux was required to reach these conditions, since an appreciable amount of heat was contributed to the loop from the uranium heater and reactor heating of the in-pile section. At the start of any MTR cycle, it was possible to attain bulk fluid temperatures ranging from 650 to 680°F, but as the fuel charge was depleted, bulk fluid temperatures ranged from 600 to 620°F. The heat transfer runs at the higher temperatures were therefore generally taken at several velocities in a bulk temperature range of 600 to 650°F. Heat transfer data was also collected at a bulk temperature of 500°F, which could be controlled to within ± 10°F.

a. Test Heater

The equation

$$h = \frac{Q}{A\Delta t}$$

was used to compute the heat transfer coefficient from thermocouple and electrical measurements at the test heater. The heat input, Q, was calculated from the power generation in the tube, based on the current flowing through the tube and the resistivity of the tube at the wall temperature. The analytical technique for computing the heat transfer coefficient at the test heater is described in detail in Appendix II.

Tables VIII to XII present the experimentally determined heat transfer coefficients as a function of HBR content at varying velocities and at bulk fluid

TABLE VIII

TEST HEATER HEAT TRANSFER COEFFICIENTS

ISOPROPYL DIPHENYL – MTR CYCLE 77

Run	Date	Velocity (ft/sec)	% High Boiler Residue	Wall Temp. (°F)	Bulk Temp. (°F)	ΔT (°F)	Heat Flux q/A x 10^{-3} (Btu/hr-ft^2)	Heat Transfer Coefficient (Btu/hr-°F-ft^2)
IPD-1-1	10/22	13.6	5.0	625	501	124	130	1064
IPD-1-2	10/25	13.2	18.0	632	500	132	109	834
IPD-1-3	10/28	13.3	23.5	635	499	136	117	862
IPD-1-4	11/2	12.9	24.0	663	508	135	131	847
IPD-2-1	10/22	13.6	7.0	697	571	126	135	1087
IPD-2-2	10/24	13.2	13.5	665	563	102	113	1099
IPD-2-3	10/27	13.3	20.0	780	560	220	229	1053
IPD-2-4	10/29	13.4	25.0	725	601	124	116	934
IPD-2-5	10/31	13.2	26.5	741	587	154	144	934
IPD-2-6	11/2	13.2	23.5	733	579	154	144	934
IPD-2-7	11/4	13.2	25.0	770	616	154	146	952
IPD-3-1	10/22	21.9	5.0	579	492	87	128	1470 (1305)*
IPD-3-2	10/24	19.0	13.5	593	505	88	110	1255
IPD-3-3	10/26	18.9	18.5	592	503	89	115	1289
IPD-3-4	10/28	18.8	24.0	599	499	100	116	1153
IPD-3-5	11/2	17.4	24.0	624	505	119	132	1099 (1180)*
IPD-4-1	10/29	18.6	25.0	691	598	93	116	1245
IPD-4-2	10/31	18.7	26.5	689	579	110	141	1277
IPD-5-1	10/25	9.0	18.5	668	501	167	113	676
IPD-5-2	10/28	8.7	24.0	690	512	178	120	676
IPD-5-3	11/2	8.9	24.3	718	514	204	136	662
IPD-6-1	10/24	8.7	13.5	716	563	153	109	714
IPD-6-2	10/27	8.9	21.5	790	554	236	187	794
IPD-6-3	10/29	9.1	25.0	769	597	172	116	671
IPD-6-4	10/31	9.1	26.5	783	586	197	147	746
IPD-6-5	11/2	8.9	23.5	773	579	194	146	752

*Value in parenthesis was corrected for velocity and was used for plotting the effect of HBR content on heat transfer. The value not in parenthesis is measured value of the heat transfer coefficient at the velocity shown.

TABLE IX

TEST HEATER HEAT TRANSFER COEFFICIENTS

DIPHENYL — MTR CYCLE 78

Run	Date	Velocity (ft/sec)	% High Boiler Residue	Wall Temp. (°F)	Bulk Temp. (°F)	ΔT °F	Heat Flux $q/A \times 10^{-3}$ (Btu/hr-ft^2)	Heat Transfer Coefficient (Btu/hr-°F-ft^2)
DIP-1-1	11/10	8.3	3.0	675	509	166	141	847 (891)*
DIP-1-2	11/12	8.8	10.5	715	513	202	177	877
DIP-1-3	11/15	9.0	17.0	734	524	210	179	847
DIP-1-4	11/16	8.9	21.0	736	518	218	175	800
DIP-1-5	11/19	8.8	24.7	738	511	227	175	769
DIP-2-1	11/10	9.0	2.5	784	652	132	154	1170
DIP-2-2	11/12	8.9	10.0	774	608	166	170	1031
DIP-2-3	11/14	8.8	15.5	780	623	157	178	1124
DIP-2-4	11/16	8.9	20.5	784	644	140	129	917
DIP-2-5	11/19	8.9	24.5	794	655	139	138	990
DIP-3-1	11/10	13.8	3.0	638	489	149	183	1228 (1181)*
DIP-3-2	11/12	13.7	10.5	687	522	165	179	1075 (1040)*
DIP-3-3	11/15	13.2	17.0	678	519	159	174	1099
DIP-3-4	11/16	13.1	21.0	674	509	165	170	1031
DIP-3-5	11/19	13.1	24.7	686	509	177	171	964
DIP-4-1	11/10	13.3	2.0	784	645	139	182	1311
DIP-4-2	11/12	13.4	10.0	755	616	139	169	1214
DIP-4-3	11/14	13.3	15.5	765	627	138	177	1277
DIP-4-4	11/16	13.3	20.5	806	655	151	172	1144
DIP-4-5	11/19	13.2	24.5	793	665	128	148	1152
DIP-5-1	11/10	17.8	3.0	597	485	112	173	1550
DIP-5-2	11/12	17.8	10.5	632	518	114	172	1502
DIP-5-3	11/15	17.8	17.0	634	516	118	172	1456
DIP-5-4	11/16	17.3	21.0	613	488	125	167	1333 (1369)*
DIP-5-5	11/19	17.3	25.0	623	493	130	169	1300 (1331)*
DIP-6-1	11/10	17.9	2.0	764	654	110	185	1681
DIP-6-2	11/12	17.6	10.0	714	601	113	172	1520
DIP-6-3	11/15	17.7	16.5	752	635	117	185	1577
DIP-6-4	11/16	17.6	20.5	767	646	121	178	1473
DIP-6-5	11/19	17.6	24.5	791	668	123	179	1466

*Value in parenthesis was corrected for velocity and was used for plotting the effect of HBR content on heat transfer. The value not in parenthesis is the measured value of the heat transfer coefficient at the velocity shown.

TABLE X

TEST HEATER HEAT TRANSFER COEFFICIENTS

SANTOWAX R - MTR CYCLE 79

Run	Date	Velocity (ft/sec)	% High Boiler Residue	Wall Temp. (°F)	Bulk Temp. (°F)	ΔT (°F)	Heat Flux $q/A \times 10^{-3}$ (Btu/hr-ft^2)	Heat Transfer Coefficient (Btu/hr-°F-ft^2)
SWR-1-1	12/4	13.3	10.5	740	624	116	109	942
SWR-1-2	12/6	13.2	14.5	814	631	183	181	985
SWR-1-3	12/8	13.2	19.5	783	615	168	163	967
SWR-1-4	12/10	13.2	23.5	819	624	195	181	928
SWR-2-1	12/4	8.9	10.5	777	625	152	112	733
SWR-2-2	12/6	8.9	15.0	859	623	236	184	781
SWR-2-3	12/8	8.8	19.5	832	620	212	166	781
SWR-2-4	12/6	10.0	23.5	858	620	238	185	775 (701)*
SWR-3-1	12/4	17.7	10.5	711	625	86	111	1286
SWR-3-2	12/6	17.5	14.5	770	628	142	178	1251
SWR-3-3	12/8	17.3	19.5	731	602	129	159	1231
SWR-3-4	12/10	18.4	23.5	769	626	143	178	1242 (1200)*

*The value in parenthesis was corrected for velocity and was used for plotting the effect of HBR content on heat transfer. The value not in parenthesis is measured value of the heat transfer coefficient at the velocity shown.

TABLE XI

TEST HEATER HEAT TRANSFER COEFFICIENTS

SANTOWAX O - SANTOWAX M - MTR CYCLE 81

Run	Date	Velocity (ft/sec)	% High Boiler Residue	Wall Temp. (°F)	Bulk Temp. (°F)	ΔT (°F)	Heat Flux $q/A \times 10^{-3}$ (Btu/hr-ft^2)	Heat Transfer Coefficient (Btu/hr-°F-ft^2)
SOM-1-1	1/12	8.9	2.5	777	630	147	130	890
SOM-1-2	1/16	9.0	11.0	775	643	132	118	892
SOM-1-3	1/20	8.8	18.3	773	578	195	146	748
SOM-2-1	1/12	13.4	2.5	771	633	138	162	1180
SOM-2-2	1/16	13.4	11.0	771	652	119	142	1188
SOM-2-3	1/20	13.3	18.0	780	593	187	197	1047
SOM-2-4	1/23	13.2	26.5	747	628	119	126.5	1060
SOM-2-5	1/24	13.4	28.0	705	585	120	123	1029
SOM-2-6	1/27	13.1	31.5	683	583	100	96.5	965
SOM-3-1	1/12	17.8	2.5	779	655	124	216	1753
SOM-3-2	1/16	17.5	11.2	787	663	124	196	1582
SOM-3-3	1/20	17.3	18.3	755	595	160	220	1369
SOM-3-4	1/24	17.5	28.5	694	598	96	123.5	1287
SOM-3-5	1/27	17.6	31.5	686	595	91	120.5	1333
SOM-4-1	1/15	9.1	9.0	741	537	204	167	820
SOM-5-1	1/15	13.4	9.0	691	532	159	163.5	1030
SOM-5-2	1/25	13.2	29.5	758	480	278	218	780
SOM-5-3	1/28	13.1	31.5	745	462	283	221	779
SOM-6-1	1/12	20.0	2.7	775	687	88	178	2021
SOM-6-2	1/16	19.6	11.3	773	666	107	189	1762
SOM-6-3	1/20	19.7	18.5	728	593	135	217.5	1606
SOM-6-4	1/24	19.2	28.5	683	596	87	123.5	1428 (1459)*
SOM-6-5	1/27	19.3	31.8	682	596	86	121	1405 (1485)*
SOM-7-1	1/15	17.9	9.0	643	526	117	164.5	1415
SOM-7-2	1/28	17.8	32.7	672	463	209	215.5	1031
SOM-8-1	1/15	18.9	9.0	634	525	109	161	1472
SOM-8-2	1/28	18.6	32.7	665	466	199	209	1054

*The value in parenthesis was corrected for velocity and was used for plotting the effect of HBR content on heat transfer. The value not in parenthesis is the heat transfer coefficient at the velocity shown.

TABLE XIIA

TEST HEATER HEAT TRANSFER COEFFICIENTS

EXTENDED DIPHENYL IRRADIATION- MTR CYCLE 82

Run	Date	Velocity (ft/sec)	% High Boiler Residue	Wall Temp. (°F)	Bulk Temp. (°F)	ΔT (°F)	Heat Flux q/A x 10^{-3} (Btu/hr-ft^2)	Heat Transfer Coefficient (Btu/hr-°F-ft^2)
DIP 3-1-1	2/3	13.2	4.4	631	501	130	145	1118
DIP 3-1-2	2/10	13.0	21.0	706	504	202	223	1101
DIP 3-1-3	2/11	13.0	21.5	646	493	153	165	1079
DIP 3-1-4	2/17	13.1	32.3	668	510	158	169	1070
DIP 3-1-5	2/18	13.1	29.4	710	509	201	222	1101
DIP 3-1-6	2/22	12.9	29.4	705	501	204	222	1091
DIP 3-2-1	2/3	17.3	4.6	589	492	97	135	1390
DIP 3-2-2	2/10	17.5	21.0	662	520	142	218	1526
DIP 3-2-3	2/11	17.4	21.6	615	502	113	166	1474
DIP 3-2-4	2/17	17.2	32.5	625	499	126	167	1327
DIP 3-2-5	2/18	17.2	29.4	661	503	158	217	1372
DIP 3-2-6	2/22	17.2	29.4	651	495	156	218	1394
DIP 3-3-1	2/3	20.4	4.7	577	495	82	134	1620
DIP 3-3-2	2/10	19.8	21.0	645	518	127	217	1710
DIP 3-3-3	2/11	19.9	21.7	600	498	102	165	1626
DIP 3-3-4	2/17	19.5	32.6	610	497	113	168	1499
DIP 3-3-5	2/22	19.8	28.9	626	498	128	216	1681
DIP 3-4-1	2/3	9.1	4.5	674	513	161	144	892
DIP 3-4-2	2/10	8.9	21.1	744	522	222	225	1013
DIP 3-4-3	2/11	8.5	21.5	700	498	202	166	823
DIP 3-4-4	2/17	8.7	32.4	701	511	190	172	906
DIP 3-4-5	2/18	8.5	29.4	738	514	224	225	1004
DIP 3-4-6	2/22	8.4	29.4	722	505	217	223	1028
DIP 3-5-1	2/3	13.4	5.0	767	659	108	146	1353
DIP 3-5-2	2/7	13.3	15.2	766	640	126	179	1420
DIP 3-5-3	2/7	13.2	15.8	767	642	125	185	1480
DIP 3-5-4	2/11	13.1	22.0	782	651	131	177	1355
DIP 3-6-1	2/3	17.8	5.0	741	654	87	144	1646
DIP 3-6-2	2/7	17.5	15.4	749	645	104	178	1702
DIP 3-6-3	2/7	17.5	15.9	753	648	105	185	1762
DIP 3-6-4	2/11	17.3	22.0	752	650	102	176	1727
DIP 3-6-5	2/14	17.2	26.0	741	634	107	175	1636
DIP 3-6-6	2/16	17.2	29.0	737	628	109	175	1602
DIP 3-7-1	2/4	20.7	5.3	728	650	78	146	1881
DIP 3-7-2	2/7	20.5	16.0	752	654	98	187	1915
DIP 3-7-3	2/11	20.5	22.0	743	653	90	175	1940
DIP 3-7-4	2/14	20.2	26.0	721	630	91	174	1917
DIP 3-7-5	2/16	20.2	29.0	722	628	94	174	1851

TABLE XIIB

TEST HEATER HEAT TRANSFER COEFFICIENTS

EXTENDED DIPHENYL IRRADIATION - MTR CYCLES 83 AND 84

Run	Date	Velocity (ft/sec)	% High Boiler Residue	Wall Temp. (°F)	Bulk Temp. (°F)	T (°F)	Heat Flux $q/A \times 10^{-3}$ (Btu/hr-ft^2)	Heat Transfer Coefficient (Btu/hr-°F-ft^2)
DIP 3-8-1	3/2	12.8	32.7	649	478	171	170	996
DIP 3-8-2	3/2	13.2	32.7	680	525	155	170	1085
DIP 3-8-3	3/4	13.2	32.6	684	521	163	172	1059
DIP 3-8-4	3/7	12.8	36.0	692	519	173	171	992
DIP 3-8-5	3/10	12.6	35.6	706	526	180	177	985
DIP 3-8-6	3/11	12.7	33.6	707	461	246	223	904
DIP 3-8-7	3/14	12.7	33.6	703	492	211	213	1011
DIP 3-8-8	3/21	12.8	35.9	686	511	175	171	978
DIP 3-8-9	3/23	12.8	35.1	718	492	226	224	990
DIP 3-8-10	3/30	12.6	38.8	666	501	165	171	1040
DIP 3-9-1	2/28	17.0	33.5	633	468	165	217	1316
DIP 3-9-2	3/2	17.1	32.7	610	483	127	168	1317
DIP 3-9-3	3/4	17.4	32.6	658	545	113	169	1496
DIP 3-9-4	3/7	17.1	36.0	645	519	126	168	1333
DIP 3-9-5	3/10	17.2	35.6	657	527	130	169	1297
DIP 3-9-6	3/21	17.1	36.0	638	504	134	168	1251
DIP 3-9-7	3/30	16.9	39.8	623	500	123	167	1357
DIP 3-10-1	3/2	19.5	32.2	596	483	113	167	1480
DIP 3-10-2	3/7	19.5	34.9	631	518	113	169	1502
DIP 3-10-3	3/10	19.5	35.7	642	528	114	168	1473
DIP 3-10-4	3/21	19.2	36.1	624	506	118	167	1426
DIP 3-10-5	3/30	18.1	38.9	621	503	118	167	1407
DIP 3-11-1	3/2	8.6	32.1	715	483	232	173	747
DIP 3-11-2	3/21	8.1	36.2	742	519	223	175	786
DIP 3-11-3	3/30	8.4	38.8	697	500	197	171	867
DIP 3-12-1	2/24	13.3	31.0	752	610	142	176	1247
DIP 3-12-2	3/17	13.2	35.9	740	599	141	175	1244
DIP 3-12-3	3/19	12.9	38.2	757	606	151	176	1170
DIP 3-12-4	3/22	13.1	37.5	732	582	150	174	1164
DIP 3-12-5	3/25	13.0	36.4	737	585	152	175	1154
DIP 3-12-6	3/27	13.0	37.0	748	623	125	176	1410
DIP 3-12-7	3/29	12.7	38.0	763	627	136	177	1305
DIP 3-13-1	2/24	17.9	31.0	726	625	101	173	1708
DIP 3-13-2	3/2	17.5	32.2	684	574	110	171	1552
DIP 3-13-3	3/17	17.2	36.5	709	593	116	174	1493
DIP 3-13-4	3/19	17.2	38.4	724	607	117	174	1490
DIP 3-13-5	3/22	16.9	37.6	707	584	123	173	1412
DIP 3-13-6	3/25	17.0	37.0	712	590	122	173	1412
DIP 3-13-7	3/27	17.1	37.1	737	629	108	175	1612
DIP 3-13-8	3/29	17.0	38.3	746	625	121	176	1442
DIP 3-14-1	3/2	20.3	32.3	678	581	97	170	1749
DIP 3-14-2	3/4	19.6	32.7	651	551	100	168	1683
DIP 3-14-3	3/17	19.5	35.9	693	591	102	171	1678
DIP 3-14-4	3/19	19.8	38.4	704	602	102	173	1703
DIP 3-14-5	3/22	19.3	37.7	691	582	109	171	1567
DIP 3-14-6	3/25	19.4	36.4	696	590	106	171	1618
DIP 3-14-7	3/29	19.5	38.3	723	622	101	174	1727

temperatures of 500 and 600°F to 650°F. The coefficients were plotted as a function of HBR with bulk temperature and fluid velocity as a parameter. A least-squares fit of a straight line appeared adequate to represent the data. Figures 17 through 21 present the experimentally determined heat transfer coefficients as a function of HBR content. The standard deviation of the data from the straight line fit of the points varies from approximately 4 to 8 percent. Only those sets of data containing more than four points and having a change in HBR content of from 15 to 20 percent were plotted, so that evaluation of the effect of coolant decomposition could be made with more certainty.

The decrease in the heat transfer coefficients as presented in Figs. 17 through 21 was noted to be approximately 15 to 20 percent for a 30 percent increase in HBR content. The decrease noted is what might be expected from the measured increase in viscosity. Viscosity data are presented in Figs. 28 through 31.

It is felt that this decrease noted is real; however, in analyzing the data, several additional points should be considered:

1) Allowance must be made for temperature effects on the physical properties when comparing measurements at different bulk temperatures but at the same velocity. It is estimated from the general polyphenyl relation, $Nu = 0.015 Re^{0.85} Pr^{0.3}$,[12] the measured physical properties, and the estimated thermal conductivity and specific heat values presented in Section D 2 that a 50°F difference in bulk temperatures would be equivalent to an approximate 5 percent change in the heat transfer coefficient.

2) The number of measurements made at any one concentration of HBR was limited, and the curves presented put a great deal of emphasis on single points.

3) The measurements of heat transfer for the Santowax O - Santowax M and the extended diphenyl irradiation are approximately 10 percent higher than those measured for the single-cycle diphenyl and the Santowax R irradiations. The test heater was replaced at the beginning of the Santowax O - Santowax M irradiation due to burnout caused by a loss-of-flow accident. Although no explanation can be advanced to explain the discrepancy, a difference of 10 percent in heat transfer measurements is well within the precision of the experiment.

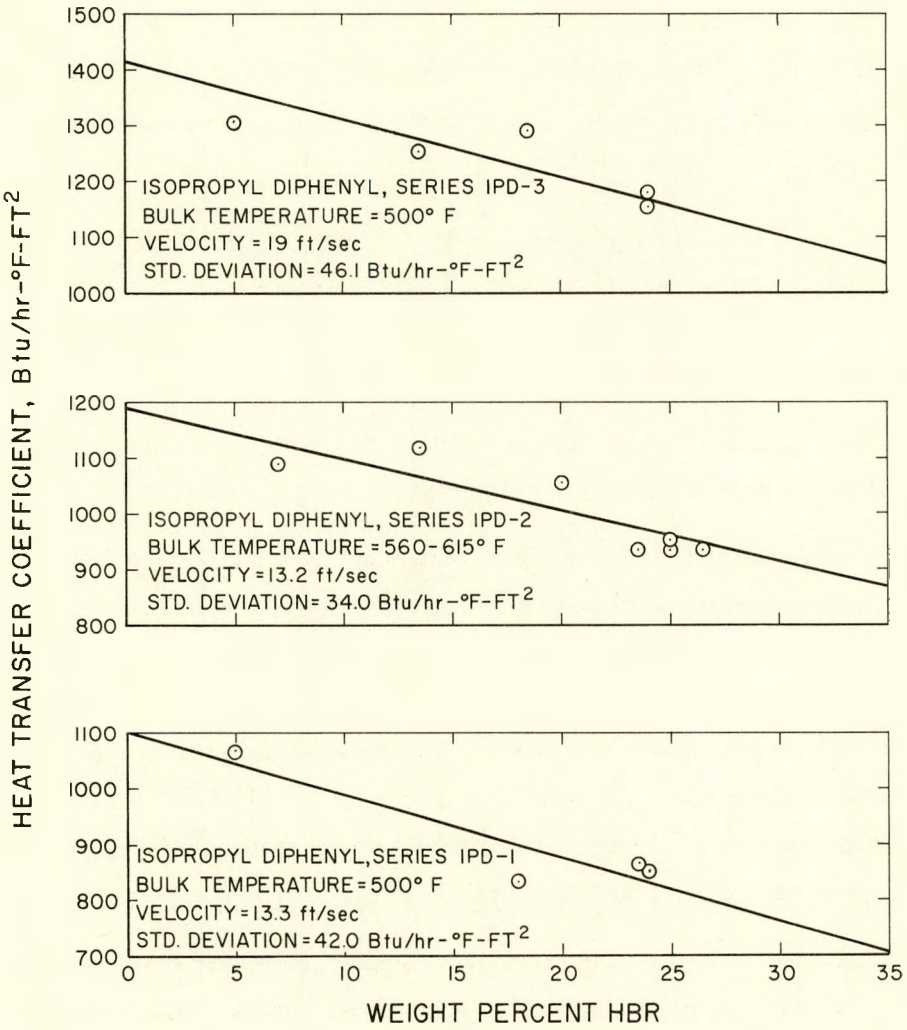

Fig. 17. Heat Transfer vs HBR Content for Isopropyl Diphenyl - MTR Cycle 77

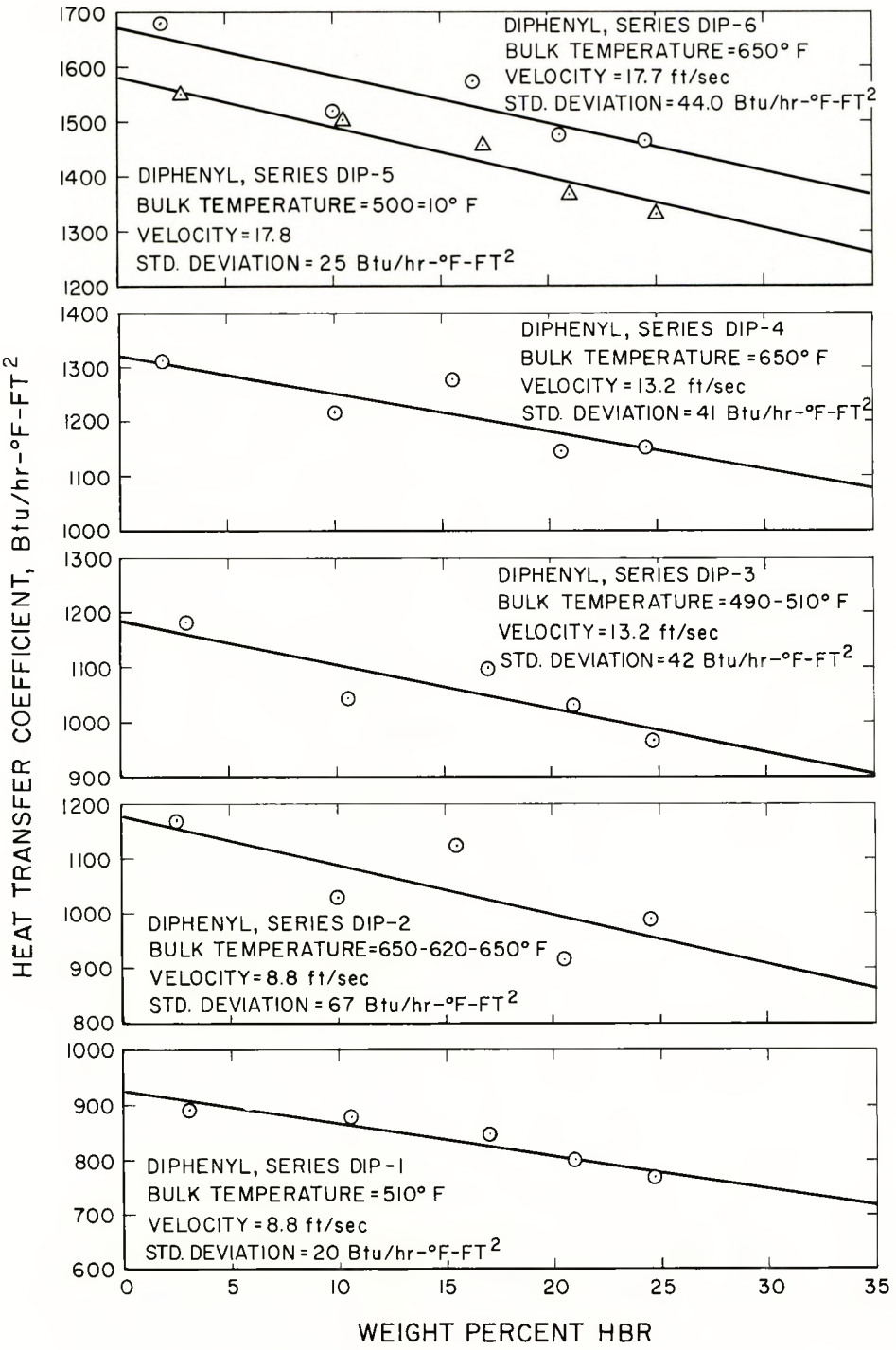

Fig. 18. Heat Transfer vs HBR Content for Diphenyl Irradiation - MTR Cycle 78

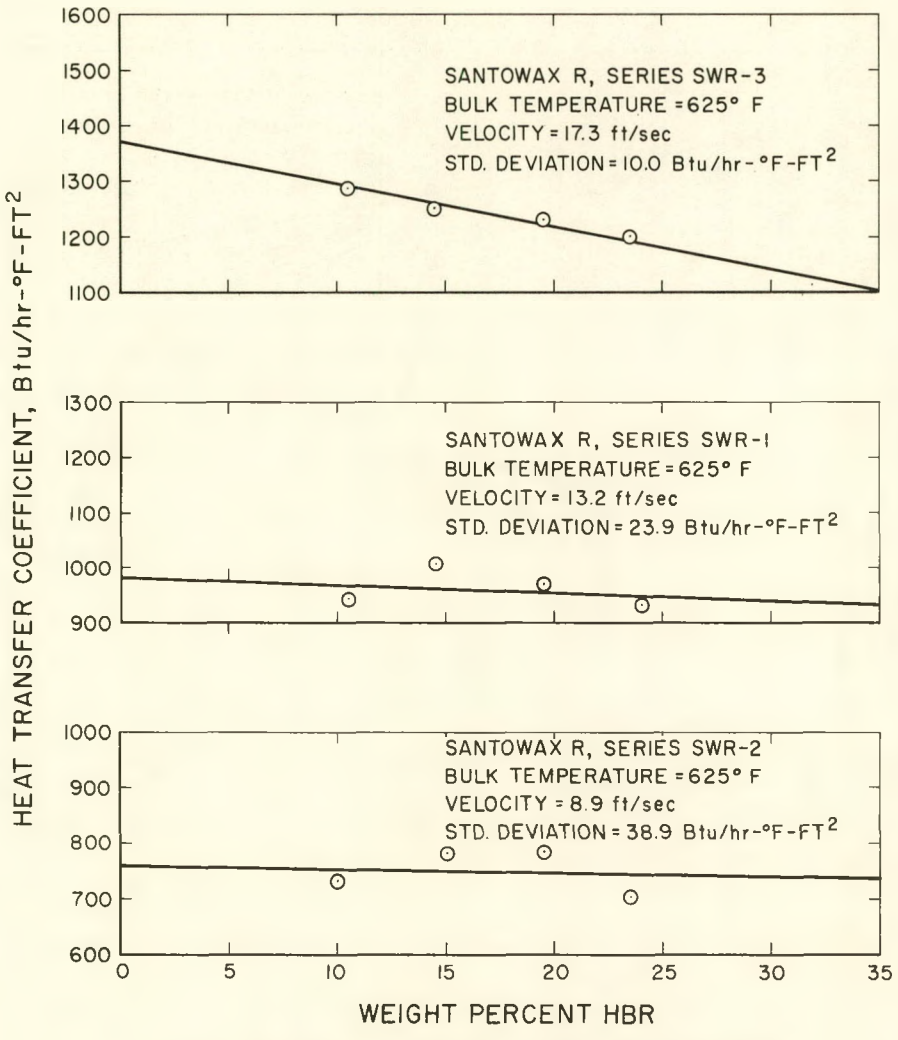

Fig. 19. Heat Transfer vs HBR Content for Santowax R - MTR Cycle 79

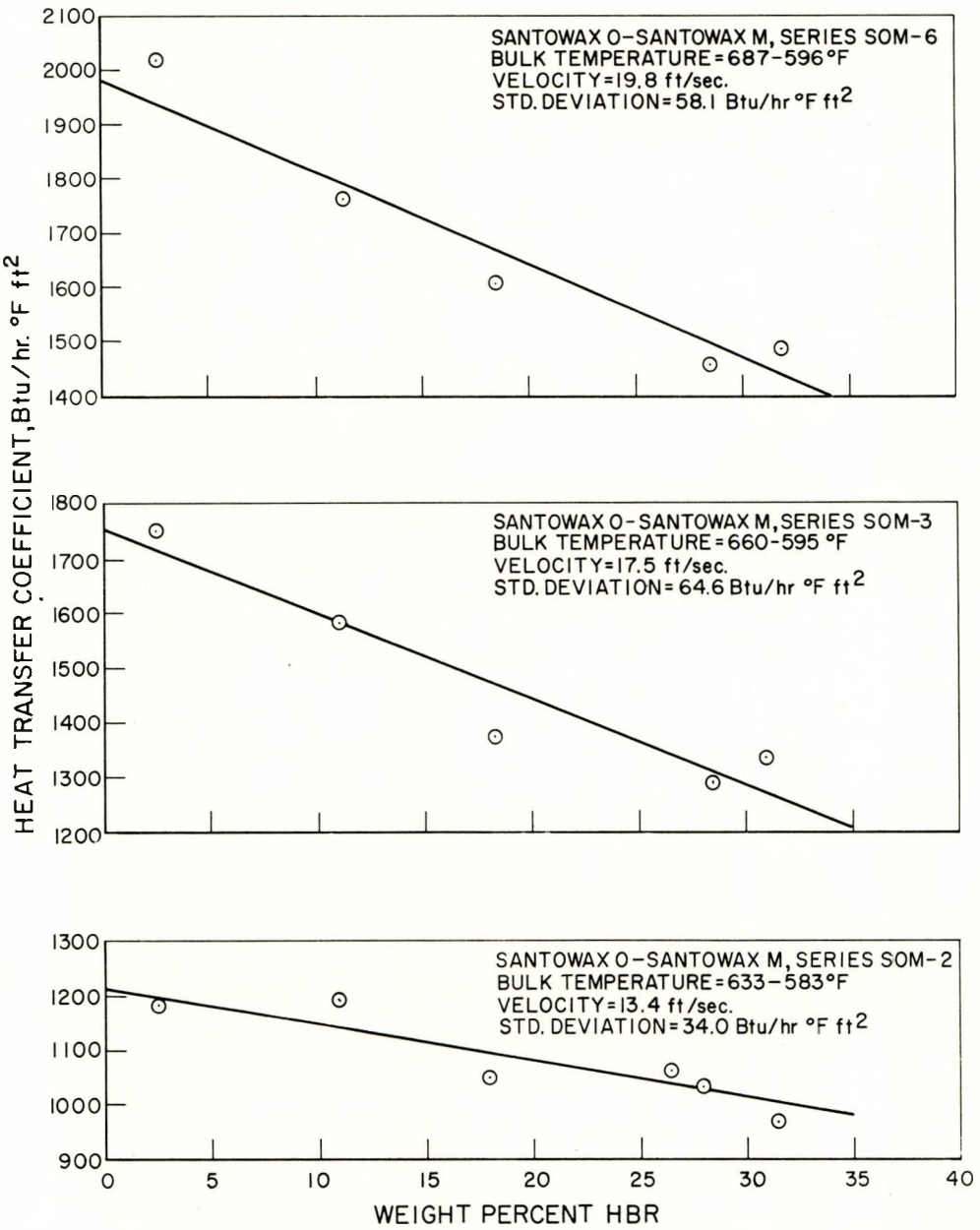

Fig. 20. Heat Transfer vs HBR Content for Santowax — Santowax M - MTR Cycle 81

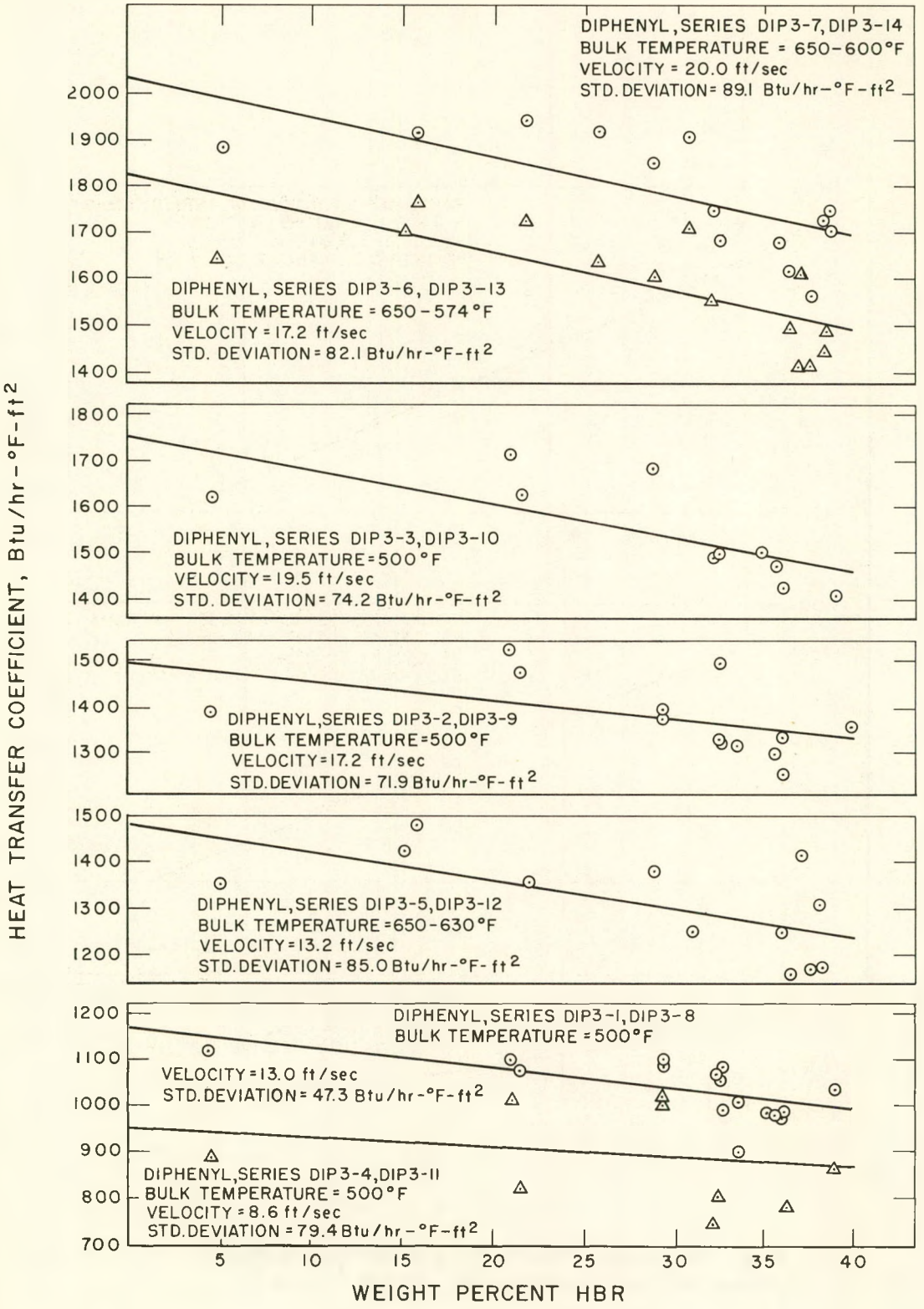

Fig. 21. Heat Transfer vs HBR Content for Extended Diphenyl Irradiation - MTR Cycles 82, 83, and 84

4) The small decreases noted in the Santowax R coefficients are not considered to be significant in the light of the small number of measurements made.

During the second and third MTR cycles (Cycles 83 and 84), heat transfer determinations were made at regular intervals while the HBR content was maintained at an approximate concentration of 33 to 35 percent by weight by replacement of portions of the damaged coolant with unirradiated coolant. The period of time covered was 6 weeks. No additional decrease in the heat transfer coefficient was noted during this period of time, indicating that there was no fouling occurring at the test heater. The values of the heat transfer coefficients measured during this period are presented in Table XII B for the second and third cycles. The coefficients in the last column do not vary more than ± 5 percent from some mean value.

Assuming that the thermocouple accuracy is ± 0.5 percent, the maximum possible error in Δt is estimated to be approximately ± 7 percent. The maximum possible error in the heat flux, estimated from the accuracy of the electrical instruments, is ± 2 percent. Allowing for a 1 percent variation in the test heater tube dimensions, the absolute accuracy of the coefficients measured at the test heater is ± 10 percent.

In summing up the data presented, it should be noted that the coefficients are within ± 10 percent of a constant value, independent of HBR content.

b) Uranium Heater

A uranium heater was used to simulate heat transfer in a reactor core by exposing the circulating polyphenyl to both radiation and high temperature. Thermocouples provided temperature information for heat transfer coefficient calculations.

Experimental heat transfer coefficients were obtained for isopropyldiphenyl, diphenyl, Santowax R, and Santowax O - Santowax M under conditions as nearly identical as possible to those experienced in the resistance heater. The detailed results are listed in Tables XIII to XVII where column 13 lists the corrected heat transfer coefficients and column 14 lists the predicted heat transfer coefficients using the resistance heater results normalized for the difference in the hydraulic diameter between the two heaters.

TABLE XIII

URANIUM HEATER HEAT TRANSFER COEFFICIENTS

ISOPROPYL DIPHENYL - MTR CYCLE 77

1 Run	2 Date	3 (Mwh)$_o$	4 Velocity (ft/sec)	5 % High-Boiler Residue	6 Wall Temp. Measured (°F)	7 Wall Temp. Corrected (°F)	8 Bulk Temp. (°F)	9 ΔT (°F)	10 Heat Flux-Thermal Neutron q/A (Btu/hr-ft^2)	11 Inside Uranium Temp. (°F)	12 Heat Flux-Thermo-Couples q/A (Btu/hr-ft^2)	13 Uranium Heater Heat Transfer Coefficient Measured (Btu/hr-°F-ft^2)	14 *Heat Transfer Coefficient Predicted from Test Heater (Btu/hr-°F-ft^2)
IPD-1-1	10/22	1,588	14.2	5.0	638	615	506	109	122,000	818	149,000	1,367	1,362
IPD-1-2	10/25	4,684	13.8	18.0	642	617	509	108	128,000	817	145,000	1,345	1,068
IPD-1-3	10/28	6,880	14.0	23.5	640	618	504	114	113,000	811	141,000	1,235	1,103
IPD-1-4	11/2	10,604	13.6	24.0	658	635	513	122	123,000	841	151,000	1,240	1,084
IPD-2-1	10/22	1,628	14.2	7.0	701	678	575	103	122,000	878	146,000	1,415	1,391
IPD-2-2	10/24	3,324	13.8	13.5	682	655	562	93	141,000	865	151,000	1,625	1,407
IPD-2-3	10/27	5,940	14.0	20.0	687	665	564	101	117,000	859	142,000	1,405	1,348
IPD-2-4	10/29	7,884	14.1	25.0	729	706	603	103	121,000	910	150,000	1,455	1,196
IPD-2-5	10/31	9,168	13.8	26.5	716	692	588	104	124,000	896	149,000	1,430	1,196
IPD-2-6	11/2	10,252	13.9	23.5	713	690	582	108	122,000	891	147,000	1,360	1,196
IPD-2-7	11/4	12,152	13.9	25.0	738	715	620	95	122,000	881	118,000	1,240	1,219
IPD-3-1	10/22	1,668	23.0	5.0	587	564	496	68	122,000	773	154,000	2,265	1,882
IPD-3-2	10/24	3,444	19.9	13.5	594	567	508	59	140,000	782	155,000	2,630	1,606
IPD-3-3	10/26	4,304	19.8	18.5	601	576	507	69	128,000	778	146,000	2,120	1,650
IPD-3-4	10/28	7,000	19.7	24.0	597	575	502	73	116,000	776	148,000	2,030	1,476
IPD-3-5	11/2	10,512	18.3	24.0	618	595	510	85	122,000	800	150,000	1,765	1,407
IPD-4-1	10/29	7,912	19.5	25.0	691	668	601	67	122,000	889	164,000	2,450	1,594
IPD-4-2	10/31	9,238	19.6	26.5	672	649	579	70	122,000	855	151,000	2,335	1,635
IPD-5-1	10/25	4,264	9.4	18.5	691	668	511	157	122,000	860	140,000	891	865
IPD-5-2	10/28	6,950	9.1	24.0	697	675	518	157	115,000	860	135,000	860	865
IPD-5-3	11/2	10,700	9.3	24.3	711	688	521	167	122,000	886	145,000	858	847
IPD-6-1	10/24	3,554	8.6	13.5	735	712	565	147	122,000	908	143,000	973	914
IPD-6-2	10/27	6,040	9.3	21.5	732	710	560	150	117,000	892	132,000	880	1,016
IPD-6-3	10/29	7,972	9.5	25.0	765	742	600	142	122,000	942	146,000	1,030	859
IPD-6-4	10/31	9,208	9.5	26.5	752	729	588	141	122,000	927	145,000	1,030	753
IPD-6-5	11/2	10,316	9.3	23.5	752	729	581	148	122,000	925	143,000	967	963

*Normalized to annular flow channel.

TABLE XIV

URANIUM HEATER HEAT TRANSFER COEFFICIENTS

DIPHENYL - MTR CYCLE 78

1 Run	2 Date	3 $(Mwh)_o$	4 Velocity (ft/sec)	5 % High Boiler Residue	6 Wall Temp. Measured (°F)	7 Wall Temp. Corrected (°F)	8 Bulk Temp. (°F)	9 ΔT (°F)	10 Heat Flux-Thermal Neutron $q/A \times 10^{-3}_2$ (Btu/hr-ft^2)	11 Inside Uranium Temp. (°F)	12 Heat Flux Thermo-Couples $q/A \times 10^{-3}_2$ (Btu/hr-ft^2)	13 Heat Transfer Coefficient Measured (Btu/hr-°F-ft^2)	14 *Heat Transfer Coefficient Predicted from Test Heater (Btu/hr-°F-ft^2)
DIP-1-1	11/10	305	8.7	3.0	674	680	525	155	159.6	905	177.8	1,148	1,120
DIP-1-2	11/12	2,468	9.2	10.5	668	675	516	159	164.6	894	174.0	1,095	1,140
DIP-1-3	11/15	4,480	9.4	17.0	675	682	530	152	161.3	897	170.9	1,125	1,120
DIP-1-4	11/16	5,864	9.3	21.0	673	680	527	153	161.3	868	150.2	981	1,032
DIP-1-5	11/18	7,472	9.2	24.7	692	698	522	176	175.3	928	181.7	1,033	1,014
DIP-1-6	11/21	9,363	9.2	28.7	647	653	522	133	172.5	874	177.1	1,352	995
DIP-1-7	11/23	11,401	9.2	35.5	681	690	526	163	167.5	906	173.3	1,063	975
DIP-1-8	11/24	12,545	9.1	34.4	629	637	481	156	163.4	846	165.6	1,061	966
DIP-2-1	11/10	244	9.4	2.5	756	764	653	111	159.3	962	158.6	1,429	1,530
DIP-2-2	11/12	2,328	9.3	10.0	730	738	595	143	166.2	933	156.3	1,093	1,363
DIP-2-3	11/14	3,893	9.2	15.5	740	748	620	128	164.2	943	156.3	1,221	1,470
DIP-2-4	11/16	5,684	9.3	20.5	767	776	545	131	160.1	967	154.0	1,176	1,220
DIP-2-5	11/19	7,400	9.3	24.5	783	790	552	138	174.8	1,004	170.2	1,233	1,300
DIP-2-6	11/21	9,274	9.1	28.5	753	762	628	134	172.8	973	169.4	1,264	1,181
DIP-2-7	11/23	11,447	9.2	32.5	772	780	641	139	166.7	985	164.0	1,180	1,134
DIP-2-8	11/25	12,632	9.1	34.5	725	732	601	131	162.8	935	161.7	1,234	1,114
DIP-3-1	11/10	283	14.5	3.0	590	595	491	104	159.3	810	169.4	1,629	1,610
DIP-3-2	11/12	2,447	14.4	10.5	627	634	505	129	164.6	826	156.3	1,212	1,410
DIP-3-3	11/15	4,460	13.9	17.0	628	634	517	117	161.7	844	166.3	1,422	1,440
DIP-3-4	11/16	5,844	13.7	21.0	574	581	492	89	161.7	786	163.2	1,834	1,350
DIP-3-5	11/19	7,452	13.7	24.7	645	650	516	134	175.3	883	183.3	1,367	1,258
DIP-3-6	11/21	9,348	13.7	28.7	644	650	507	143	172.4	844	154.0	1,077	1,210
DIP-3-7	11/23	11,323	13.5	32.3	629	637	503	134	167.8	863	180.2	1,345	1,158
DIP-3-8	11/24	12,505	13.5	34.4	615	621	509	112	163.8	834	168.6	1,506	1,133
DIP-4-1	11/10	217	14.0	2.0	737	748	650	98	158.8	945	160.2	1,632	1,720
DIP-4-2	11/12	2,308	14.1	10.0	712	720	614	106	166.3	901	145.5	1,373	1,600
DIP-4-3	11/14	3,867	14.0	15.5	714	722	624	98	164.6	922	160.2	1,639	1,680
DIP-4-4	11/16	5,674	14.0	20.5	747	755	655	100	160.1	950	156.3	1,563	1,501
DIP-4-5	11/19	7,372	13.9	24.5	780	788	564	124	174.5	992	160.2	1,292	1,520
DIP-4-6	11/21	9,232	13.8	28.5	729	738	621	117	172.8	955	181.7	1,553	1,477

*Normalized to annular flow channel

TABLE XIV (Continued)

URANIUM HEATER HEAT TRANSFER COEFFICIENTS

DIPHENYL - MTR CYCLE 78

1 Run	2 Date	3 $(Mwh)_o$	4 Velocity (ft/sec)	5 % High Boiler Residue	6 Wall Temp. Measured (°F)	7 Wall Temp. Corrected (°F)	8 Bulk Temp. (°F)	9 ΔT (°F)	10 Heat Flux-Thermal Neutron $q/A \times 10_2^{-3}$ (Btu/hr-ft^2)	11 Inside Uranium Temp. (°F)	12 Heat Flux Thermo-Couples $q/A \times 10_2^{-3}$ (Btu/hr-ft^2)	13 Heat Transfer Coefficient Measured (Btu/hr-°F-ft^2)	14 *Heat Transfer Coefficient Predicted from Test Heater (Btu/hr-°F-ft^2)
DIP-4-7	11/23	11,460	13.7	32.5	736	743	624	119	166.7	954	167.9	1,411	1,400
DIP-4-8	11/24	12,592	13.7	34.5	707	714	600	114	163.0	916	161.0	1,412	1,382
DIP-5-1	11/10	312	18.7	3.0	714	722	651	71	159.3	922	160.2	2,256	2,017
DIP-5-2	11/12	2,488	18.7	10.5	592	597	524	73	164.2	802	161.7	2,215	1,970
DIP-5-3	11/15	4,420	18.7	17.0	593	598	513	85	162.1	807	164.8	1,939	1,910
DIP-5-4	11/16	5,884	18.2	21.0	574	581	492	89	161.7	786	163.2	1,834	1,750
DIP-5-5	11/19	7,500	18.2	25.0	594	600	497	103	175.7	835	185.6	1,802	1,700
DIP-5-6	11/21	9,388	16.7	28.8	605	611	512	99	172.0	837	178.6	1,804	1,647
DIP-5-7	11/23	11,305	18.0	32.3	586	592	487	105	167.9	819	179.4	1,709	1,559
DIP-5-8	11/24	12,485	15.8	34.3	607	613	507	106	163.8	826	170.2	1,605	1,537
DIP-6-1	11/10	228	18.8	2.0	714	722	651	71	159.3	922	160.2	2,256	2,200
DIP-6-2	11/12	2,346	18.5	10.0	668	675	596	79	165.4	874	158.6	2,008	2,000
DIP-6-3	11/15	4,318	18.6	16.5	700	708	629	79	163.0	909	160.9	2,037	2,050
DIP-6-4	11/16	5,693	18.5	20.5	712	720	642	78	160.5	913	154.8	1,984	1,930
DIP-6-5	11/19	7,412	18.5	24.5	750	757	666	91	175.1	969	168.6	1,853	1,910
DIP-6-6	11/21	9,308	18.2	28.7	733	741	652	89	172.8	954	170.2	1,911	1,818
DIP-6-7	11/23	11,560	18.2	32.7	731	737	648	89	166.3	948	167.1	1,877	1,779
DIP-6-8	11/24	12,578	17.9	34.5	684	690	605	85	163.0	896	163.2	1,920	1,757

*Normalized to annular flow channel

TABLE XV

URANIUM HEATER HEAT TRANSFER COEFFICIENTS

SANTOWAX R - MTR CYCLE 79

1 Run	2 Date	3 (Mwh) o	4 Velocity (ft/sec)	5 % High Boiler Residue	6 Wall Temp. Measured (° F)	7 Wall Temp. Corrected (° F)	8 Bulk Temp. (°F)	9 ΔT (°F)	10 Heat Flux-Thermo-Couples q/A (Btu/hr-ft^2)	11 Inside Uranium Temp. (°F)	12 Heat Flux Thermo-Couples q/A (Btu/hr-ft^2)	13 Uranium Heater Heat Transfer Coefficient Measured (Btu/hr-°F-ft^2)	14 * Heat Transfer Coefficient Predicted from Test Heater (Btu/hr-°F-ft^2)
SWR-1-1	12/4	3,064	13.9	10.5	741	715	622	93	159,000	910	118,200	1,271	1,235
SWR-1-2	12/6	4,565	13.8	14.5	741	716	623	93	156,000	903	113,400	1,225	1,229
SWR-1-3	12/8	6,484	13.7	19.5	731	708	612	96	146,000	888	109,900	1,145	1,220
SWR-1-4	12/10	8,357	13.8	23.5	738	716	617	99	139,000	892	107,800	1,090	1,212
SWR-2-1	12/4	3,084	8.9	10.5	783	758	623	135	158,000	944	112,700	835	933
SWR-2-2	12/6	4,643	8.9	15.0	774	749	617	132	156,000	934	112,000	848	1,003
SWR-2-3	12/8	6,496	8.8	19.5	778	755	616	139	146,000	933	108,500	781	996
SWR-2-4	12/6	8,417	10.5	23.5	769	747	615	132	138,000	916	102,000	773	1,988
SWR-3-1	12/4	3,097	18.6	14.5	710	685	623	62	158,000	879	118,200	1,900	1,630
SWR-3-2	12/6	4,514	18.4	14.5	715	690	625	65	156,000	878	114,100	1,750	1,615
SWR-3-4	12/10	8,334	18.3	23.5	715	690	621	69	139,000	866	107,800	1,562	1,574

*Normalized to Annular Flow Channel

TABLE XVI

URANIUM HEATER HEAT TRANSFER COEFFICIENTS

SANTOWAX O - SANTOWAX M - MTR CYCLE 81

1 Run	2 Date	3 $(Mwh)_o$	4 Velocity (ft/sec)	5 % High Boiler Residue	6 Wall Temp. Measured (°F)	7 Wall Temp. Corrected (°F)	8 Bulk Temp. (°F)	9 ΔT (°F)	10 Heat Flux-Thermal Neutron q/A (Btu/hr-ft^2)	11 Inside Uranium Temp. (°F)	12 Heat Flux-Thermo-Couples q/A (Btu/hr-ft^2)	13 Uranium Heater Heat Transfer Coefficient Measured (Btu/hr-°F-ft^2)	14 *Heat Transfer Coefficient Predicted from Test Heater (Btu/hr-°F-ft^2)
SOM-1-1	1/12	850	9.3	2.5	816	776	638	138	167,897	971	145,700	1,055	1,169
SOM-1-2	1/16	3,745	9.4	11.0	847	803	647	156	181,800	1,010	153,220	982	1,075
SOM-1-3	1/20	6,468	9.2	18.3	871	829	586	143	176,100	1,029	148,520	1,089	998
SOM-2-1	1/12	832	14.1	2.5	770	743	639	104	168,715	928	148,520	1,428	1,530
SOM-2-2	1/16	3,715	14.1	11.0	799	755	656	99	181,000	967	157,970	1,595	1,453
SOM-2-3	1/20	6,398	13.9	18.0	765	721	601	120	177,700	917	142,880	1,191	1,395
SOM-2-5	1/24	10,625	14.0	28.0	768	730	596	134	159,600	908	131,600	982	1,302
SOM-2-6	1/27	12,295	13.7	31.5	774	733	592	141	168,700	922	139,120	986	1,011
SOM-3-1	1/12	867	18.7	2.5	763	731	661	70	167,900	918	145,700	2,081	2,182
SOM-3-2	1/16	3,770	18.4	11.2	778	751	669	82	182,700	952	163,560	2,240	2,022
SOM-3-3	1/20	6,491	18.1	18.3	735	693	601	92	175,300	891	146,600	1,593	1,873
SOM-3-4	1/24	10,758	18.4	28.5	748	705	606	99	159,660	874	118,400	1,669	1,196
SOM-3-5	1/27	12,354	18.5	31.5	753	712	599	113	169,540	885	124,080	1,097	1,613
SOM-4-1	1/15	3,122	19.5	9.0	775	735	551	184	172,000	883	177,660	966	883
SOM-5-1	1/15	3,103	14.1	9.0	707	664	543	121	172,000	924	169,200	1,398	1,285
SOM-6-1	1/12	890	21.0	2.7	789	753	692	61	167,900	945	144,760	2,372	2,560
SOM-6-2	1/16	3,781	20.6	11.3	776	749	673	76	182,700	927	141,950	2,087	2,298
SOM-6-3	1/20	6,533	20.7	18.5	724	681	599	82	174,480	879	145,700	1,777	2,088
SOM-6-4	1/24	10,778	20.1	28.5	732	694	606	88	160,070	875	134,420	1,527	1,792
SOM-6-5	1/27	12,385	20.2	31.5	723	682	599	83	169,540	878	145,700	1,755	1,824
SOM-7-1	1/15	3,075	18.8	9.0	704	662	535	127	171,200	881	166,380	1,320	1,811
SOM-8-1	1/15	3,035	19.8	9.0	700	656	533	123	170,360	878	165,440	1,345	1884

*Normalized to Annular Flow Channel

TABLE XVIIA

URANIUM HEATER HEAT TRANSFER COEFFICIENTS-EXTENDED DIPHENYL IRRADIATION

MTR CYCLE 82

1 Run	2 Date	3 $(Mwh)_o$	4 Velocity (ft/sec)	5 % High-Boiler Residue	6 Wall Temp. Measured (°F)	7 Wall Temp. Corrected (°F)	8 Bulk Temp. (°F)	9 ΔT (°F)	10 Heat Flux-Thermal Neutron $q/A \times 10^{-3}$ (Btu/hr-ft^2)	11 Inside Uranium Temp. (°F)	12 Heat Flux-Thermo-Couples $q/A \times 10^{-3}$ (Btu/hr-ft^2)	13 Heat Transfer Coefficient Measured (Btu/hr-°F-ft^2)	14 *Heat Transfer Coefficient Predicted from Test Heater (Btu/hr-°F-ft^2)
DIP-3-1-1	2/3	1,358	13.9	4.4	615	610	503	107	197	799	189	1,750	1,428
DIP-3-1-3	2/11	8,077	13.6	21.5	635	630	497	133	179	803	173	1,300	1,403
DIP-3-1-4	2/17	14,050	13.7	32.3	651	646	510	136	172	812	166	1,220	1,391
DIP-3-2-1	2/3	1,392	18.2	4.6	583	578	491	87	187	769	180	2,010	1,860
DIP-3-2-3	2/11	8,134	18.3	21.6	609	604	502	102	182	780	176	1,730	1,816
DIP-3-3-1	2/3	1,422	21.7	4.7	571	572	495	76	200	761	195	2,300	2,129
DIP-3-3-3	2/11	8,154	20.9	21.7	597	592	499	93	185	770	178	1,920	2,083
DIP-3-4-1	2/3	1,379	9.5	4.5	659	654	514	140	188	836	182	1,300	1,062
DIP-3-4-3	2/11	8,090	8.9	21.5	687	682	506	176	175	851	169	1,250	1,197
DIP-3-4-4	2/17	14,090	9.1	32.4	694	699	515	134	171	856	165	1,230	1,244
DIP-3-5-1	2/3	1,493	14.1	5.0	756	753	656	97	186	931	179	1,840	1,791
DIP-3-5-2	2/7	4,919	14.0	15.2	744	739	635	104	182	915	176	1,710	1,788
DIP-3-5-3	2/7	5,061	13.8	15.8	747	743	637	106	179	915	172	1,670	2,435
DIP-3-5-4	2/11	8,254	13.7	22.0	767	763	652	111	169	926	163	1,470	1,788
DIP-3-5-5	2/16	12,610	13.8	28.9	746	742	624	118	166	902	160	1,450	1,792
DIP-3-6-1	2/3	1,534	18.7	5.0	727	723	655	68	185	901	178	2,500	2,186
DIP-3-6-2	2/7	4,946	18.4	15.4	727	723	640	83	175	892	169	2,040	2,158
DIP-3-6-3	2/7	5,082	18.4	15.9	730	726	643	83	171	892	166	2,000	2,157
DIP-3-6-4	2/11	8,274	18.2	22.0	742	738	647	91	171	904	166	1,830	2,269
DIP-3-6-5	2/14	10,750	18.0	26.0	728	724	629	95	166	885	161	1,760	2,130
DIP-3-6-6	2/16	12,630	18.0	29.0	725	723	623	100	160	878	156	1,560	2,122
DIP-3-7-1	2/4	1,634	21.7	5.3	716	713	645	68	184	890	177	2,580	2,436
DIP-3-7-2	2/7	5,102	21.5	16.0	725	722	650	72	173	888	167	2,310	2,433
DIP-3-7-3	2/11	8,294	21.5	22.0	735	732	652	80	171	897	165	2,080	2,435
DIP-3-7-4	2/14	10,770	21.2	26.0	717	714	627	87	167	875	161	1,850	2,432
DIP-3-7-5	2/16	12,650	21.2	29.0	715	712	623	89	162	868	156	1,750	2,380

*Normalized to annular flow channel.

TABLE XVIIB

URANIUM HEATER HEAT TRANSFER COEFFICIENTS-EXTENDED DIPHENYL IRRADIATION

MTR CYCLES 83 AND 84

1 Run	2 Date	3 $(Mwh)_o$	4 Velocity (ft/sec)	5 %High-Boiler Residue	6 Wall Temp. Measured (°F)	7 Wall Temp. Corrected (°F)	8 Bulk Temp. (°F)	9 ΔT (°F)	10 Heat Flux-Thermal Neutron $q/A \times 10^{-3}$ (Btu/hr-ft^2)	11 Inside Uranium Temp. (°F)	12 Heat Flux-Thermo-Couples $q/A \times 10^{-3}$ (Btu/hr-ft^2)	13 Heat Transfer Coefficient Measured (Btu/hr-°F-ft^2)	14 *Heat Transfer Coefficient Predicted from Test Heater (Btu/hr-°F-ft^2)
DIP-3-8-1	3/2	20,603	13.4	32.7	656	653	479	174	151	798	142	820	1,300
DIP-3-8-2	3/2	20,706	13.9	32.7	682	680	524	156	153	825	143	920	1,420
DIP-3-8-3	3/4	22,503	13.8	32.6	678	675	518	157	159	827	149	950	1,390
DIP-3-8-4	3/7	24,173	13.4	36.0	687	685	521	164	149	827	140	850	1,299
DIP-3-8-5	3/10	27,901	13.2	35.6	700	696	539	157	132	823	124	790	1,298
DIP-3-9-2	3/2	20,653	17.9	32.7	615	613	480	133	181	775	170	1,280	1,730
DIP-3-9-3	3/4	22,533	18.3	32.6	663	660	538	122	179	823	168	1,380	1,950
DIP-3-9-4	3/7	24,198	17.9	36.0	647	645	518	127	187	802	175	1,380	1,750
DIP-3-9-5	3/10	27,928	18.0	25.6	659	656	528	128	156	806	147	1,150	1,700
DIP-3-9-6	3/21	33,518	17.9	36.0	616	613	510	103	165	771	155	1,500	1,640
DIP-3-10-1	3/2	20,663	20.5	32.2	603	600	480	120	172	764	161	1,340	1,940
DIP-3-10-2	3/7	24,216	20.5	34.9	633	630	516	114	170	791	160	1,410	1,970
DIP-3-10-3	3/10	27,995	20.5	35.7	648	645	527	118	162	799	152	1,290	1,930
DIP-3-10-4	3/21	33,538	20.1	36.1	648	642	505	137	133	736	125	920	1,860
DIP-3-11-1	3/2	20,630	9.0	32.1	656	654	479	175	192	846	180	1,030	980
DIP-3-12-1	2/24	15,334	14.0	31.0	724	720	611	109	155	868	146	1,340	1,630
DIP-3-12-2	3/17	29,758	13.8	35.9	728	724	599	125	160	878	150	1,200	1,620
DIP-3-12-3	3/19	31,362	13.5	38.2	727	723	602	121	175	891	164	1,350	1,530
DIP-3-12-4	3/22	34,278	13.7	37.5	709	706	581	125	165	864	155	1,240	1,520
DIP-3-13-1	2/24	15,351	18.8	31.0	706	703	610	93	190	864	178	1,210	2,100
DIP-3-13-2	3/2	20,733	18.4	32.2	685	682	570	112	162	837	152	1,350	2,050
DIP-3-13-3	3/17	29,778	18.1	36.5	696	693	593	100	165	851	155	1,550	1,950
DIP-3-13-4	3/19	31,385	18.0	38.4	694	691	606	85	177	861	167	1,970	1,940
DIP-3-13-5	3/22	34,308	17.7	37.6	682	679	582	97	174	845	163	1,690	1,910
DIP-3-13-7	3/27	37,825	17.9	37.1	712	709	625	84	193	893	181	2,150	1,860
DIP-3-13-8	3/29	39,598	17.8	38.3	707	704	623	81	193	888	180	2,220	1,890
DIP-3-14-1	3/2	20,743	21.3	32.3	663	660	576	84	166	839	156	1,860	2,300
DIP-3-14-2	3/4	22,550	20.6	32.7	657	654	544	110	175	821	164	1,490	2,200
DIP-3-14-3	3/17	29,798	20.5	35.9	685	682	589	93	171	845	160	1,720	2,190
DIP-3-14-4	3/19	31,408	20.8	38.4	686	683	599	84	180	855	169	2,020	2,240
DIP-3-14-5	3/22	34,328	20.2	37.7	672	669	580	89	176	837	165	1,860	2,060
DIP-3-14-7	3/29	39,615	20.4	38.3	696	693	622	71	204	881	191	2,680	2,270

*Normalized to annular flow channel.

The heat flux at the uranium heater was determined by two independent methods. The first method entailed the use of cobalt-aluminum wire monitors. The monitors gave the neutron flux integrated over the entire cycle and over the length of the in-pile section. From the flux distribution around the pipe, the attenuated flux at the heater was calculated by trial and error solution on the IBM 704, utilizing diffusion and transport theory. The thermal neutron flux at any time during an irradiation was determined by multiplying the average integrated flux by the ratio of the radial temperature drop in the uranium heater at the time in question to the average temperature drop in the uranium heater throughout the cycle.

The heat flux was also calculated from the radial temperature difference between the inside of the uranium heater and the outside wall of the heater, considering the uranium as a volumetric heat source and the NaK and stainless steel as ordinary thermal resistances, the values of which were determined by their thermal conductivities and geometries. Appendix III gives the detailed equations for computing the heat transfer coefficients at the uranium heater.

Preliminary analysis of heat flux determinations using the methods outlined above indicated that the methods did not give the same result. The heat flux as determined from the temperature drop was lower than that determined by using the monitors, thus indicating that the measured wall temperatures were too high. The source of error in calculating the heat flux and the heat transfer coefficient arises from the use of thermocouples imbedded in the wall of the heater. It is improbable that these thermocouples read the true interface temperatures between the hydrocarbon and the stainless-steel wall of the heater. Location under the wall would cause the thermocouple to read too high and would consequently cause a low radial temperature drop and a high film temperature drop. This double error would result in calculations showing excessively low heat flux and low heat transfer coefficients.

Originally it was thought that the thermocouple was located at the hydrocarbon-steel interface and read too high due to its being imbedded in silver solder. The higher conductivity of the silver solder would offer a heat flow path of lower resistance, with the net result that the thermocouple would read too high. In an effort to determine the effect of silver solder on the temperature relationship

of the wall thermocouples, an analog solution using the IBM 704 was initiated. The approach to the problem was to use a modified form of the numerical method of Dusinberre[13] for the two-dimensional-transient-conduction case with a source term. The analog solution indicated that the higher conductivity of the silver solder did not have any significant effect on the temperature at the point of measurement for the heat flow rates considered. Thus, the only other conclusion that could be reached was that the thermocouples were located below the surface of the heater wall.

To provide an adequate means of comparing in-pile results with external heater results in order to detect if any adverse effects occurred when the material was subjected to both radiation and high temperature, a procedure was initiated to determine the exact location of the thermocouple under the wall. Standard equations were used to determine depth which expressed the temperature drop through a series of resistances by using the initial value of heat flux as determined by fission heating, based on neutron flux measurements and the values of the heat transfer coefficient for unirradiated material. Once the depth was known, the corrected value of the wall temperature could be determined by using standard conduction equations. Using the corrected value of wall temperature, the bulk fluid temperature, and the value of heat flux as determined by radial temperature drops, the local heat transfer coefficient was determined.

The measured heat transfer coefficients corrected for the position of the wall thermocouples are presented in column 13 in Tables XIII through XVII Columns 10 and 12 give the values of the heat flux at the uranium heater as determined from the thermal neutron flux and the temperature drop, respectively. The heat transfer coefficients in column 12 were computed from thermocouple values as described above. Heat fluxes computed from the thermal neutron flux are presented in column 12 for comparison. Considering the accuracy of heat transfer measurements, the agreement between columns 10 and 12 are generally within ±15 percent. Some values differ by as much as 50 percent, however.

To determine the effect of radiation on heat transfer, the heat transfer coefficients as measured under the same bulk temperatures, HBR contents, and fluid velocity conditions as at the test heater were compared to the coefficients measured at the uranium heater. The values of the coefficients measured at the test heater

are presented in column 14 and should be compared to those in column 13. Correction has been made on the test heater coefficients for the differences in the flow channel, since the uranium heater coolant channel is annular, while the test heater coolant channel is tubular.

An attempt was made to correlate the uranium heater heat transfer coefficients by plotting them and comparing them to the general polyphenyl relation, $Nu = 0.015Re^{0.85}Pr^{0.3}$,[12] but due to the scatter of the points, no conclusion could be reached. However, if columns 13 and 14 are compared directly, there does not appear to be any great difference between the coefficients or any trend of a greater decrease in heat transfer indicated at the uranium heater. An approximate ±10 percent agreement between the test heater values of h and the measured values of h at the uranium heater is the general case for the single-cycle irradiations. During the extended diphenyl irradiation, in which considerable in-pile thermocouple difficulty was experienced, the difference between the test heater and uranium heater values of h are in some cases greater than 10 percent. However, in these cases, it is apparent that the difference between the values in columns 13 and 14 remain unchanged, indicating that whatever the normalized value of h is, the measured value of h at the uranium heater follows the same decrease as predicted from the test heater data.

In conclusion, no fouling effect or decrease in the heat transfer coefficient could be detected at the uranium heater greater than the ± 10 percent uncertainty which existed between the values of h measured at the uranium heater and the values of h predicted from the test heater.

2. Hot Cell Examination of the Uranium Heaters

Five uranium heater assemblies were used to irradiate the different materials. Four assemblies were utilized for the first four single-cycle irradiations and one assembly was used to test diphenyl for the extended 3 MTR cycle test.

All five in-pile sections with the loop lines cut off just above the top of the square aluminum section were removed from the reactor via the reactor discharge chute to the canal. Storage in the canal was for a period of one to two months, until at least two assemblies could be made available for hot cell examination of the in-pile heaters, removal of the flux monitor wires, and weighing of the specimens.

It was necessary to seal the tubes after severing to prevent the entrance of reactor or canal water into the reservoir. Crimping the tubes was the method used to effect the seal before removing the in-pile assemblies for the isopropyl diphenyl (MTR Cycle 77) and the diphenyl (MTR Cycle 78) irradiations. When these two assemblies were examined in the hot cell, the reservoir was found to contain excessive water. Tube fittings were used to seal the remaining in-pile pieces to ensure the exclusion of water while they were stored in the canal.

Circulation of the irradiated hydrocarbon was continued for approximately 18 to 24 hours after reactor shutdown before the coolant was drained from the in-pile reservoir. After draining the system, use was made of the uranium thermocouples which were still intact to note any excessive heating of the uranium element heat transfer surface due to afterglow heat. In all cases, the element temperatures never exceeded 130°F, which was approximately reactor ambient water temperature after draining the hydrocarbon from the in-pile assembly.

The examination procedure consisted of cutting through the 3-inch-square aluminum housing and the steel reservoir at previously scribed points. The central tube with the uranium heater and the corrosion samples were then completely freed from the reservoir walls. The uranium heater was slipped out of the central tube and dipped in methyl-chloroform for cleansing. No scrubbing of the surface of the element was used. The heaters were mounted in a block which contained a dummy stainless-steel element which had never been heated or exposed to the hydrocarbon. The dummy element was scribed to indicate the length of the heat transfer area.

Visual examination of all the uranium elements revealed the presence of a very thin, hard, and adherent film or coating covering the heat transfer area. It was not possible to remove any of the film from the surface by rubbing nor was it possible to measure its thickness in the hot cell. Figure 22, which is a photograph of the element from the Santowax R irradiation, best illustrates the noted effect. The thinness of the film is apparent from the metallic lustre which is detectable on the heat transfer area. In general, all of the heaters showed some coating on the heat transfer area. No differences in the coating could be ascertained from visual examination of the heaters.

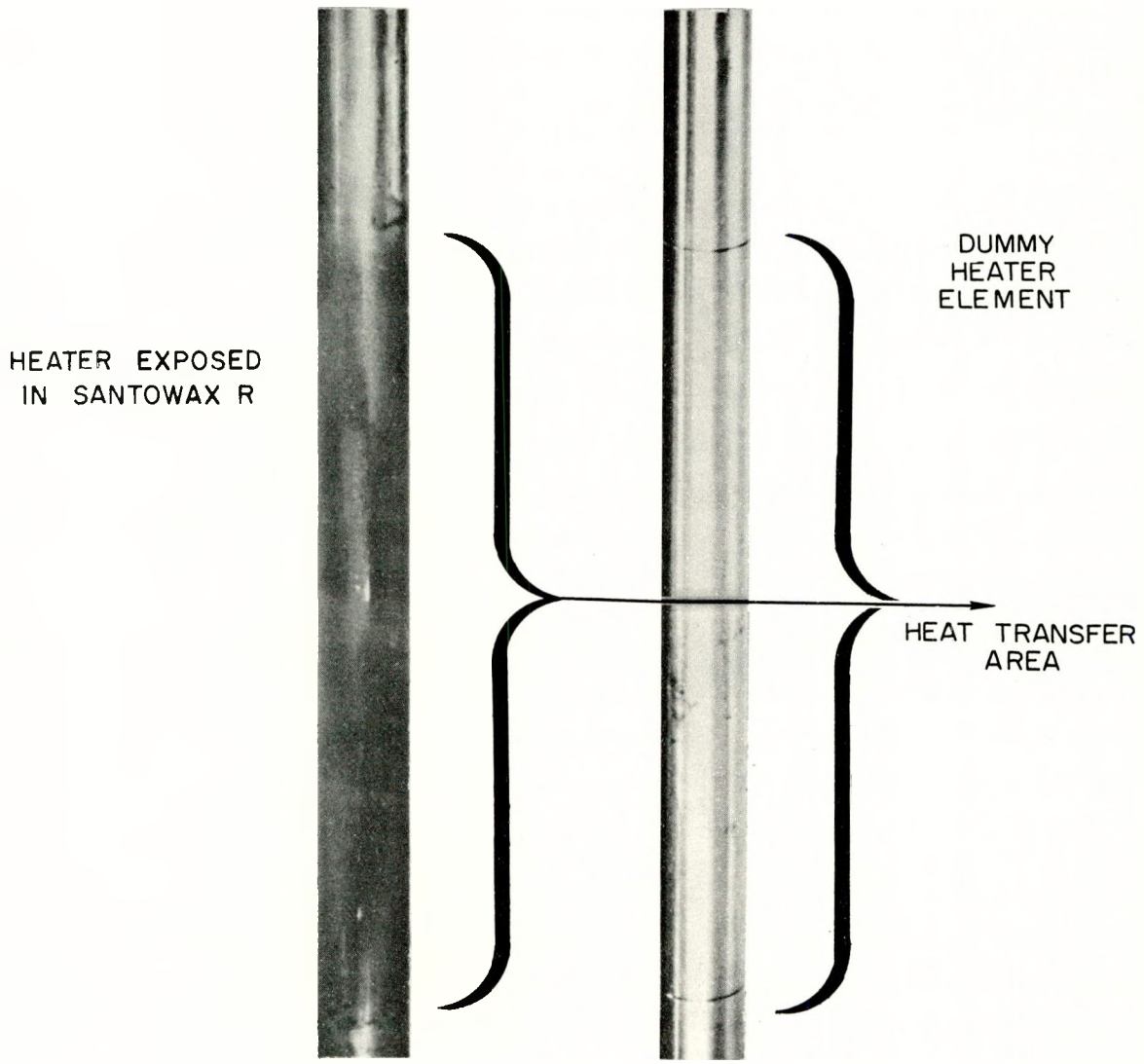

Fig. 22. In-Pile Heat Transfer Surface of Uranium Heater Exposed to Irradiated Santowax R

In analyzing the formation of the surface film, the long storage in the canal before hot-cell examination should be considered. It is possible that the residual organic film may have decomposed during storage in the canal. However, since the temperature of the element was 100° F or lower during storage and the radioactivity of the uranium portions of the element is probably not significantly greater than the radiation dosage from the steel parts due to low uranium enrichment and burnup, preferential radiation decomposition on this portion of the element is felt to be improbable.

C. CORROSION OF STRUCTURAL METALS IN IRRADIATED POLYPHENYLS

During the course of the experiment, a general screening of common structural metals which might be considered for use in an organic moderated reactor was also conducted. Loop operating conditions were dictated by the parameters of coolant decomposition rates and heat transfer. Therefore, the conditions under which the corrosion specimens were exposed varied and the experiment cannot really be considered as wholly adequate as a corrosion test. The time of exposure was relatively short, considering the normal procedures used in corrosion testing.

Mild steel, aluminum, stainless steel, magnesium, and zirconium were exposed in the in-pile assembly adjacent to the uranium heater and in an out-of-pile position in the piping, as shown in Figs. 1 and 2. The linear flow rate past the specimens was calculated to be approximately 0.5 feet per second in the expanded flow path where the samples were mounted.

In general, the corrosion resistance of the stainless steels and aluminum was excellent. The mild steel and alloy steel exhibited slightly greater weight changes and more discoloration. However, the steel specimens would still be considered to have good corrosion resistance for use in a reactor. Magnesium and zirconium were found to be unsatisfactory due to their tendency to become oxidized or hydrided.

Although no water analysis was done on the coolant, it is estimated from the traces of water detected during gas solubility sampling that the water concentration was approximately 10 ppm. Magnesium oxide may have been formed

from the trace amounts of water estimated to be present in the system. Since hydrogen was the most prevalent gas in the system, it is assumed that zirconium hydride was formed from reaction with this hydrogen. Table XVIII lists the weight change data for all the samples exposed. There were greater weight changes indicated for the samples which were exposed at the in-pile position. However, since these specimens were weighed remotely in the hot cell, it is felt that the weighings were subject to larger experimental errors.

The periodic activation analysis of the coolant indicated no buildup of any activities which may have come from corrosion. Although Fe^{59} did account for some of the activation of the coolant, it is felt that this activity was caused by the rusting of the carbon steel parts of the system prior to use.

There were no indications of any radiation effect on the corrosion resistance of any of the materials tested.

A more detailed report on the corrosion studies conducted has been published by H. E. Kline et al.[14]

D. COOLANT ACTIVATION AND PHYSICAL PROPERTIES

1. Coolant Activation

One-gram portions of the samples removed for HBR analysis were counted on a multichannel gamma spectrometer at four to five day intervals to detect active isotopes in the coolant. In comparison with activation occurring in pressurized water systems, the activation of the polyphenyl coolants was very low. The console and the piping emerging from the reactor was monitored daily by Health Physics. The radiation level on the surface of the piping and the console was found to be between 50 and 150 mr/hr. Levels decreased somewhat as the irradiations progressed. This was probably due to removal of particles of rust or metal which were introduced with the installation of each new in-pile assembly. The system filter always required replacement once or twice immediately after initiation of circulation through the new assemblies. The coolant and system cleanup was accomplished before the reactor was brought to power. After the commencement of irradiation, it did not appear to be necessary to use the filter to maintain coolant purity. During the second and

TABLE XVIII

CORROSION TEST RESULTS ON MATERIALS EXPOSED TO IRRADIATED POLYPHENYLS

Material	Identity Code		Polyphenyl	Wt. Change (mg)		Average Wt. Change (mg)	
	In-Pile	Out-of-Pile		In-Pile	Out-of-Pile	In-Pile	Out-of-Pile
410 Stainless Steel	-	10A	Isopropyl	-	-0.3		
	-	11A	Diphenyl	-	-0.5	-	-0.4
	-	12A		-	-0.4		
	10	25A	Santowax R	+0.2	+0.1		
	11	26A		+0.6	+0.3	+0.3	+0.2
	12	27A		+0.1	+0.1		
304 Stainless Steel	1A	1	Diphenyl	0.0	+0.2		
	2A	2	(1 MTR Cycle)	+0.2	+0.1	+0.1	+0.1
	-	3		-	+0.1		
4130 Alloy Steel	-	13A	Isopropyl	-	0.0		
	-	14A	Diphenyl	-	0.0	-	0.0
	-	15A		-	-0.1		
	31	31A	Diphenyl	+0.1	+0.1		
	32	32A	(3 MTR Cycles)	+1.3	+0.1	+0.6	0.0
	33	33A		+0.4	-0.2		
	34	34A	Santowax O-	-1.6	-0.7		
	35	35A	Santowax M	-2.2	+0.3	-2.3	-0.2
	36	-		-3.2	-		
ASTM A 212 Steel	A-3	A-4	Diphenyl	+1.0	+0.4	+1.1	+0.5
	A-1	A-6	(3 MTR Cycles)	+1.2	+0.6		
ASTM A 7 Carbon Steel	19	19A	Diphenyl	-	+0.2		
	20	20A	(1 MTR Cycle)	-0.3	+0.3	-0.3	+0.3
	-	21A		-	+0.3		
	55	55A	Santowax O-	+1.6	-0.3		
	56	56A	Santowax M	+1.2	-1.1	+1.1	-1.0
	57	57A		+0.5	-1.5		
2S Aluminum	4A	4	Diphenyl	-0.2	0.0		
	5A	5	(1 MTR Cycle)	-0.5	+0.1	-0.3	0.0
	-	6		-	-0.1		
	22	22A	Santowax R	+0.2	-0.1		
	23	23A		+0.4	0.0	+0.4	-0.1
	24	24A		+0.5	-0.3		
	79	79A	Santowax O-	+0.1	-0.1		
	80	80A	Santowax M	-0.5	-0.2	-0.1	-0.2
	81	-		+0.1	-		
	73	73A	Diphenyl	+1.1	+0.2		
	74	74A	(3 MTR Cycles)	+0.9	0.0	+0.8	+0.2
	75	75A		+0.2	+0.3		
	76	76A		+0.9	+0.1		
Magnesium	-	16A	Isopropyl	-	+3.0		
	-	17A	Diphenyl	-	+2.9	-	+2.8
	-	18A		-	+2.6		
	16	40A	Santowax R	+0.6	+0.1		
	17	41A		+0.6	+0.1	+0.8	+0.1
	18	42A		+1.3	0.0		
	40	43A	Diphenyl	+41.7	+44.6		
	41	44A	(3 MTR Cycles)	+45.5	+44.4	+38.5	+46.3
	42	45A		+28.2	+50.0		
SRE Zirconium	52	52A	Santowax O-	+4.0	+2.2		
	53	53A	Santowax M	+7.2	+2.2	+5.3	+2.4
	54	54A		+4.8	+2.8		
Crystal Bar Zirconium (KAPL)	-	ZAI 1	Diphenyl	-	+2.7		
	-	ZAI 2	(1 MTR Cycle)	-	+3.0	-	+2.8
	-	ZAI 3		-	+2.7		
	B1	-	Santowax R	+1.4	-		
	B2	-		-0.4	-	+1.0	-
	B4	-		+2.1	-		

third cycles of the extended diphenyl irradiation, the filter was bypassed for approximately 80 percent of the time. No increase or change in the coolant activity was noted. With the exception of a similar sintered bronze filter in the feed line, no special care was taken in the preparation of the makeup coolant. The coolants circulated were all of industrial grade or purity. The only precaution used before a coolant could be accepted for irradiation was that a neutron activation of the charge material should indicate an acceptable level of contamination. This technique for acceptance was developed prior to and concurrently with the in-pile loop experiment. Isotopic impurities expected to be present had been previously identified and their concentrations determined from capsule irradiations. Activities noted during the first two irradiations and additional computations concerning activation from various isotopes resulted in the establishment of the acceptance standards for the OMRE coolant. The most active impurities in the charge materials were found to be Na^{23}, Cl^{37}, Mn, Hg^{207}, and a trace amount of Co^{60}. All concentrations were only a few parts per million.

Figure 23 is a graph of a typical change-in-activity spectrum of the charge material due to continued irradiation in the system. The activity increased by a factor of ten. This increase may be for the most part due to the appearance of the isotopes Cu^{64}, Fe^{59}, Cr^{51}, and Zn^{65}. Subsequent counting of both samples accentuated the peaks for these isotopes. No attempt was made to determine the concentration of the impurities present in the coolant once the irradiation began because of the large amount of sampling taking place and the varied radiation history. It is significant that the activity level did not change during irradiation and no new isotopes appeared except those previously mentioned. The isotopes Cu^{64} and Zn^{65} may have come from either the silver solder used in the preparation of the uranium heater wall thermocouple installation or the sintered bronze filter in the system. Silver, cadmium, and nickel were also present. It is probable that bronze may not be too usable at temperatures of 650 to 700°F. The isotopes Fe^{59} and Cr^{51} probably came from the rusting of the steel parts of the in-pile assemblies previous to their use. The type 4130 steel used in the loop lines contained chromium.

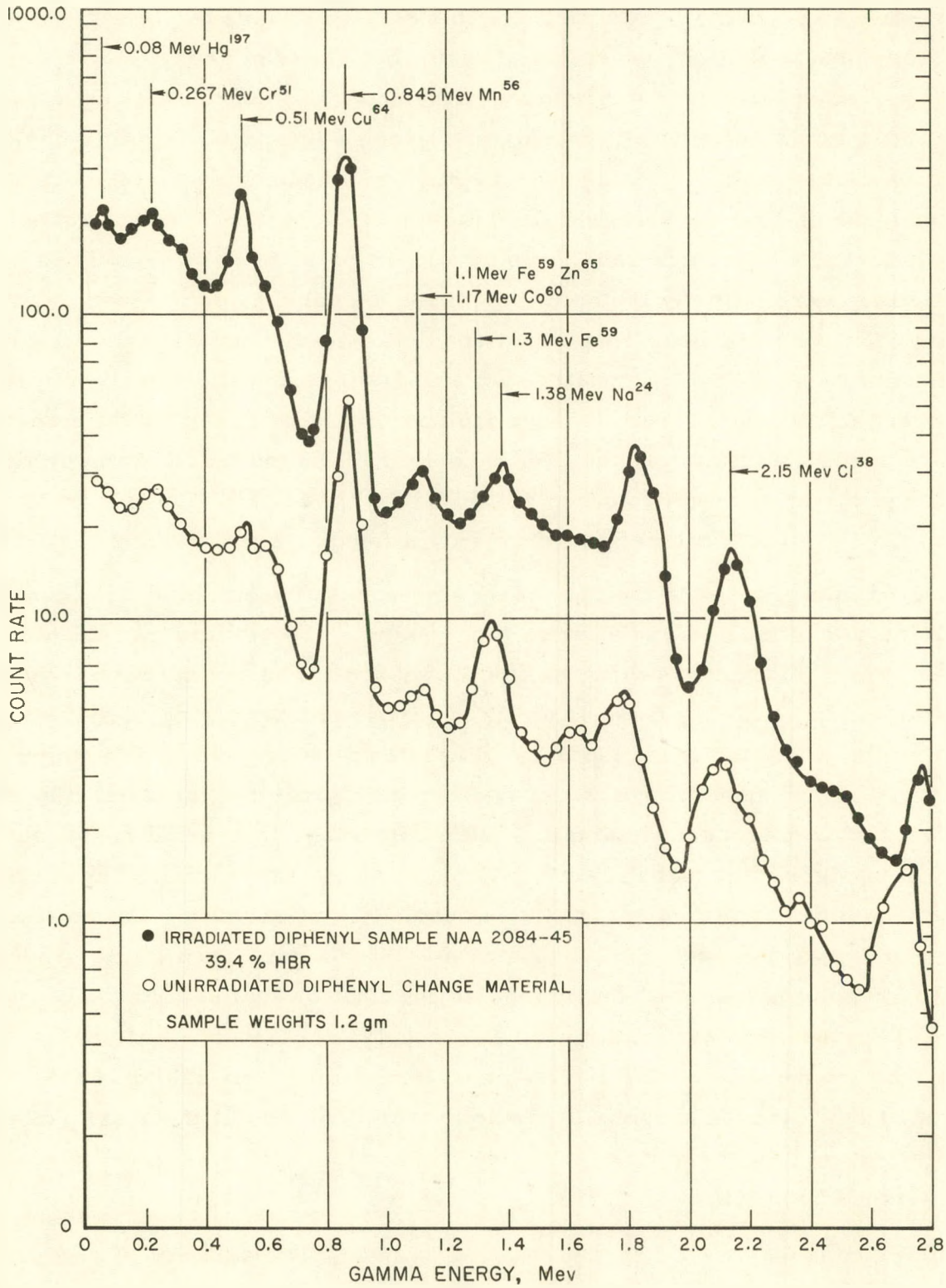

Fig. 23. Typical Gamma Spectra of Irradiated and Unirradiated Diphenyl

A sample of the same irradiated material characterized in Fig. 23 was counted approximately one year after removal from the reactor. The Co^{60} could then be positively identified, since only Zn^{65} remained to mask the peaks. Due to the long half life of the Co^{60}, the changes in reactor power, shutdowns, and sampling would only make small differences in determining the radiation history. It is estimated that the Co^{59} concentration in the coolant was approximately 2×10^{-3} ppm.

Counts were made as early as 2 to 3 minutes after collection of a sample in an attempt to detect short-lived isotopes such as Mg^{27} and Al^{28}. No characteristic peaks for these isotopes could be detected.

No beta counting of the samples was attempted. However, combined beta and gamma activity amounted to approximately 10 mr/hr for a 1-gram sample at contact. Gammas amounted to approximately 2 mr/hr of the 10 mr/hr total activity. Both the betas and gammas were soft and the radiation level dropped off rapidly with distance.

Two spills occurred with the irradiated materials during the course of the experiment. In one, a valve was inadvertently opened, resulting in the spillage of irradiated diphenyl on personnel and in the air. The second case was the rupture of the test heater during the Santowax R irradiation, resulting in spillage on the floor adjacent to the console. It is significant that in both cases decontamination was easily accomplished. Air monitors which were sprayed directly did not indicate any undue air activity. Soap and water were adequate to effect decontamination of the personnel and the contaminated area.

During the sampling process, organic vapors were always emitted when the connections from the sampling valve was broken after the samples were collected. Tubes connected to the air monitors did not show an increase in activity.

Based on the fact that the activity in the system was primarily due to impurities introduced with the coolant and by cleaning of the system from startup, it is probable that the activity to be expected in a reactor may be lower than was experienced during loop operation. As a result of a smaller surface-to-volume ratio which would exist in a reactor system, a lower concentration of contaminants from system cleanup would be the case after reactor startup. It is also possible that continuous purification would aid in reducing the activity levels.

2. Physical Properties

Concurrent with the irradiation phase of the experiment, the physical properties of the irradiated samples were determined by R. H. J. Gercke. The work has been published[15] and is presented herewith as information used to correlate the parameters studied in this experiment.

a. Densities and Viscosities

The densities and viscosities were measured and found to increase as the HBR content increased. Densities increased from 4 percent to 8 percent as the residue content rose to 35 weight percent. Larger increases in the density were found for isopropyl diphenyl and the diphenyl than were found for the terphenyls.

A two- to two-and-one-half-fold increase was measured for the viscosities as the HBR concentration rose to 35 weight percent. This is not an unreasonable increase insofar as pumping power and heat transfer properties in a reactor are concerned.

Density data is presented in Figs. 24 through 27. Viscosity data is presented in Figs. 28 through 31.

Additional density and viscosity measurements of samples from the latter cycles of the extended diphenyl irradiation revealed no changes in these properties other than would be expected from the HBR content in the coolant.

b. Specific Heat

The specific heats of an 89 percent ortho-, 11 percent meta-terphenyl mixture and an irradiated Santowax O - Santowax M mixture at 32 percent HBR content were determined experimentally. The data is presented in Fig. 32. The diphenyl data of Forrest et al,[16] are also shown. Irradiation to approximately 35 percent HBR decreased the specific heat by approximately 10 percent.

c. Thermal Conductivity

Thermal conductivities have not yet been determined experimentally. However, it is generally accepted that the thermal conductivity of organic materials can be predicted and will fall within a narrow range. Figure 33 is a plot of the equation, as used to estimate the thermal conductivity of the organic coolants.

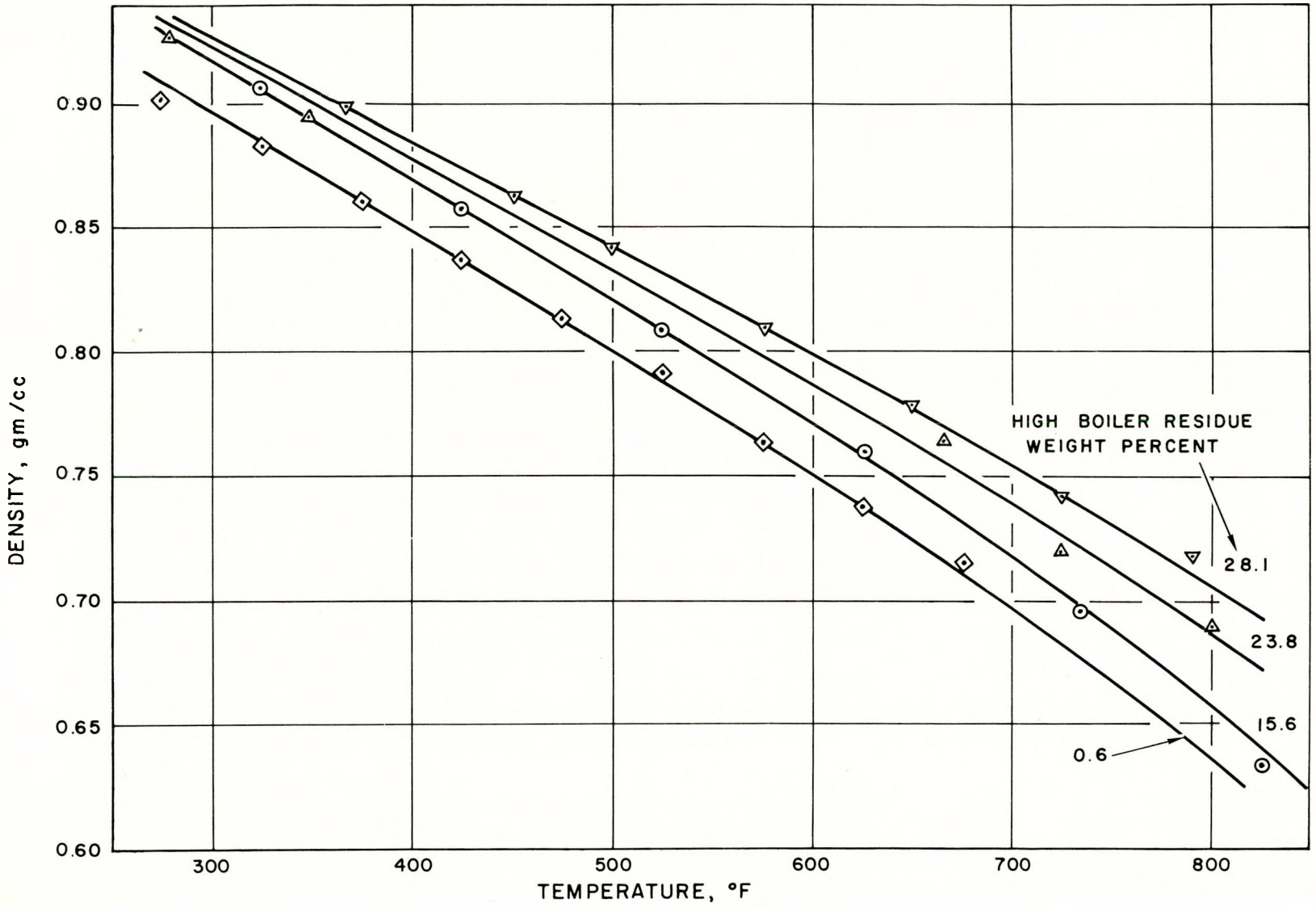

Fig. 24. Density of Irradiated Isopropyl Diphenyl

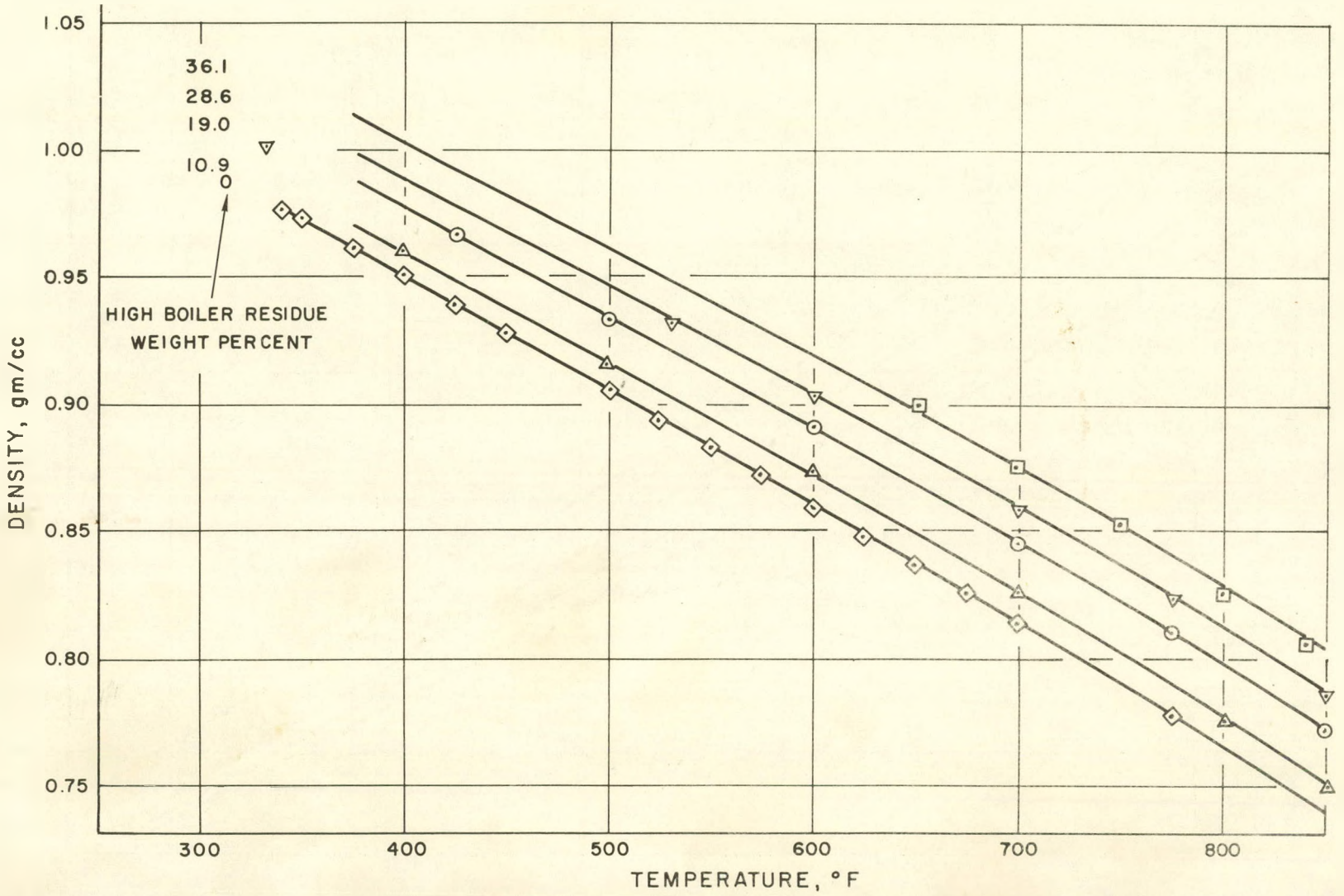

Fig. 25. Density of Irradiated Santowax O–Santowax M

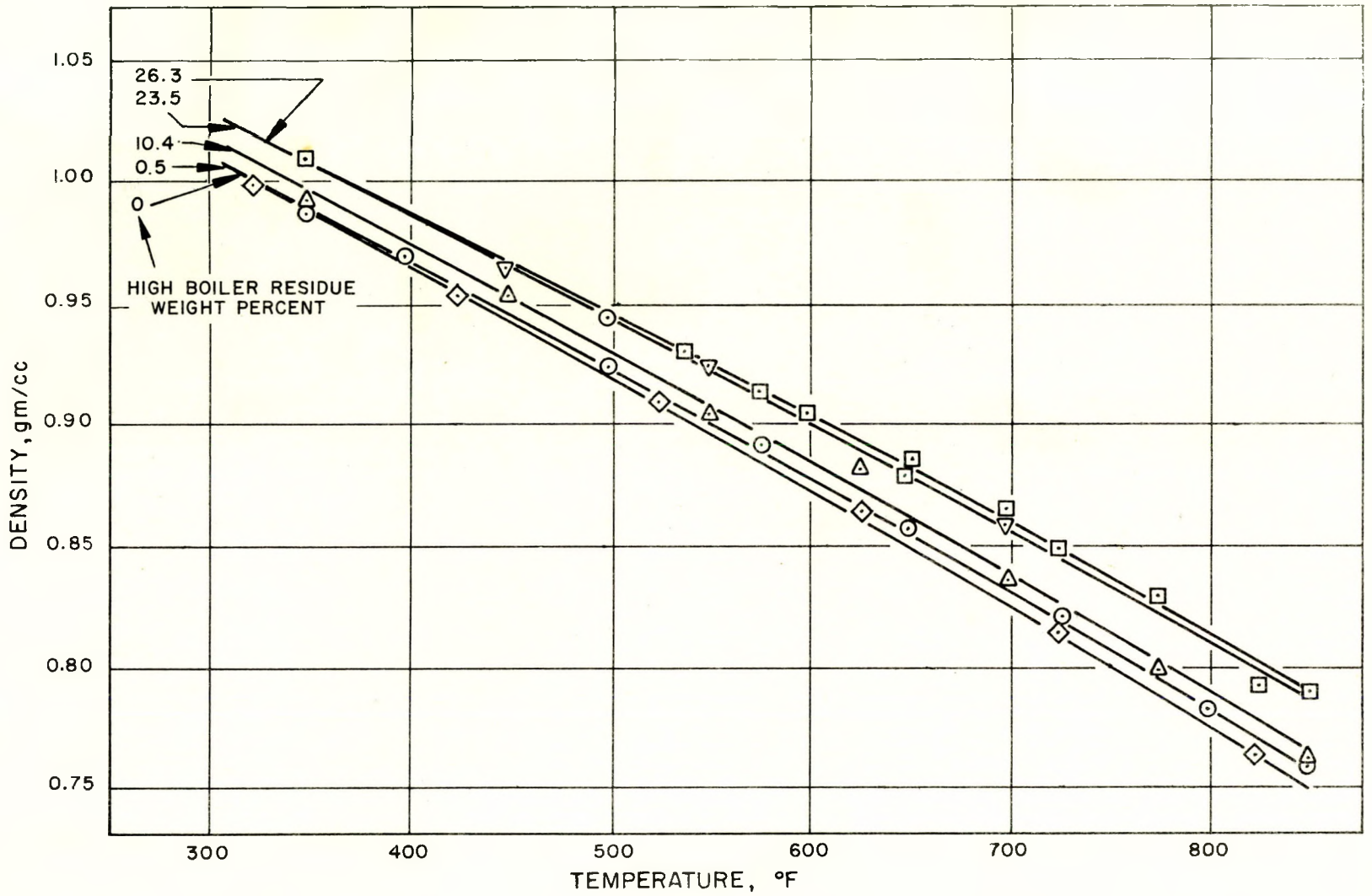

Fig. 26. Density of Irradiated Santowax R

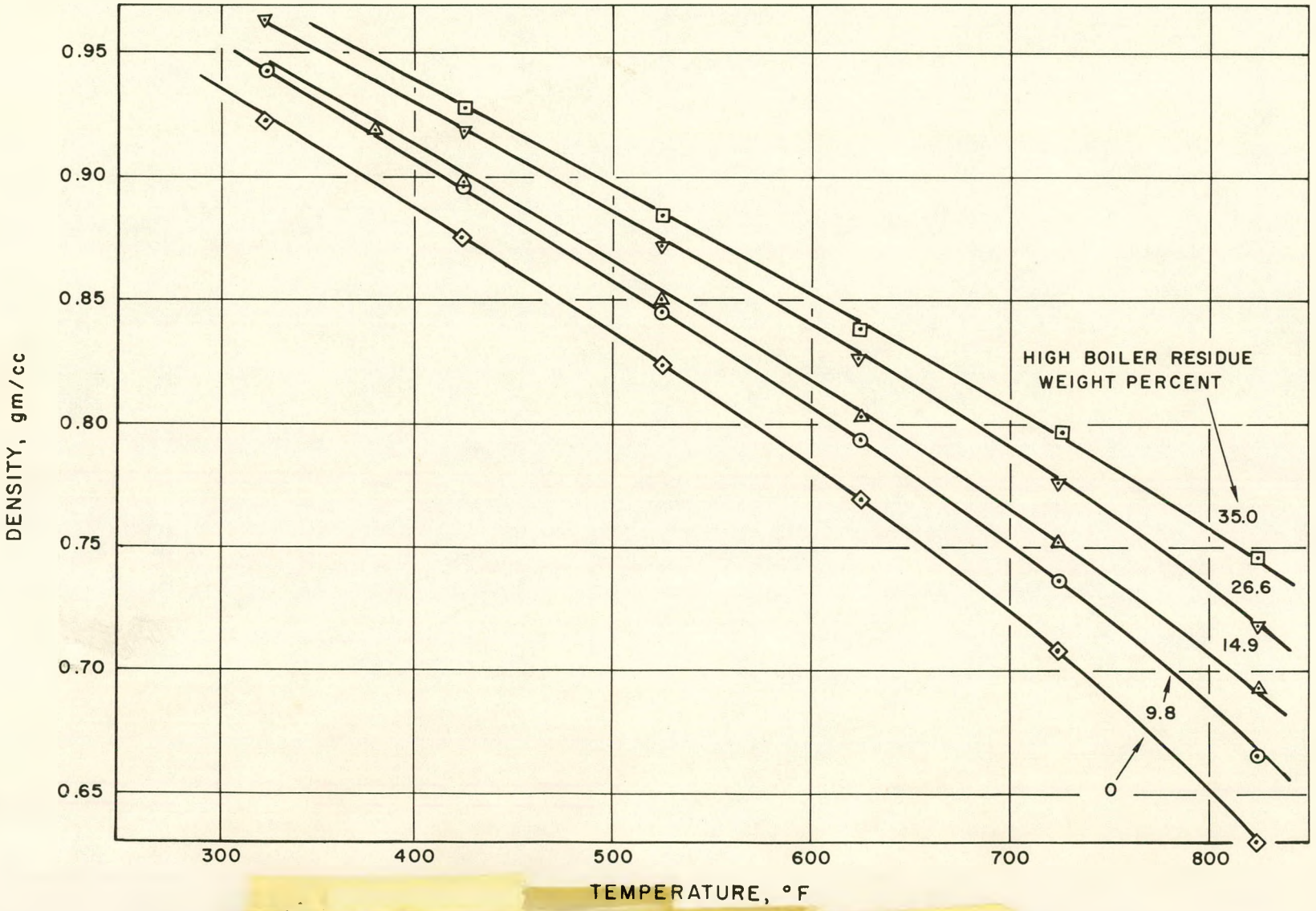

Fig. 27. Density of Irradiated Diphenyl

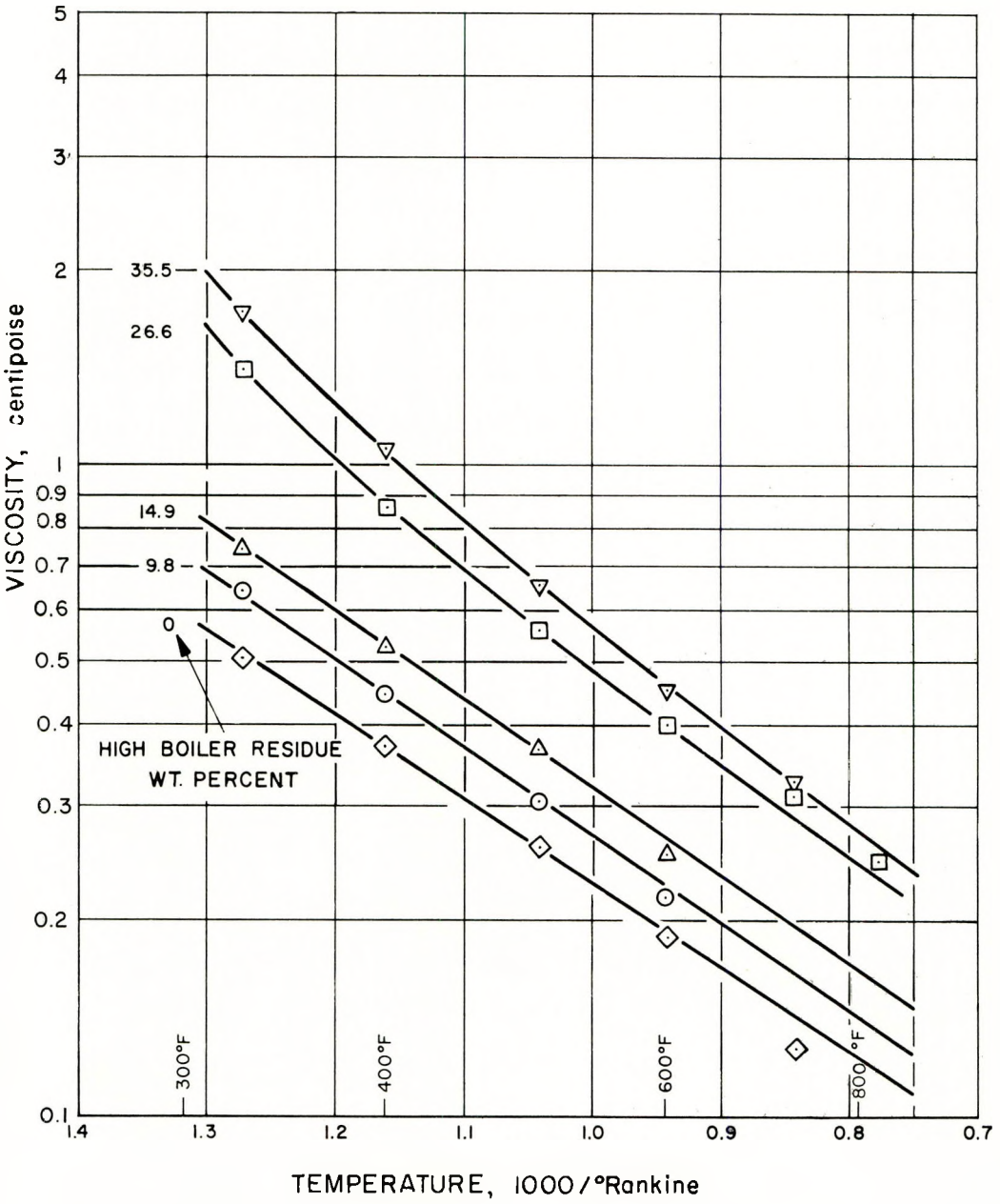

Fig. 28. Viscosity of Irradiated Isopropyl Diphenyl

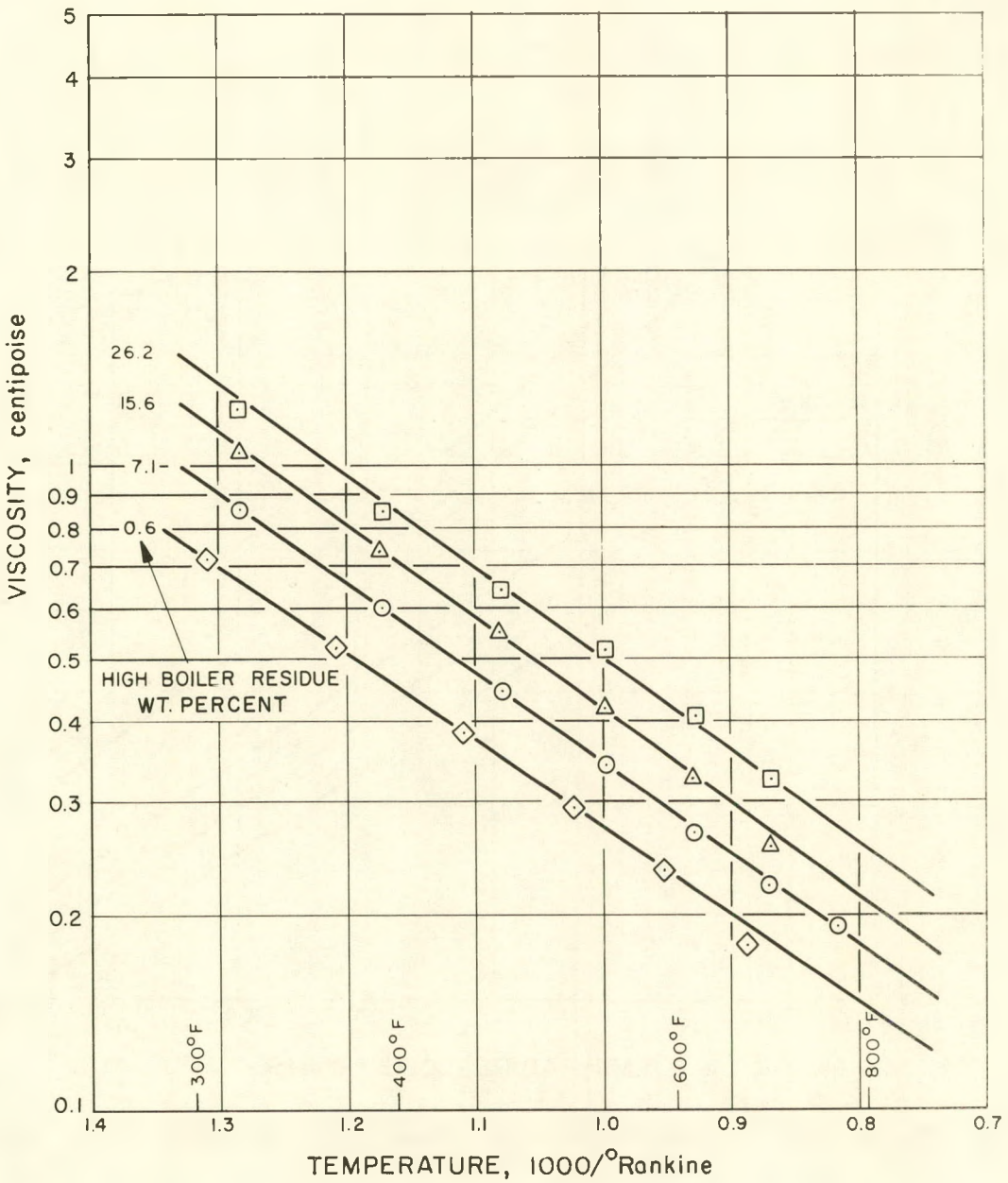

Fig. 29. Viscosity of Irradiated Diphenyl

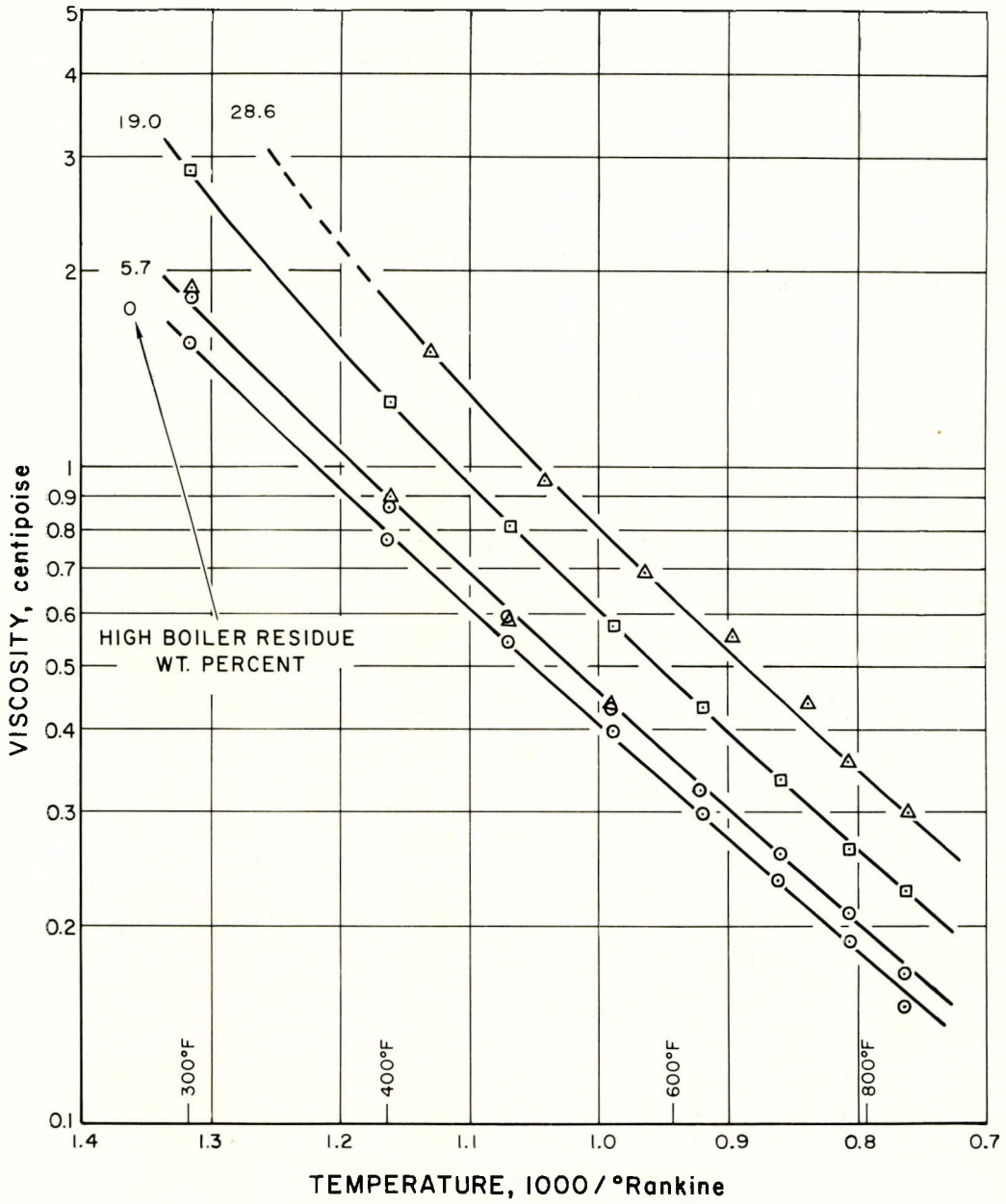

Fig. 30. Viscosity of Irradiated Santowax R

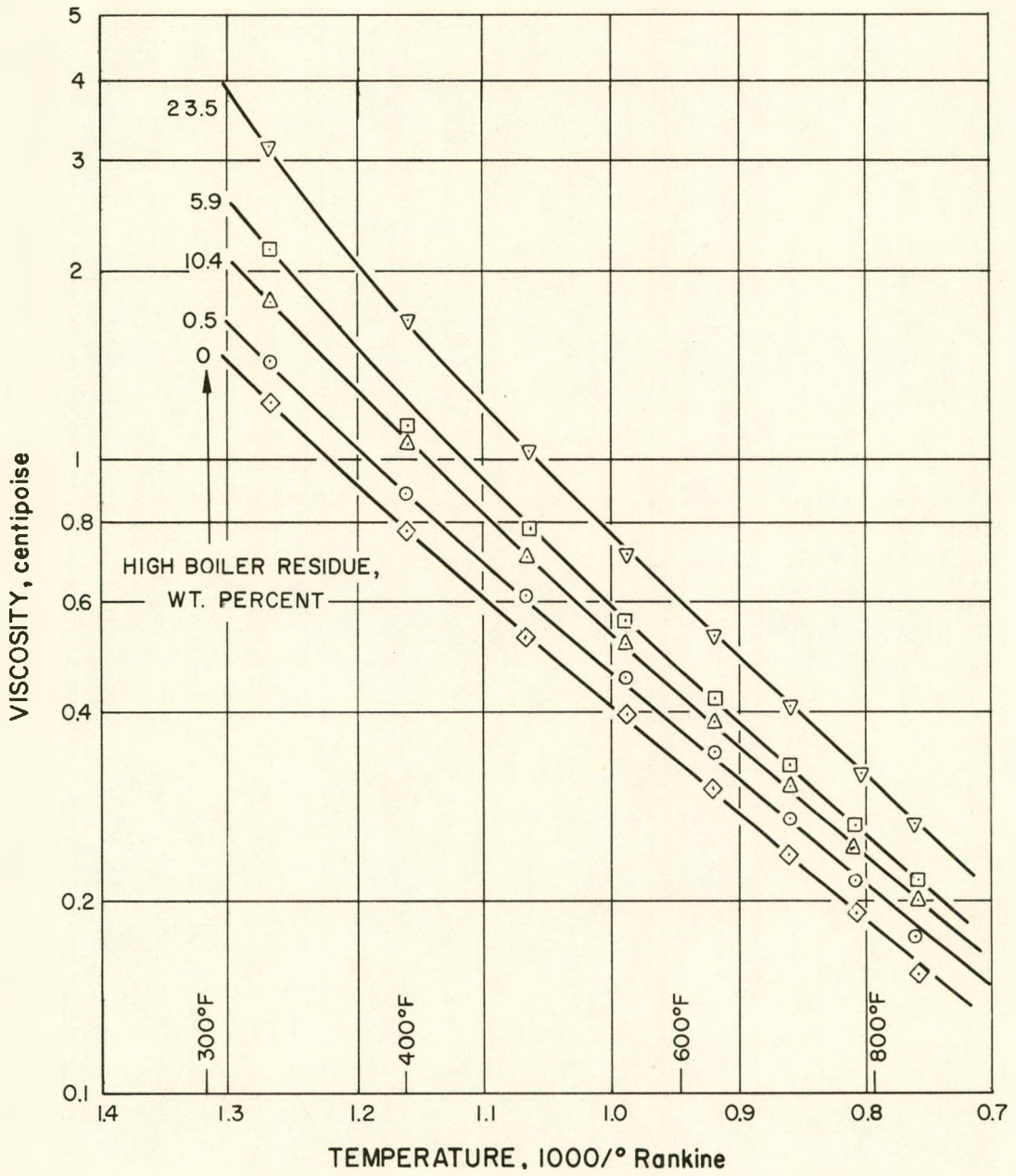

Fig. 31. Viscosity of Irradiated Santowax O - Santowax M

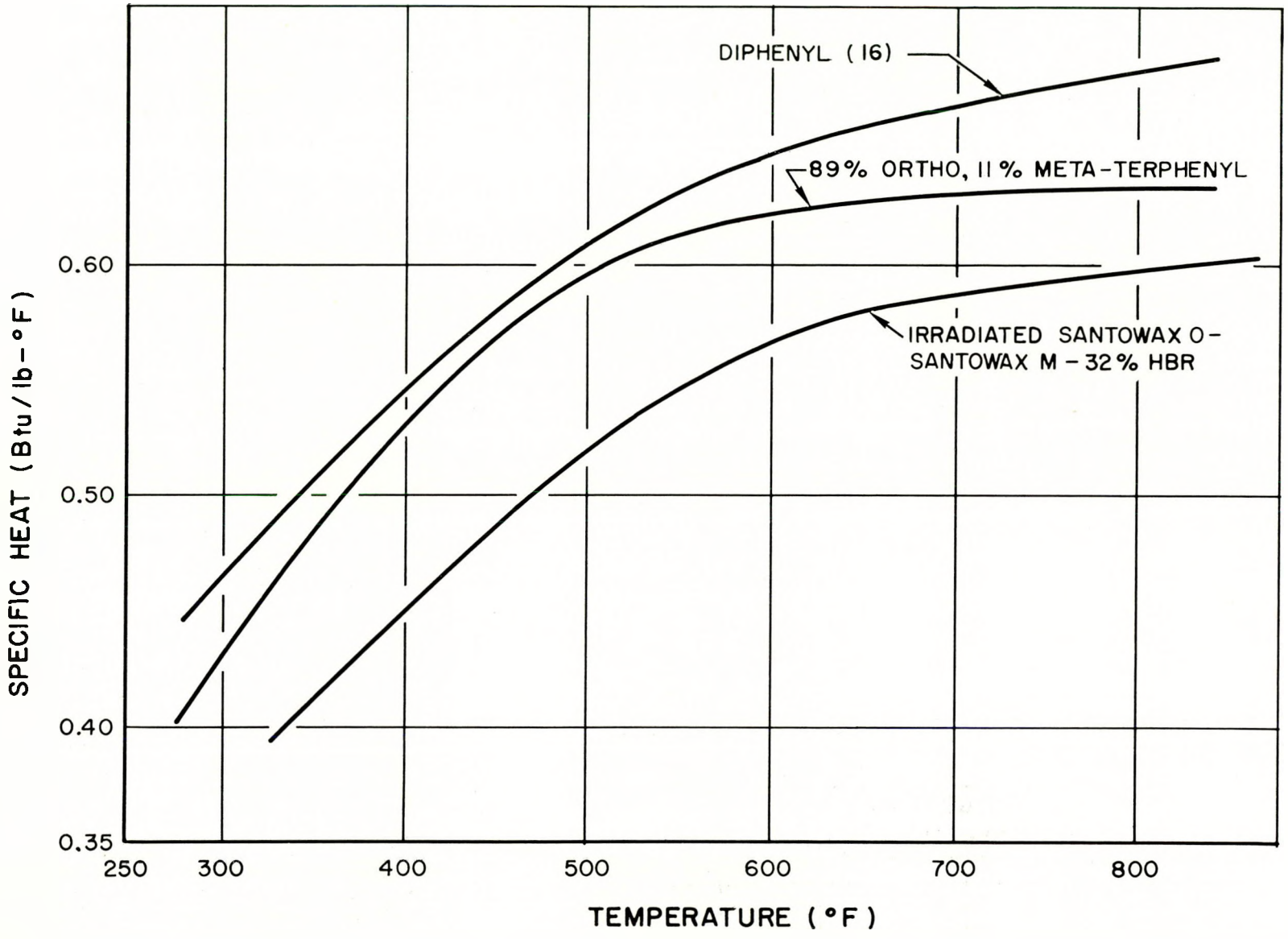

Fig. 32. Specific Heat of Polyphenyls

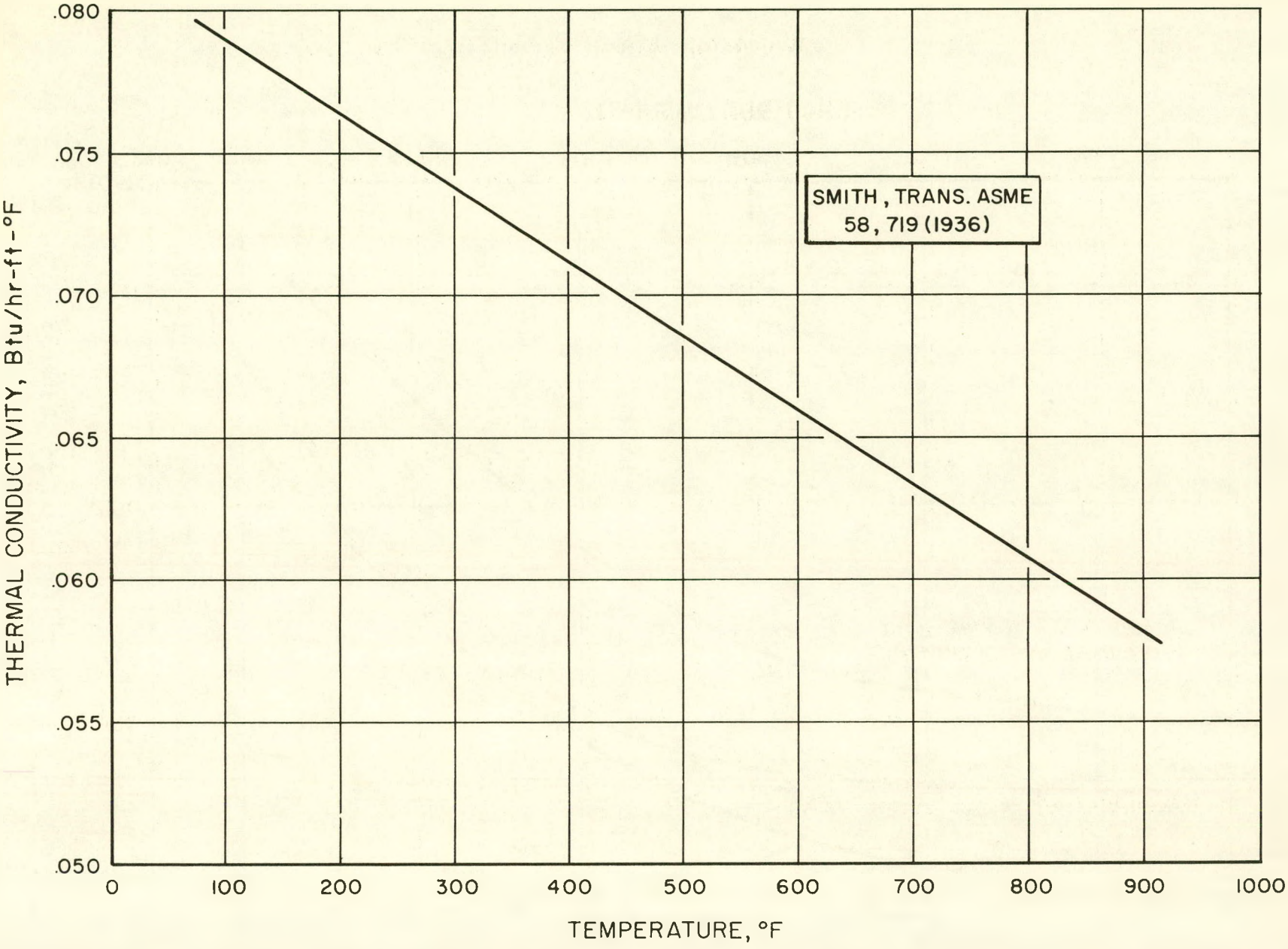

Fig. 33. Estimated Thermal Conductivity of Polyphenyl Coolants

d. Carbon-Hydrogen Ratios

The carbon-to-hydrogen ratio increased as would be expected since hydrogen is the most prevalent gaseous decomposition product. However, this effect was smaller than the effect of the increase in density, with the net result that the hydrogen density actually increased. The hydrogen density increased by approximately 3 percent to 5 percent for diphenyl and isopropyl diphenyl, respectively. A 2 percent increase was noted for the terphenyls (Santowax R and Santowax O - Santowax M).

e. Physical Appearance

All irradiated samples were darker in color and opaque except for thin films. The thin films on laboratory glassware were brown in color and transparent with no particulate matter discernible.

f. Melting Points

The melting points of all the materials decreased with increasing HBR content. The decrease in the final liquidus point was approximately 35°F at 35 percent HBR for all the coolants except Santowax O - Santowax M. For Santowax O - Santowax M, a 55°F drop was noted. Figure 34 presents the melting point data. In general, the irradiated materials had a tendency to subcool. The first appearance of liquid started at a lower temperature than for the pure material. Irradiated diphenyl from the extended diphenyl irradiation was still soft several months after completion of the irradiation when the console was dissassembled and inspected.

E. EQUIPMENT EXAMINATION

Irradiated polyphenyls were circulated for approximately 130 days through the console at high temperatures. During this period, the HBR content was above 30 percent for approximately 50 days. During the last 42 days of operation of the equipment, the HBR content was between 30 and 40 percent by weight.

Upon completion of the extended diphenyl irradiation, the system was drained and the console lines were sealed off for later examination of the valves, rotameter, surge tank, and pump. No flushing of the console was done with pure diphenyl. Between the other cycles, the previously irradiated material was flushed from the equipment by charging the system with the new polyphenyl to be irradiated,

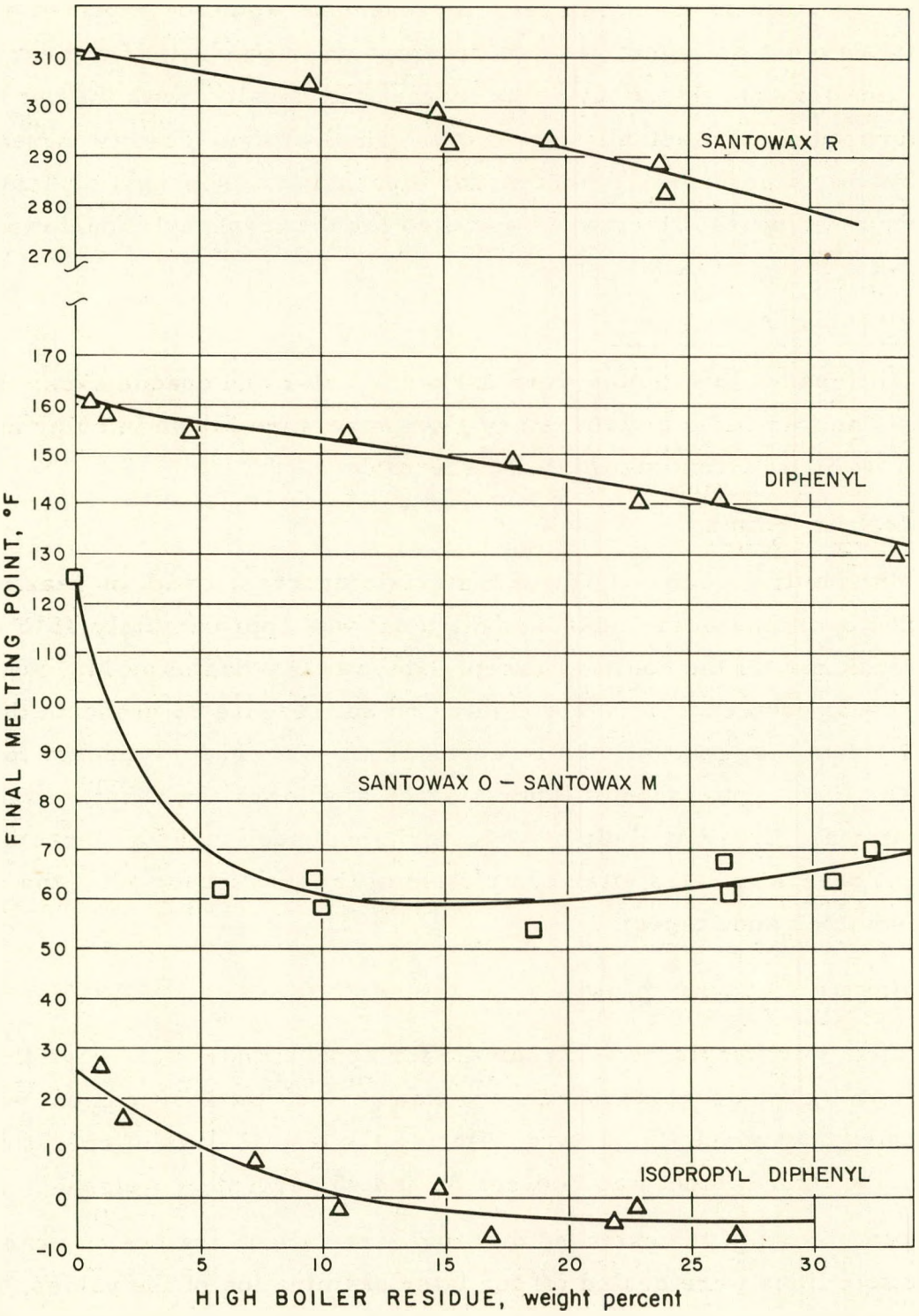

Fig. 34. Melting Points of Irradiated Polyphenyls

circulating the material at elevated temperatures, and then draining the system and refilling with pure unirradiated material. No solvents were used at any time to clean the system after organic materials were once used. This included the time when high-temperature shakedown runs were made prior to installation at the MTR.

Portions of the piping and pump were examined to detect concentration or buildup of any insoluble material in the cooler or stagnant regions of the system.

The rotor chamber and bearing portions of the pump were always operated very close to the freezing point of the material irradiated. There were no indications at any time that plugging of the small bypass coolant line on the pump was occurring. The temperature of the irradiated coolant in this line was generally 300°F or below. Figures 35, 36, and 37 are photographs of the pump rotor, the pump impeller housing, and the bearings. The material adhering to the pump rotor and bearings was irradiated diphenyl and was found to be quite soft, although not liquid. No heat was required to disassemble the pump, which indicates the softness of solidified irradiated diphenyl. The impeller housing shows the characteristic thin (machine marks are visible), hard, and adherent film which was found on all portions of loop exposed to high-temperature irradiated or unirradiated polyphenyls.

Figures 38, 39, and 40 are photographs of the surge tank sight glass, valve bellows assemblies, and the rotameter float with magnetic follower extension. The cleanliness of the parts is apparent. Of particular significance is the cleanliness of the sight glass. There was no stain or organic film on the inside of the glass. Since the valve bellows assemblies were installed horizontally, one side of the bellows shows the material which adhered to the walls after draining the irradiated polyphenyl. The assembly from valve 4 was in constant use for the high temperature polyphenyl, since it was the valve just upstream of the test heater. Valve 5 is the feed tank valve, which was generally much cooler and was exposed to the pure feed material. Comparison of the two valves indicates that irradiation of the polyphenyl to high HBR concentrations does not result in accumulation of deposits on equipment.

It should be noted that the rotor of the pump and the magnetic follower on the rotameter were not discolored by the polyphenyl.

The test heater was sectioned and examined to detect any fouling or scaling. No heat-affected zone was found, nor could any difference between the appearance of the test heater and other portions of the piping be detected.

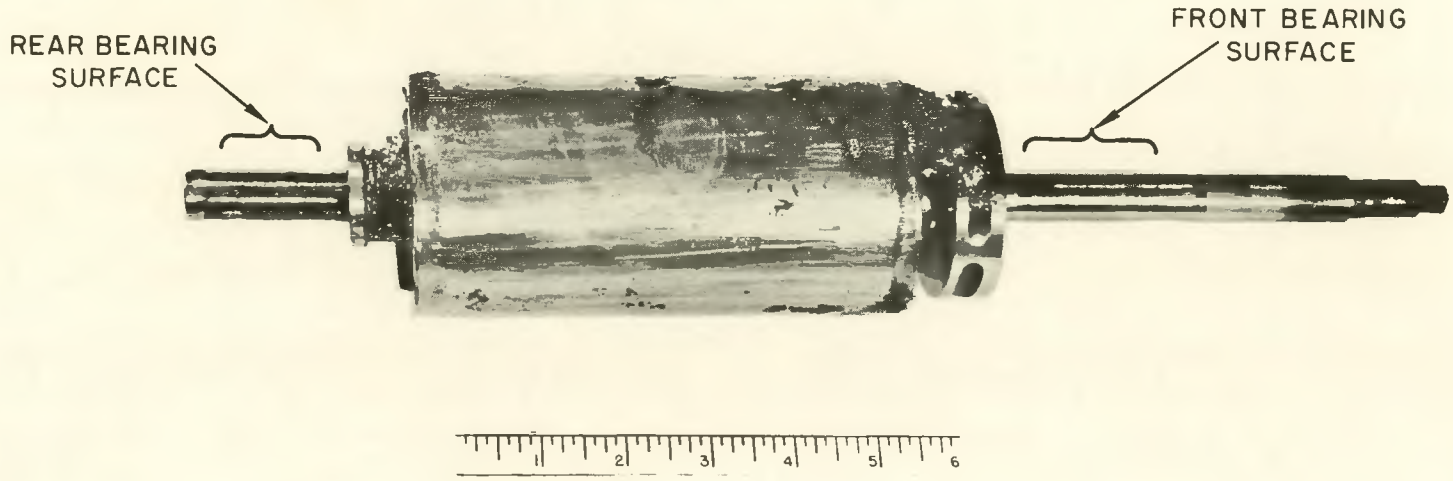

Fig. 35. Pump Rotor

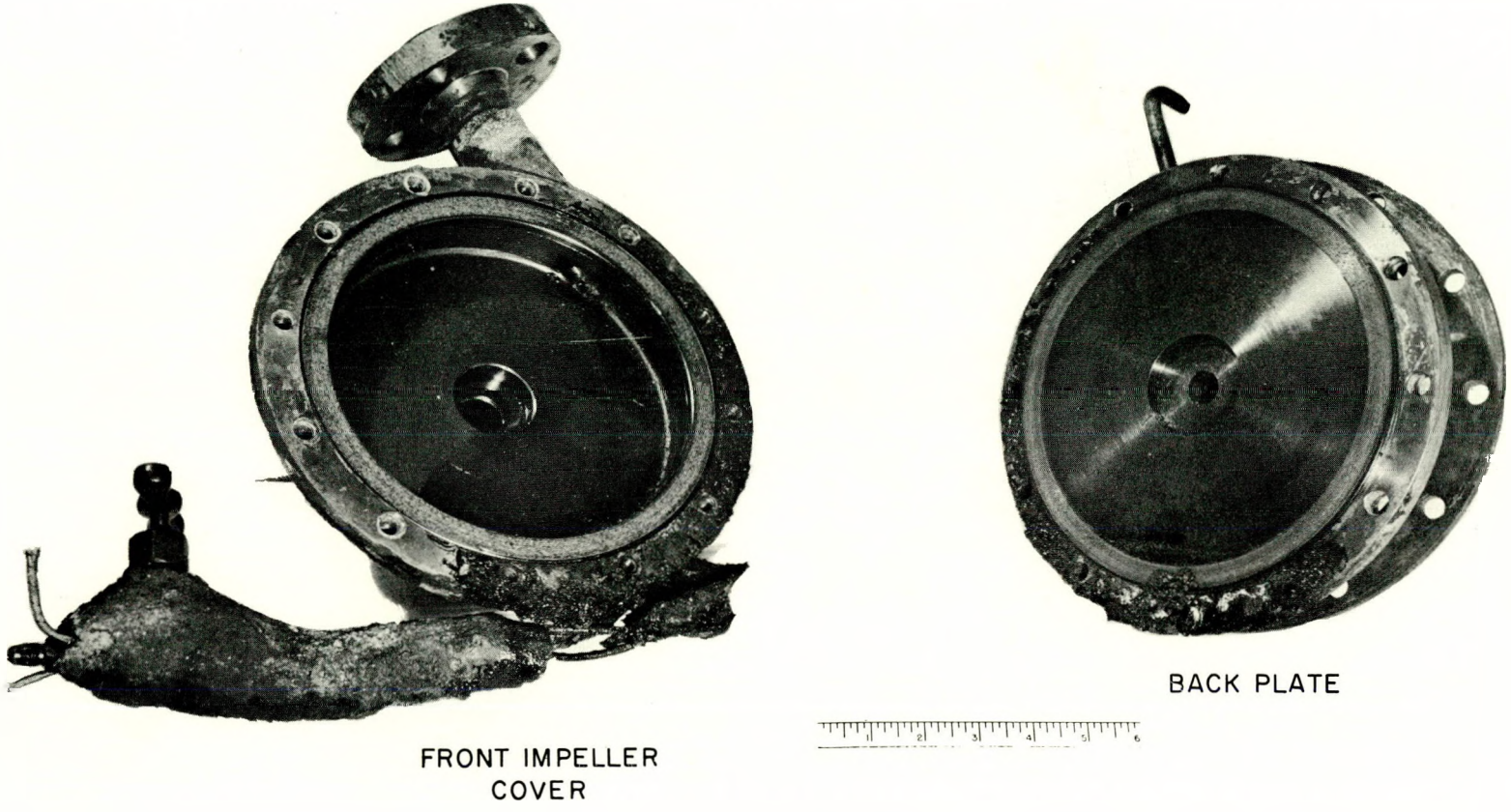

Fig. 36. Pump Impeller Housing

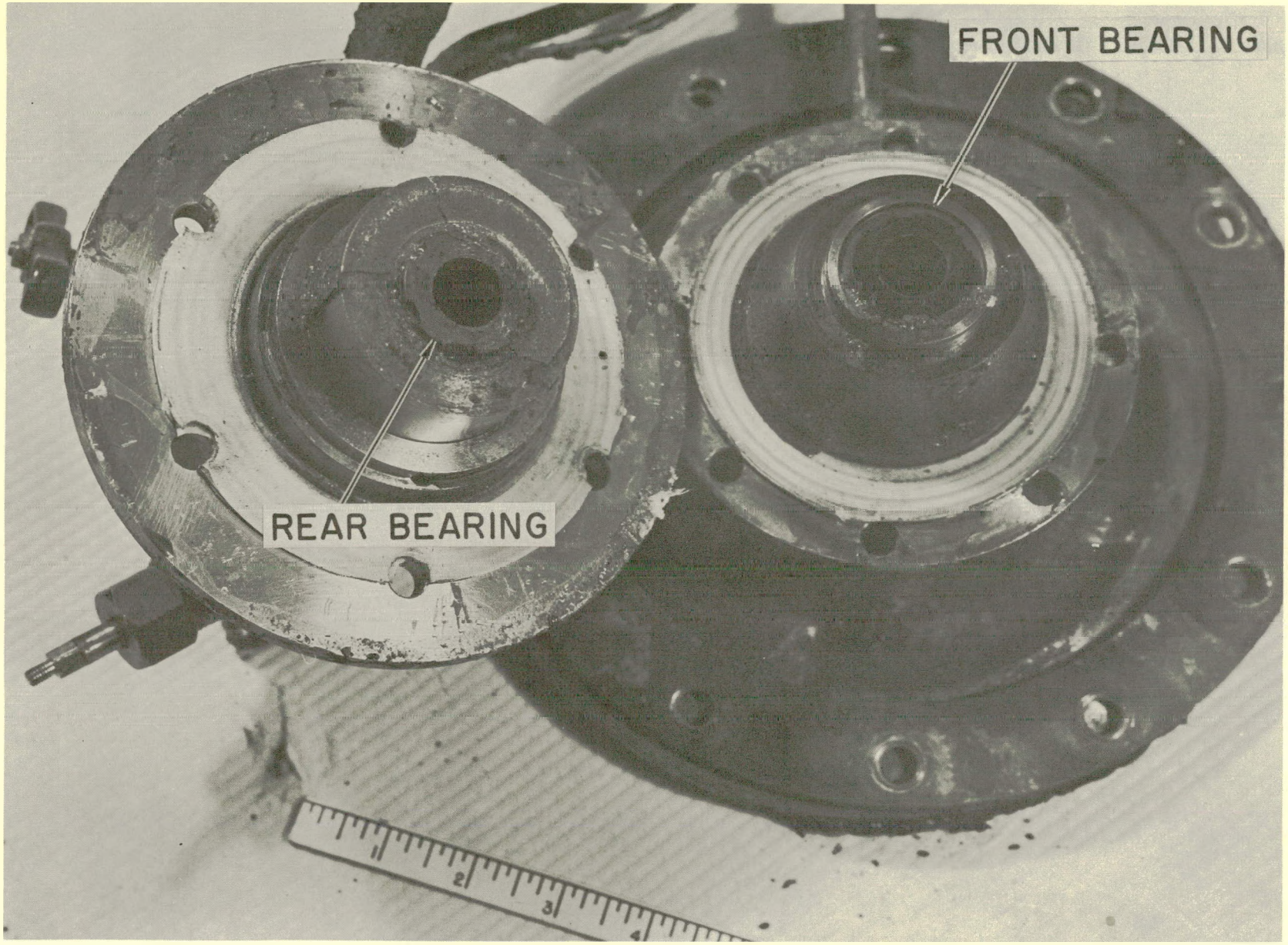

Fig. 37. Pump Bearings

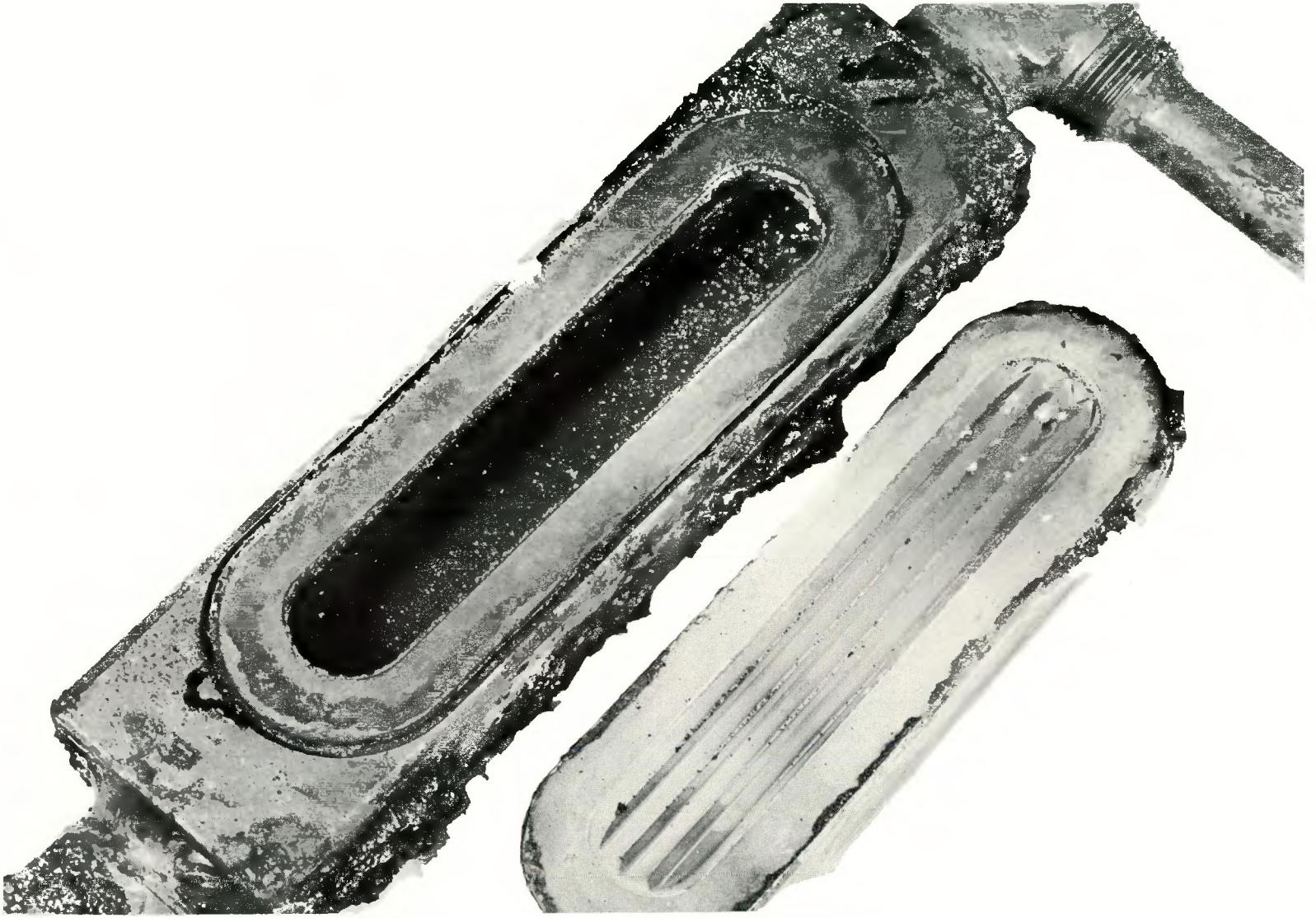

Fig. 38. Surge Tank Sight Glass

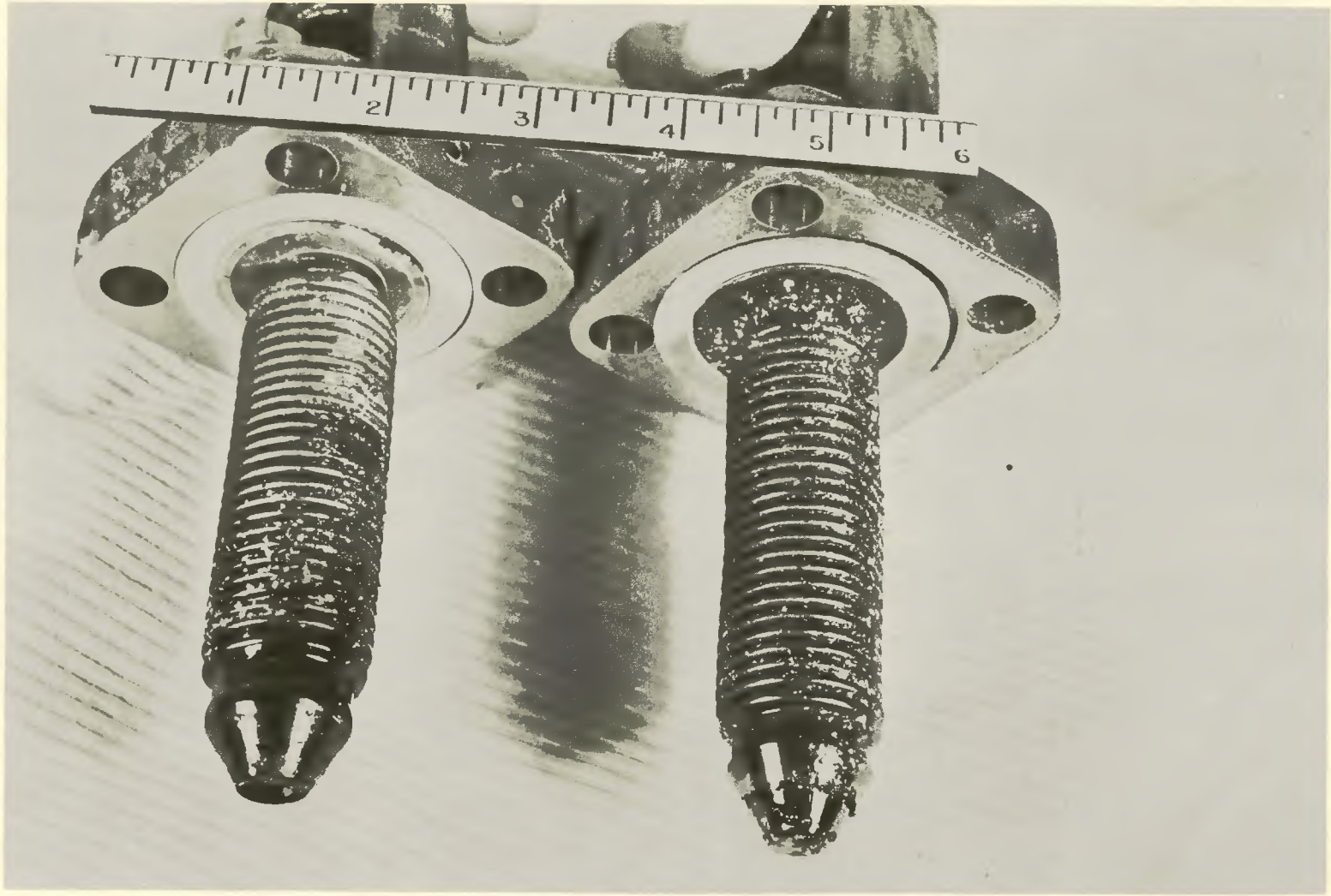

VALVE No. 5 VALVE No. 4

Fig. 39. Valve Stem Assemblies

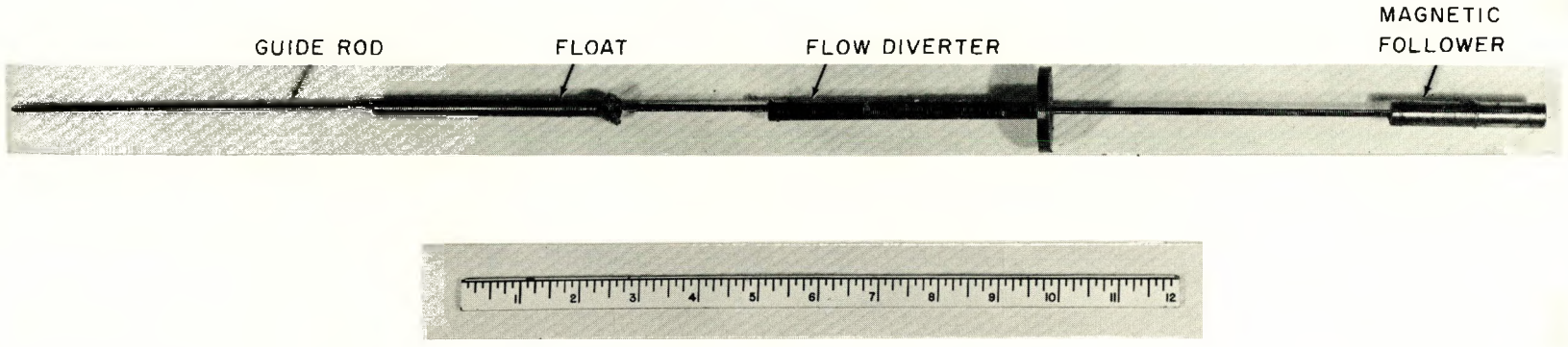

Fig. 40. Rotameter Float Assembly

APPENDICES

APPENDIX I
RADIATION DECOMPOSITION CALCULATIONS

A. GENERAL

The decomposition of the polyphenyls was assumed to be a function of the total amount of energy absorbed in the coolant from ionizing radiation and was assumed to be independent of the type of ionizing radiation to which the material is exposed. Energy is absorbed from fast and epithermal neutron moderation and the Compton scattering of the gamma photons. The scattering of fast and epithermal neutrons results in proton recoils which are highly ionizing for short distances. Interaction with thermal neutrons is not considered to cause any damage in the organic fluid, since the energy absorbed from these neutrons is negligible.

The amount of decomposition products in the coolant was determined by a semi-micro distillation at reduced pressure. Fractional distillations of large samples were in good agreement with the semi-micro technique.

High boiler residue (HBR) is defined as that portion of the coolant which is less volatile than para-terphenyl. G_{HBR} is the index used to define the decomposition rate occurring. The units of G_{HBR} are "pounds of HBR produced per megawatt-hour of energy absorbed in the coolant."

The following calculations illustrate how the HBR buildup rate was correlated with the energy absorption rate to determine G_{HBR}. The total production of HBR was plotted as a function of time. The slope of this curve at any time was then the HBR generation rate vs time. The time scale used was the accumulated reactor power in megawatt-hours $(Mwh)_o$, since the MTR operated at full power for over 98 percent of the time. The time scale is presented in megawatt-hours operating, and is abbreviated $(Mwh)_o$. Reactor fluxes are proportional to the reactor power and are stated when the reactor is operating at $40(Mwh)_o/hr$.

The energy absorption rate was determined from the fast-flux traverse plotted from the nickel monitor wires. Gamma heat generation was measured directly by the use of three calorimeters which were spaced to give a gamma traverse over the in-pile section. The separate contributions were added to give the total energy absorption rate in megawatt-hours absorbed per megawatt-hour operating $(Mwh)_a/(Mwh)_o$.

Dividing the HBR generation rate by the energy absorption rate gives G_{HBR}:

$$G_{HBR} = \frac{lbs\ HBR/(Mwh)_o}{(Mwh)_a/(Mwh)_o} = lbs\ HBR/(Mwh)_a$$

B. HIGH BOILER RESIDUE GENERATION RATE

During each irradiation, periodic sampling and analysis of the coolant resulted in a plot of HBR content vs time. Figure 41 shows such a plot for the irradiation of Santowax O - Santowax M. Discontinuities in the curve result from the dilution of the coolant by fluid additions to the system. Mass balances on the system using irradiated densities and allowing for material removed from the system through sampling and leakage results in a curve as shown in Fig. 42 for the total amount of HBR produced vs reactor operating time $(Mwh)_o$. Assuming the slope of the curve to be constant over short periods of time, the generation rate for different periods was determined by dividing the amount of HBR generated in the period by the reactor operating time. The rate thus computed has the units of lbs HBR generated/$(Mwh)_o$.

C. RADIATION ENERGY ABSORPTION IN THE COOLANT

The gamma and neutron fluxes were plotted as a traverse along the in-pile reservoir. Areas under the curves were used to determine average flux values to which all the hydrocarbon in the reservoir was exposed. Figure 43 presents the flux traverses for MTR Cycle 81, during which Santowax O - Santowax M was irradiated. It was found that although the individual fluxes varied somewhat during each cycle, the net energy deposited was nearly equal for all the cycles. Table XIX presents the individual contributions from each type of radiation for each of the cycles. There were no gamma calorimeters in MTR Cycles 77 and 78. However, the fast and thermal neutron monitors from these cycles indicated that these two fluxes were in good agreement with the fluxes measured during the cycles in which gamma calorimeters were utilized. It was therefore assumed that the energy deposition during these two cycles were the same as the rates observed in MTR Cycles 78, 81, 82, 83, and 84.

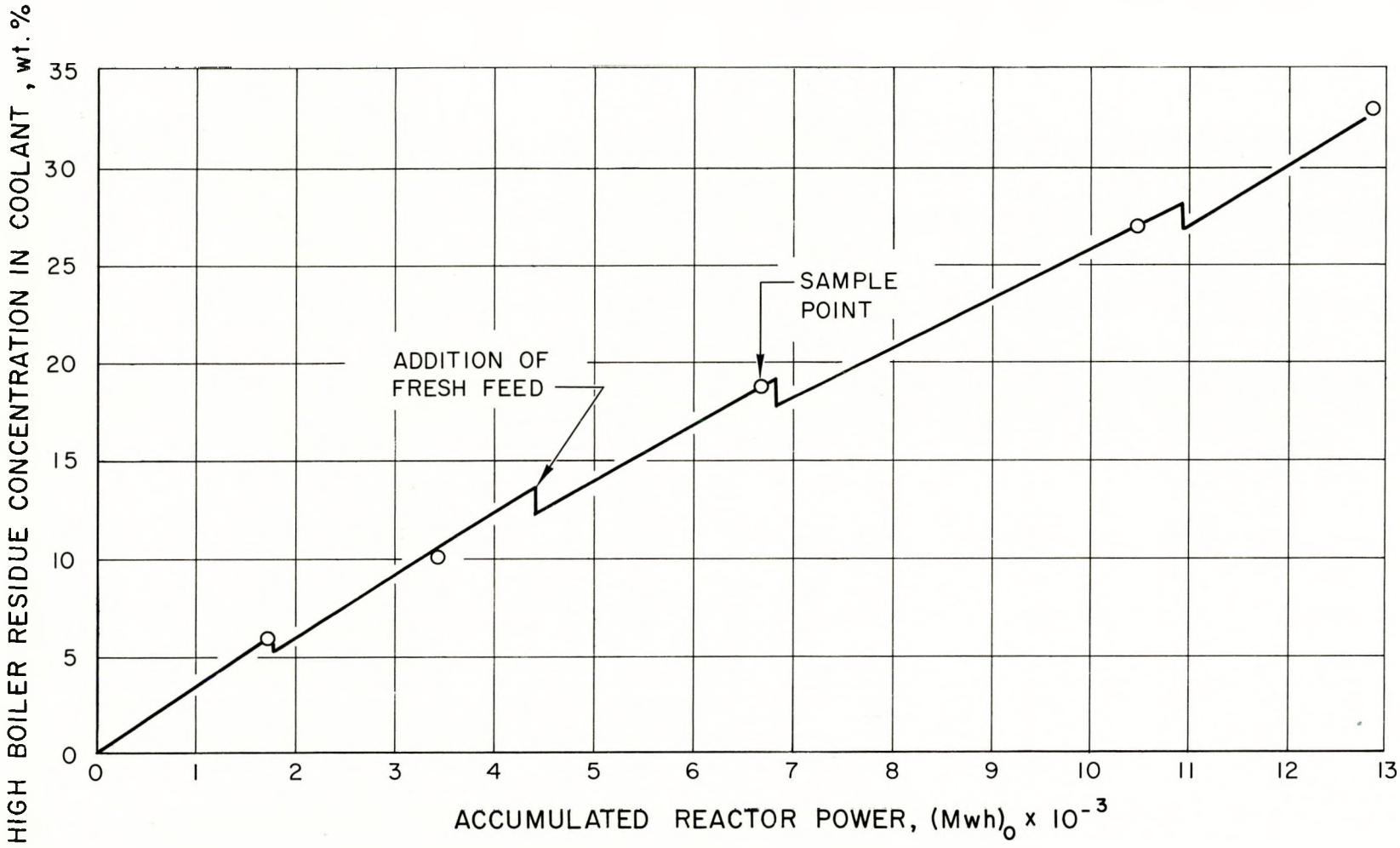

Fig. 41. High Boiler Residue Buildup vs Time

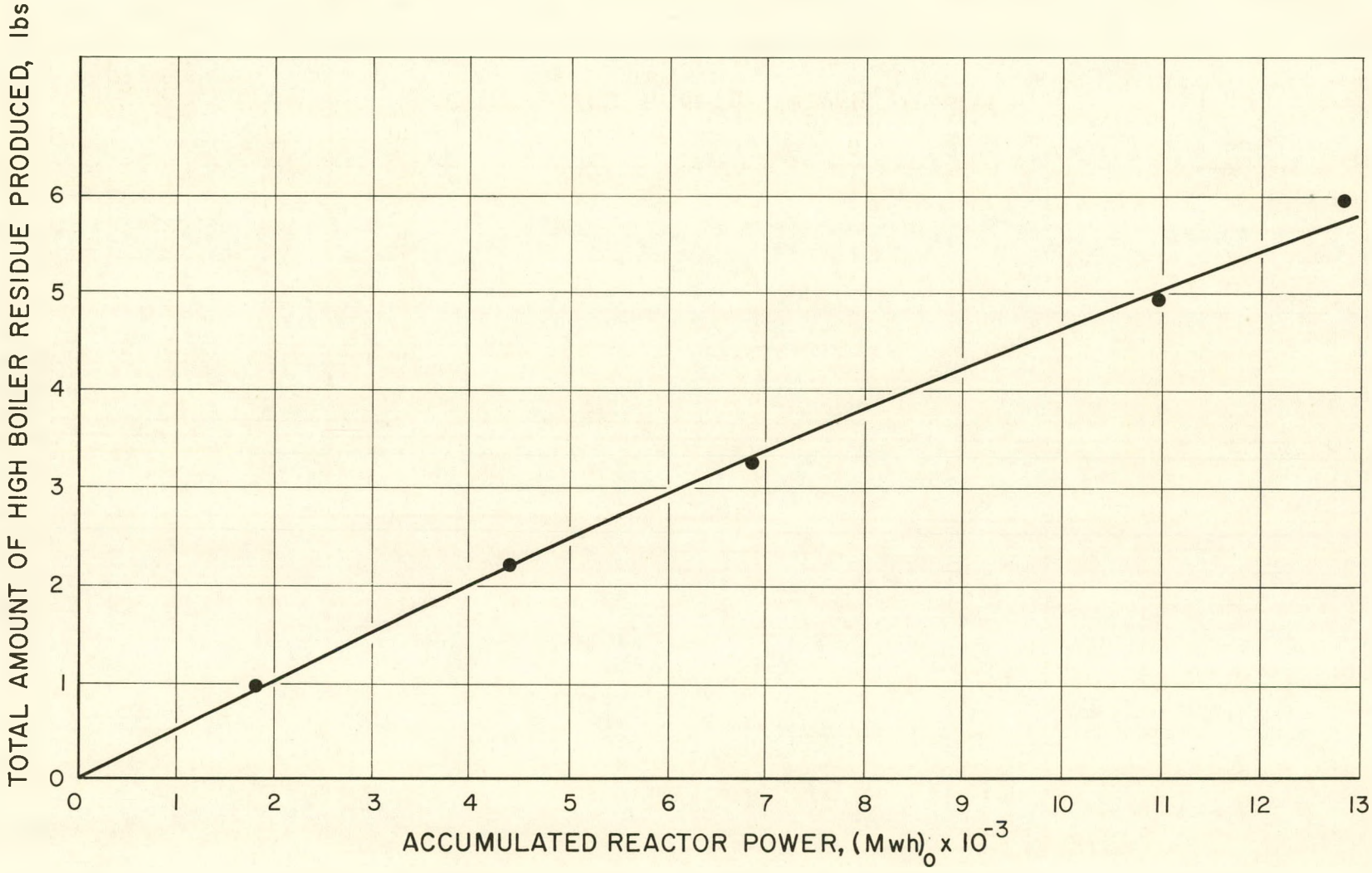

Fig. 42. High Boiler Residue Produced vs Time

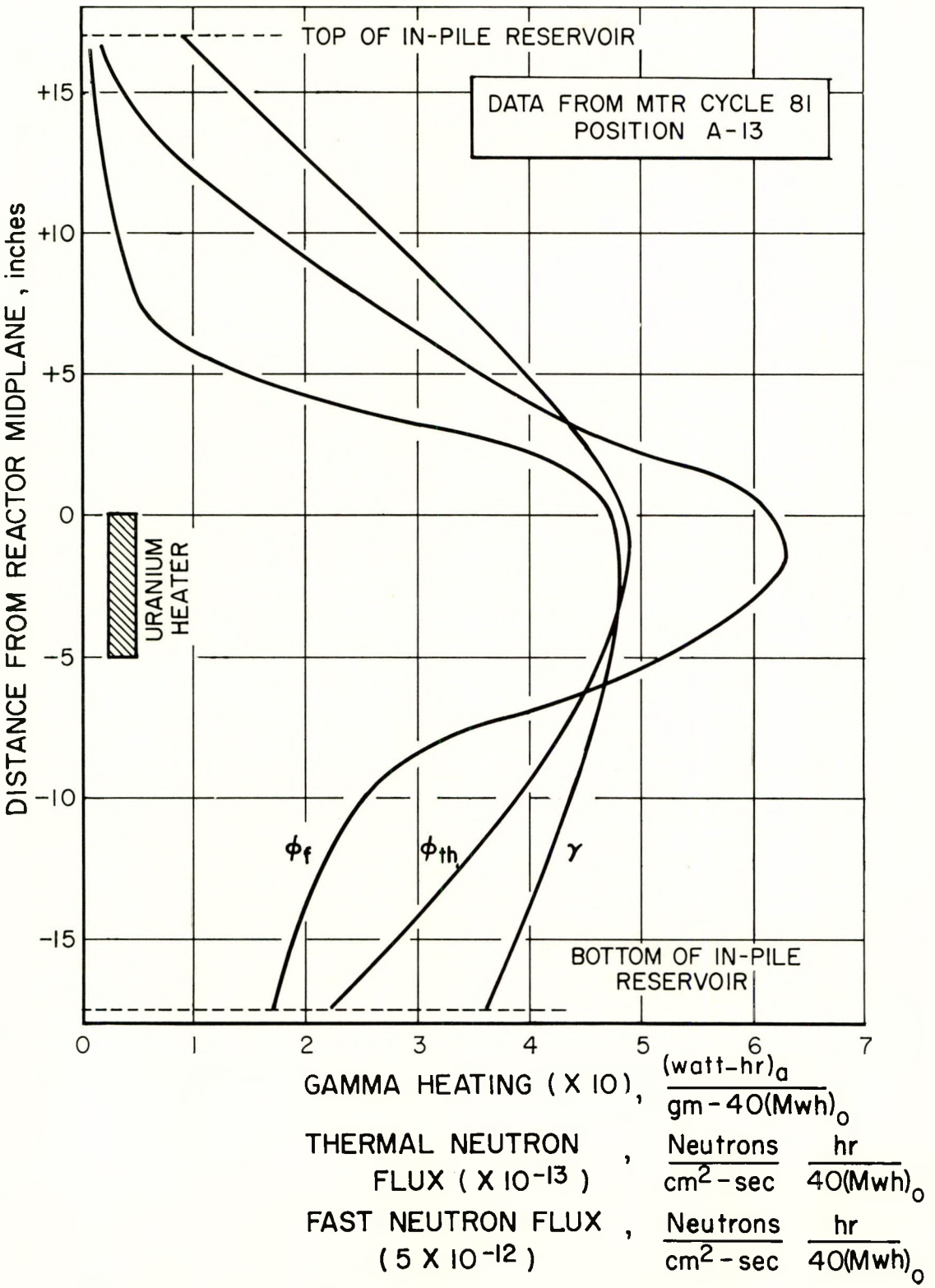

Fig. 43. Typical Flux Traverse Over In-Pile Section

TABLE XIX

INDIVIDUAL REACTOR FLUX CONTRIBUTIONS FOR ALL MATERIALS

Polyphenyl Irradiated	Distance from Reactor Midplane	Calorimeter Data: Heat Generation Rate in Calorimeter	Calorimeter Data: Thermal Neutron* Flux at Calorimeter ϕ_{th} (10^{-13})	Calorimeter Data: Self Absorption Heating in Calorimeter $0.0248(10^{13})\phi_{th}$	Calorimeter Data: Energy Absorption Rate from Gammas	Average Energy† Absorption from Gammas	Fast Neutron* Flux $\phi_f(10^{-12})$	Average Fast Neutron† Flux $\phi_f(10^{-13})$	Energy Absorption Rate from Fast Neutrons $\left[0.656(10^{-13})\phi_f\right]$	Net Energy Absorption Rate due to Gammas and Fast Neutrons
	inches	$\frac{(\text{watt-hr})_a}{\text{gm-40(Mwh)}_o}$	$\frac{\text{neutrons}}{\text{cm}^2\text{-sec}}$	$\frac{(\text{watt-hr})_a}{\text{gm-40(Mwh)}_o}$	$\frac{(\text{watt-hr})_a}{\text{gm-40(Mwh)}_o}$	$\frac{(\text{watt-hr})_a}{\text{gm-40(Mwh)}_o}$	$\frac{\text{neutrons}}{\text{cm}^2\text{-sec}}$	$\frac{\text{neutrons}}{\text{cm}^2\text{-sec}}$	$\frac{(\text{watt-hr})_a}{\text{gm-40(Mwh)}_o}$	$\frac{(\text{watt-hr})_a}{\text{gm-40(Mwh)}_o}$
Santowax R (MTR cycle 79)	+ 7.5	0.232	2.8	0.070	0.162		0.42			
	0	0.673	4.2	0.107	0.566	0.296	1.18	0.061	0.041	0.337
	-10.0	0.403	3.6	0.092	0.311		0.61			
Santowax O plus Santowax M (MTR cycle 81)	+ 7.5	0.140	3.4	0.086	0.054		0.51			
	0	0.603	4.9	0.124	0.479	0.285	1.24	0.060	0.041	0.326
	-10.0	0.538	4.0	0.103	0.435		0.50			
Extended Diphenyl Irradiation (MTR cycles 82, 83, 84)	+ 7.5	0.194	3.5	0.089	0.105		0.48			
	0	0.685	5.0	0.127	0.558	0.298	1.06	0.056	0.038	0.336
	-10.0	0.450	3.9	0.099	0.351		0.46			
§ Average for all Cycles										0.333

* Values of neutron fluxes were determined from Co-Al and Ni monitor wires.

† Determined from average area under curves. See Figure 43.

§ This energy absorption rate was used for the isopropyl diphenyl and the single cycle diphenyl irradiations since the neutron flux monitors from these cycles were not appreciably different than those presented in this table.

Two general assumptions were made in order to simplify the consideration of the energy absorption from the reactor fluxes.

It was assumed that the calorimeter rods did not depress the thermal neutron and gamma fluxes at the point of measurement. In the light of the small size of the rods (1/4 inch), this is probably a reasonable assumption.

The flux distribution in the vertical direction is known to change as the shim rods and control rods are readjusted to maintain a constant reactor power level. Since the reactor power level was constant, the number of fissions occurring over the volume of the reactor core are assumed not to change with fuel depletion. Readjustment of the shim and control rods is assumed to flatten the center peak and raise the outer edges of the flux traverses shown in Fig. 43. It is assumed that the area under these traverses is constant throughout the cycle and that the ratio of fast to thermal and gamma fluxes can be expected to remain unchanged. Therefore, the area under the traverses from the flux monitor wires is a good measure of the average flux over the entire in-pile assembly at any time during the cycle.

1. Energy Absorption from Gamma Photons

Gamma photons which interacted with the polyphenyl were primarily produced from the reactor core. However, gamma photons are also produced from thermal neutron capture reactions with the metallic components of the in-pile section, surrounding experiments, and thermal neutron capture in the calorimeter rods themselves. Since the calorimeter rods are situated in the organic reservoir, they see all the gammas produced from the above reactions. However, if a correction is applied to the calorimeter for the self-absorption gammas arising from the $(n-\gamma)$ reaction occurring within the calorimeters, then the net heat generation in the calorimeter rods is equal to the heat generation or absorption of gammas in the polyphenyl. It is assumed that the average photon energy is high enough so that Compton scattering accounts for all the absorption of the gamma photons. Under these conditions, the mass absorption cross sections for the polyphenyl and the steel calorimeter rods are approximately equal. A direct measure of the heat generation rate in watts/gm in the calorimeter rods, corrected for self absorption, is then equal to the energy absorbed in the organic medium from gamma photons.

The general equation describing the volumetric heat generation, with heat losses, in the calorimeter rods is:

$$\frac{q}{V} = k_f M^2 \left(\Delta t - \frac{\Delta t_b - \Delta t_t}{2\left[\sinh\left(\frac{Mx}{2}\right)\right]^2} \right) \frac{Btu}{hr\text{-}ft^3} \qquad (17) \qquad ...(1)$$

Heat losses from the calorimeter rod occur through the nitrogen-filled annulus surrounding the rod. This loss appears in the term M as follows:

$$M^2 = \frac{h_N \pi D_g}{k_f A_g} = \frac{4 h_N \pi D_g}{k_f \pi D_g^2} = \frac{4 h_N}{k_f D_g} \qquad ...(2)$$

The subscript N is for nitrogen and h_N is the heat transfer coefficient for the surroundings of the rod.

Since the surroundings consist of a narrow annulus, the heat losses can be approximated by conductive heat flow in the annulus:

$$\frac{q}{A} = \frac{k_N 2\pi x \, \Delta t}{\pi x D_g \ln \frac{D_{gs}}{D_g}} = h_N \Delta t = \frac{2 k_N \Delta t}{D_g \ln \frac{D_{gs}}{D_g}} \qquad (18) \qquad ...(3)$$

Cancelling Δt from eq. (3) and substituting into eq. (2) yields:

$$M^2 = \frac{8 k_N}{k_f D_g^2 \ln (D_{gs}/D_g)} \qquad ...(4)$$

Substituting the following numerical values in the expression for M^2

$$k_f = 24.7 \; Btu/hr\text{-}ft\text{-}^\circ F \; at \; 600^\circ F \qquad (19)$$

$$k_N = 0.026 \; Btu/hr\text{-}ft\text{-}^\circ F \; at \; 600^\circ F \qquad (20)$$

$$D_g = 0.0208\ ft$$

$$D_{gs} = 0.0358\ ft$$

We obtain

$$M^2 = 35.9\ ; \quad M = 5.99$$

The length of the calorimeter, x, appears in the term $\sinh\left(\frac{Mx}{2}\right)^2$ For the 1-inch calorimeter rod, x = 0.0833 ft. Also, it is more convenient to express the heat generation rate in the rod directly as G_t watts/gm instead of g/V, Btu/hr-ft^3.

Thus,

$$G_t = \frac{1}{(62.3)\,(7.87)\,(454)\,(3.413)}\left(\frac{q}{V}\right) \quad ,$$

where (62.3) (7.87) (454) is the density of the iron at 600°F in gm/ft^3, and 3.413 watt-hr = 1 Btu.

When the above conversion values and the value for x and M are substituted into eq. (1) for the heat generation rate in the calorimeter rod, the total heat generation for the 1-inch calorimeter rod becomes:

$$G_t = (1.17)\,(10^{-3})\left[\Delta t_t - \frac{\Delta t_b - \Delta t_t}{0.127}\right]\frac{(watts)_a}{gm} \quad . \qquad \ldots(5)$$

The net gamma energy absorption rate in the calorimeter and the polyphenyl may be obtained as follows:

As derived above, G_t includes all gammas from the core and the capture gammas from the interaction of thermal neutrons with materials in the in-pile assembly and surrounding experiments. G_t also includes the capture gammas produced in the calorimeter rod. Since it is assumed that negligible flux depression results at the position of the calorimeter, a correction for the self absorption of the gammas can be subtracted to obtain the net gamma absorption rate (G_N) in the calorimeter and the polyphenyl. The energy produced in the rods by the release of gammas upon neutron capture can be expressed as follows:

$$G_f = \frac{(7.6)\,(1.603)\,(10^{-13})\,(N_o)\,(\phi_{th})\,(\sigma)}{AW_{Fe}} \quad , (21) \qquad \ldots(6)$$

where 7.6 Mev is the gamma energy released per neutron capture in iron.[22] The quantity $(1.603)(10^{-13})$ is the conversion factor $\frac{(\text{watt})(\text{sec})_a}{(\text{Mev})_a}$.

Substituting the numerical values, we find that the total gamma energy released in the calorimeter rod due to the thermal neutron flux becomes:

$$G_f = (0.316)\,(10^{-13})\,\phi_{th} \ .$$

However, of the gammas produced from thermal neutron capture, only a fraction are absorbed. For a cylindrical shape with a uniform gamma flux, the following equation is applicable:

$$\textit{Fraction absorbed} = (1.3)\,(B)\,\frac{D_g}{2} \quad , (23) \qquad \ldots(7)$$

where 1.3 is the geometry constant and B is the energy absorption cross section of the iron in cm^2/cm^3.

In this case, $B = (0.024)(7.87)\ cm^2/cm^3$ for 7.6 Mev gammas.[24]

Upon substituting these values in the preceding equation, the fraction absorbed equals 0.078. Multiplying G_f by the fraction absorbed and subtracting this value from G_t, the net gamma energy absorbed in the polyphenyl for a 1-inch rod becomes:

$$G_N = \left((1.17)\,(10^{-3}) \left[\Delta t_t - \frac{\Delta t_b - \Delta t_t}{0.127} \right] - (0.078)\,(0.316)\,(10^{-13})\,\phi_{th} \right) \frac{(watt\text{-}hr)_a}{gm\text{-}40(Mwh)_o} \ . \qquad \ldots(8)$$

The addition of $\frac{\text{hr}}{40\ (\text{Mwh})_o}$ to the units is made since all fluxes and temperatures were measured when the reactor was operating at full power and generating $\frac{40\ (\text{Mwh})_o}{\text{hr}}$. Similar equations were derived for the other calorimeters which were of different lengths, x.

2. Energy Absorption Rate Due to Slowing of Fast Neutrons

The technique for these calculations has been previously derived.[25] In accordance with this reference, the following equation is utilized:

$$\Delta E = \phi_f E_1 \left[\Sigma_H \left(1 - \frac{E_2}{E_1} \right)_H + \Sigma_c \left(1 - \frac{E_2}{E_1} \right)_c \right] \frac{(Mev)_a}{cm^3\text{-}sec} \quad , \qquad \ldots(9)$$

where $\frac{E_1}{E_2}$ = energy loss per collision ratio

= 2.72 for hydrogen

= 1.172 for carbon,

ϕ_f = integrated fast flux as measured by the nickel monitor wires, and assumed to have an energy in excess of 1 Mev.

However, it is assumed that the energy absorbed from collisions occurring with fast neutrons with energies greater than 1 Mev is equal to the amount of energy absorbed from the remainder of collisions occurring down to thermal energy. Then the total energy, F, deposited in the coolant from the moderation of fast neutrons is equal to:

$$F = 2\Delta E \qquad \ldots(10)$$

Substituting the numerical values into the equation for F and using the conversion factor $(1.603)(10^{-13})$ watt-sec = 1 Mev, dividing by the average density of the organic in the in-pile reservoir = 0.78 gm/cm^3, and adding the units indicating the reactor power generation, we obtain:

$$F = (0.656)\ (10^{-13})\ \phi_f \ \frac{(watt\text{-}hr)_a}{gm\text{-}40\ (Mwh)_o} \quad . \qquad \ldots(11)$$

3. Total Energy Absorption Rate in the Coolant

The total energy absorption rate, T, in $\frac{(\text{watt-hr})\,a}{\text{gm-40(Mwh)}_o}$, is the sum of the contributions from the fast and epithermal fluxes, F, and the contribution from the gamma flux G_N. For the 1-inch rod, we have

$$T = \left[1.17\,(10^{-3})\left(\Delta t_t - \frac{\Delta t_b - \Delta t_t}{0.127}\right) - 0.0248\,(10^{-3})\,\phi_{th} + 0.656\,(10^{-13})\,\phi_f\right]\frac{(watt\text{-}hr)_a}{gm\text{-}40\,(Mwh)_o} \qquad ...(12)$$

Multiplying the above expression by the in-pile volume ($V = 0.0565\ ft^3$), the average density of the coolant (P_{av} lbs/ft^3), the conversion factor of 454 gms/lb, and $(10^{-6}\ \text{watt-hr})_a/(\text{Mwh})_a$, gives the desired expression for the rate of energy absorption.

Table IX presents the energy absorption rates for the three cycles in which all the monitors were present. It is apparent that the energy absorption rates were equal on a mass basis, and that the average value used for each irradiation was converted as discussed above to

$$T = (0.333)\,(454)\,(0.0565)\,(10^{-6})\,[G_N + F]\,P_{av}\,\frac{(Mwh)_a}{(Mwh)_o}$$

$$= 2.23\,(10^{-7})\,P_{av}\,[G_N + F]\,\frac{(Mwh)_a}{(Mwh)_o} \qquad ...(13)$$

4. Sample Calculations for Santowax O - Santowax M.

Table XX presents the calculation for G_{HBR} for the Santowax O - Santowax M irradiation. Figures 41 and 43 were utilized to compute the values in lines 2 4, and 8. Irradiated densities were used for the information presented in lines 6 and 7. Equation 13 was utilized to compute the energy absorption rate in line 10.

The value G_{HBR} for all the materials irradiated was computed in an identical manner as the sample calculation.

TABLE XX

TYPICAL CALCULATION FOR G_{HBR}

SANTOWAX O - SANTOWAX M

Date of Exposure	Jan 11-13	Jan 14-15	Jan 16-17	Jan 18-20	Jan 21-22	Jan 23-24	Jan 25-28
Period of Exposure $(Mwh)_o$	1800	1400	1170	2430	2200	1950	1905
Cumulative Exposure $(Mwh)_o$	1800	3200	4370	6800	9000	10,950	12,855
Average HBR Conc. (%)	3.1	7.4	11.7	15.6	20.3	25.4	29.6
Temp. in Reservoir, Average (°F)	670	670	620	605	590	640	620
Density During Exposure, (average) (lbs/cu-ft)	52.0	52.5	54.4	55.3	56.0	54.9	55.8
Mass of Material Irradiated (lbs)	2.94	2.97	3.07	3.12	3.16	3.10	3.15
HBR Produced (lbs)	0.94	0.67	0.57	1.08	0.93	0.81	0.75
Rate of HBR Production $[lbs/(Mwh)_o]\ 10^4$	5.22	4.79	4.87	4.44	4.23	4.15	3.94
Rate of Energy Absorption $[(Mwh)_a/(Mwh)_o]10^5$	1.11	1.12	1.16	1.18	1.19	1.17	1.19
G_{HBR}/lbs HBR/$(Mwh)_a$	47.0	42.8	42.0	37.6	35.5	35.4	33.1

APPENDIX II

TEST HEATER HEAT TRANSFER ANALYSIS

A thin-walled, electrically-heated tube was used as the test heater and was connected in series with the in-pile section. Figure 1 shows the location of the heater with respect to the rest of the apparatus. Thermocouples were silver-soldered to the tube at various points to provide a means of determining the temperature profile along the tube. A typical temperature profile is shown in Fig. 44. Inlet and outlet bulk fluid temperatures were determined by placing thermocouples in wells located in the fluid stream. The heater tube was surrounded by a trace-heated pipe which was maintained at the same temperature as the outer heater wall to prevent the transfer of heat between the tube and its surroundings.

Heat transfer runs were made at varying time intervals to determine the effect of increasing polymer concentration as a result of irradiating the organic fluid. Complete temperature profiles, inlet and outlet bulk temperatures, power-inputs, and bulk fluid velocities were recorded during each of the runs.

A. GENERAL EQUATION FOR DETERMINING COEFFICIENTS

Film heat transfer coefficients are expressed by the equation[26]

$$h = \frac{q/A}{t_w - t} \quad ,$$

where

q/A is the heat flux, Btu/hr-ft^2,

t_w is the wall temperature, °F,

t is the bulk temperature of the fluid, °F,

h is the heat transfer coefficient, Btu/hr-ft^2-°F.

Applying this equation to the external heater where the heat transfer coefficient was measured half way along the lower half of the heater gives:

$$h_t = \frac{(q/A)_L}{t_i - t_b} \quad , \qquad \ldots(1)$$

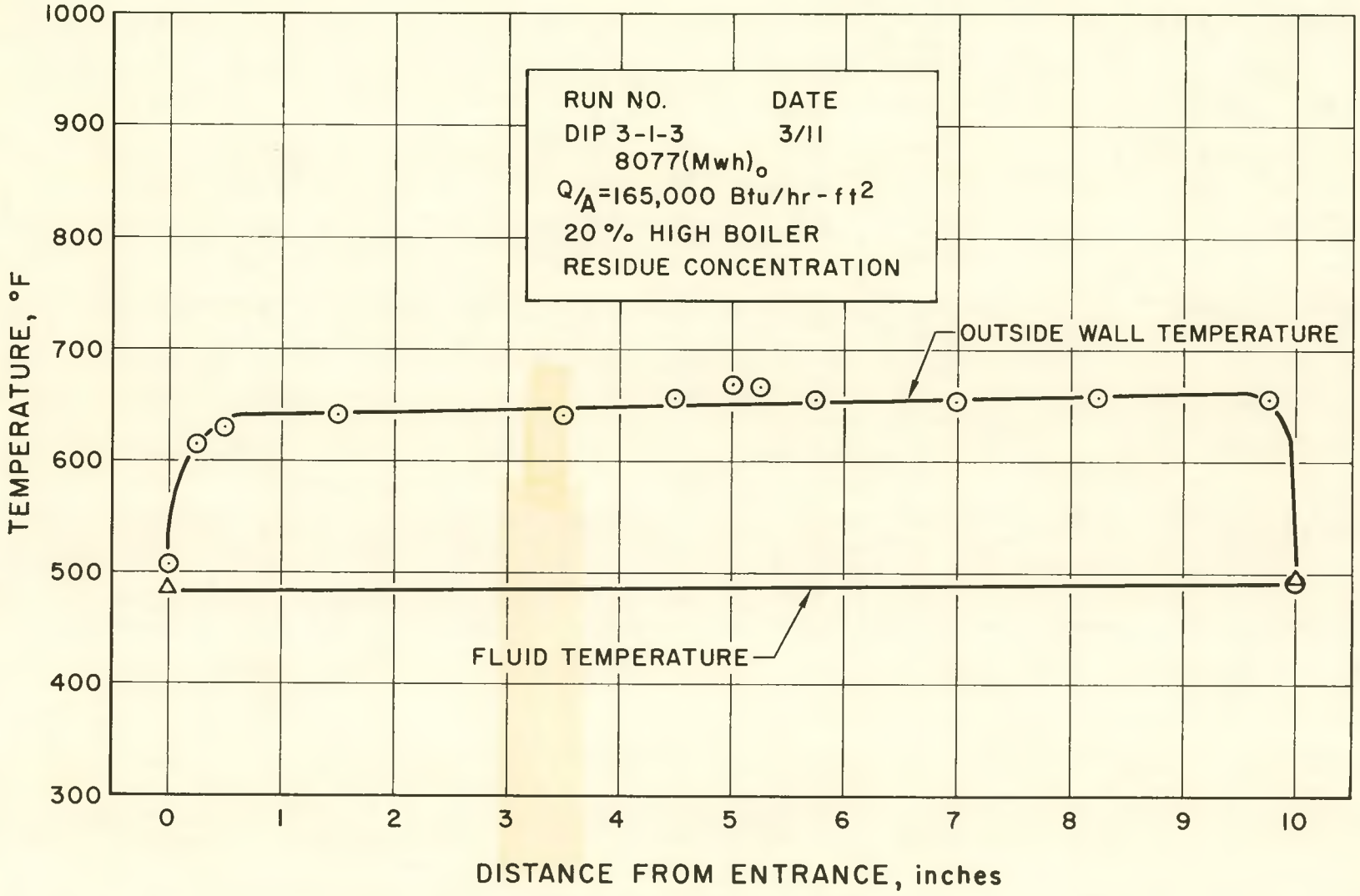

Fig. 44. Temperature Profile - Test Heater

where

$(q/A)_L$ is the external heater heat flux in the lower half of the heater, Btu/hr-ft^2,

t_i is the inner wall temperature of the external heater at the point where the heat transfer coefficient is measured, °F,

t_b is the bulk fluid temperature at the point of heat transfer coefficient measurement, °F,

h_t is the external heater heat transfer coefficient, Btu/hr-ft^2-°F.

B. DETERMINATION OF HEAT FLUX

The heat flux is obtained from the electric power input (I^2R) and the area of the heater (A):

$$q/A = C_1 I^2 R/A \quad \frac{Btu}{hr\text{-}ft^2} \quad ,$$

where

C_1 is a conversion factor,

I is the current, amperes,

R is the resistance of the heater, ohms.

A is the area of the test heater, ft^2

For the external heater, we have

$$(q/A)_L = (0.509\, I_t)^2 R_L \left(\frac{2 \times 3.413}{0.0745}\right) \frac{Btu}{hr\text{-}ft^2} \quad , \qquad \ldots(2)$$

where

$0.509 I_t$ is equal to the current through the lower half of the heater (Slight differences in resistance in either the heater tube sections or in the terminal junctions accounted for the uneven split in the current through two heater halves.),

R_L is the resistance of the lower half of the heater, ohms,

0.745/2 is the area of the lower half of the heater, ft^2,

3.413 is a conversion factor, Btu/hr-watt.

Applying measured values of resistance to eq. (2), it was possible to obtain a group of curves expressing $(q/A)_L$ as a function of I_t and the average wall temperature of the heat, t_{av} :

$$(q/A)_L = f(I_t, t_{av}) \qquad ...(2a)$$

C. DETERMINATION OF THE INNER WALL TEMPERATURE

The inner wall temperature, t_i , is obtained from the outer wall temperature, t_o , which is the average of two thermocouples located about 7/8 inch on either side of the point of measurement. The equation expressing the temperature drop through the wall is:[27]

$$t_o - b_i = (q/V)_L \left(\frac{D^2}{16k}\right) + C_2 ln \frac{D}{2} + C_3 \ °F \ ,$$

where

$(q/V)_L$ is the volumetric heat strength, Btu/hr-ft^3,

D is the diameter, ft,

k is the thermal conductivity of the tubing, Btu/hr-ft-°F,

C_2 and C_3 are constants.

Applying appropriate boundary conditions, the above equation becomes

$$t_o - t_i = (q/V)_L \left(\frac{1}{8k_{ss}}\right)\left[\frac{D_{ir}^2 - D_{or}^2}{2} + D_{or}^2 ln \left(\frac{D_{or}}{D_{ir}}\right)\right] \ °F \ , \qquad ...(3)$$

where

$(q/V)_L$ is the volumetric heat strength of the lower half of the heater, Btu/hr-ft^3,

k_{ss} is the thermal conductivity of stainless steel, Btu/hr-ft-°F,

D_{or} is the outer diameter of the heater, ft,

D_{ir} is the inner diameter of the heater, ft.

The heat generation rate, q_L, for the lower half of the heater is

$$q_L = (q/A)_L \quad \frac{0.0745}{2} \quad . \qquad \ldots(4)$$

The volume, V_L, of the lower half of the heater is

$$V_L = \frac{\pi}{4} (D_{or}^2 - D_{ir}^2) (L_L) \ . \qquad \ldots(5)$$

Substituting eqs. (4) and (5) into (3) gives

$$t_o - t_i = \frac{(q/A)_L \left(\frac{0.0745}{2}\right)}{2\pi k_{ss} L_L} \left[\frac{D_{or}^2}{D_{or}^2 - D_{ir}^2} \ ln\left(\frac{D_{or}}{D_{ir}}\right) - \frac{1}{2} \right] ,$$

where

D_{or} is 0.0311 ft,

D_{ir} is 0.0286 ft,

L_L is 0.417 ft,

k_{ss} is 12.05 Btu/hr-ft-°F.[28]

Substituting the numerical values in the above equation yields

$$t_i = t_o - 4.88 \times 10^{-5} (q/A)_L \ . \qquad \ldots(6)$$

D. DETERMINATION OF THE BULK TEMPERATURE AT THE POINT OF MEASUREMENT

The bulk temperature, t_b, was determined at a point three-quarters of the way along the heated length of the heater corresponding to the point of inner wall temperature measurement.

1. For the First Two Cycles:

For the first two cycles, i.e., those utilizing isopropyl diphenyl and diphenyl, the outlet bulk temperature was not obtained, due to a faulty thermocouple. Therefore, for these two cycles, the bulk fluid temperature (t_b) was calculated from the inlet bulk temperature and the calculated temperature rise:

$$t_b = t_{bi} + \Delta t_r \ ^\circ F \ . \qquad \ldots(7)$$

The equation expressing temperature rise due to sensible heat absorption is

$$\Delta t_r = \frac{q}{WC_p} \ ^\circ F \ , \qquad \ldots(8)$$

where

W is the mass flow rate, lb/hr,

C_p is the specific heat of the coolant, Btu/lb-°F.

The heat rate in the upper half of the heater is

$$q_{up} = \frac{0.491}{0.509}(q/A)_L \left(\frac{0.0745}{2}\right) = 0.0359\,(q/A)_L \frac{Btu}{hr} \ .$$

The heat rate to a point half way through the lower half of the heater is

$$\frac{q_{up}}{2} = (q/A)_L \left(\frac{0.0745}{4}\right) \ \frac{Btu}{hr} \ .$$

The total heat rate, q, is the sum of the above two equations:

$$q = 0.0545(q/A)_L \ \frac{Btu}{hr} \ . \qquad \ldots(9)$$

Substituting eqs. (8) and (9) in eq. (7) yields:

$$t_b = t_{bi} + \frac{0.0545\,(q/A)_L}{WC_p} \ ^\circ F \ . \qquad \ldots(10)$$

2. For the Remaining Cycles

For all remaining cycles, the bulk temperature at the point of measurement was the weighted arithmetic average of the inlet and outlet bulk temperature:

$$t_b = 0.25\,t_{bi} + 0.75\,t_{bo} \ ^\circ F \ . \qquad \ldots(11)$$

E. COMBINED EXPRESSION FOR HEAT TRANSFER COEFFICIENT

Equations (2), (6), and (10) are substituted in eq. (1) to give a combined expression for determining the heat transfer coefficient during the first two cycles:

$$h_t = \frac{L}{\dfrac{t_o - t_i}{(q/A)_L} - \dfrac{0.0545}{WC_p} - 4.88 \times 10^{-5}} \ \frac{Btu}{hr\text{-}ft^2\text{-}^\circ F} \ . \qquad \ldots(12)$$

Substitution of eqs. (2), (6), and (11) in eq. (1) results in a similar expression for the remaining cycles:

$$h_t = \frac{L}{\dfrac{t_o - 25t_{bi} - 75t_{bo}}{(q/A)_L} - 4.88 \times 10^{-5}} \ \frac{Btu}{hr\text{-}ft^2\text{-}^\circ F} \ . \qquad \ldots(13)$$

Upon substitution of data in eqs. (12) and (13), the coefficient is estimated to be accurate to ± 10 percent.

APPENDIX III

URANIUM HEATER HEAT TRANSFER ANALYSIS

A. GENERAL EQUATION USED FOR OBTAINING COEFFICIENT, h_u

By analogy with Section A, Appendix II, we have

$$h_u = \frac{(q/A)_u}{t_{os} - t_{bu}} \quad \frac{Btu}{hr\text{-}ft^2\text{-}°F} \quad ,$$

where

$(q/A)_u$ is the uranium heater heat flux, Btu/hr-ft^2,

t_{os} is the wall temperature of the heater, °F,

t_{bu} is the bulk fluid temperature at the point of measurement, °F.

B. DETERMINATION OF HEAT FLUX, $(q/A)_u$

The heat flux in the uranium heater could be determined using two methods:

1) from the radial temperature difference in the heater, and

2) from the thermal neutron flux.

1. Determination of Heat Flux from Radial Temperature Difference in the Uranium Heater

The heat flux is directly proportional to the radial temperature difference between the inside of the uranium tube and the outside of the stainless-steel tube. The radial temperature difference is the sum of two differences: 1) the temperature difference across the uranium tube $(t_{iu}-t_{ou})$, and 2) the temperature difference across the NaK and the stainless steel tube $(t_{ou}-t_{os})$. The temperature difference across the uranium tube is determined by considering it as a volumetric heat source. Using techniques similar to those in Section C, Appendix II, one obtains

$$t_{iu} - t_{ou} = \frac{q_u}{V_u 8 k_u} \left[\frac{D_{ou}^2 - D_{iu}^2}{2} - D_{iu} \ln \left(\frac{D_{ou}}{D_{iu}} \right) \right] °F \quad ,$$

where

q_u is the heat generation rate, Btu/hr,

V_u is the uranium volume, ft^3,

D_{ou} is the outer diameter of the uranium (0.0334 ft),

D_{iu} is the inner diameter of the uranium (0.0181 ft),

k_u is the thermal conductivity of uranium at 900°F (19.3 Btu/hr-ft-°F).[29]

The volume of the uranium is determined by

$$V_u = \frac{\pi}{4}(D_{ou}^2 - D_{iu}^2) L_u \quad .$$

Substituting the above equation in the previous equation, one obtains

$$t_{iu} - t_{ou} = \frac{q_u}{2\pi k_u L_u} \left[\frac{1}{2} - \frac{D_{iu}^2}{D_{ou}^2 - D_{iu}^2} \ln\left(\frac{D_{ou}}{D_{iu}}\right) \right] °F ,$$

where

L_u is the length of uranium in feet. (0.417 ft)

The temperature drop across the NaK and stainless-steel tube is controlled by thermal conductive resistance, and is expressed by

$$t_{ou} - t_{os} = \frac{q_u}{2\pi L_u} \left[\frac{\ln\left(\frac{D_{is}}{D_{ou}}\right)}{k_{NaK}} + \frac{\ln\left(\frac{D_{os}}{D_{is}}\right)}{k_{ss}} \right] °F ,$$

where

D_{is} is the inner diameter of the stainless steel (0.0382 ft),

D_{os} is the outer diameter of the stainless steel (0.0521 ft),

k_{NaK} is the thermal conductivity of the NaK at 875°F (15.6 Btu/hr-ft-°F).[30]

Adding the above two equations gives

$$t_{iu} - t_{os} = \frac{q_u}{2\pi L_u}\left[\frac{1}{2k_u} + \frac{ln\left(\frac{D_{is}}{D_{ou}}\right)}{k_{NaK}} + \frac{ln\left(\frac{D_{os}}{D_{is}}\right)}{k_{ss}} - \frac{D_{iu}^2}{k_u(D_{ou}^2 - D_{iu}^2)}\ ln\left(\frac{D_{ou}}{D_{iu}}\right)\right] {}^{\circ}F\ ,$$

where

q_u is equal to $(q/A)_u \pi D_{os} L_u$ Btu/hr .

Substituting, there results

$$t_{iu} - t_{os} = \frac{(q/A)_u D_{os}}{2}\left[\frac{1}{2k_u} + \frac{ln\left(\frac{D_{is}}{D_{os}}\right)}{k_{NaK}} + \frac{ln\left(\frac{D_{os}}{D_{is}}\right)}{k_{ss}} - \frac{D_{iu}^2}{k_u(D_{ou}^2 - D_{iu}^2)}\ ln\left(\frac{D_{ou}}{D_{iu}}\right)\right] \frac{Btu}{hr\text{-}ft^2}\ .$$

Solving for $(q/A)_u$ we obtain

$$(q/A)_u = \frac{2(t_{iu} - t_{os})}{D_{os}} \times \frac{1}{\left[\frac{1}{2k_u} + \frac{ln\left(\frac{D_{is}}{D_{os}}\right)}{k_{NaK}} + \frac{ln\left(\frac{D_{os}}{D_{is}}\right)}{k_{ss}} - \frac{D_{iu}^2}{ku(D_{ou}^2 - D_{iu}^2)}\ ln\left(\frac{D_{ou}}{D_{iu}}\right)\right]} \frac{Btu}{hr\text{-}ft^2}$$

The above equation must be slightly modified to correct for the situation where the thermocouple is located under the wall. This is accomplished by using the standard equation for conduction through a solid, the equation for temperature drop through the laminar boundary, the coefficient of heat transfer for unirradiated material, and the initial value of the thermal neutron flux.

2. Determination of Heat Flux from Thermal Neutron Flux

The thermal neutron flux in the region of the uranium heater was determined using four cobalt-aluminum wire monitors. From the flux distribution around the pipe, the flux at the heater was estimated using diffusion theory, and the absorption cross sections of the materials intervening between the flux monitors and the uranium heater.

The product of the thermal neutron flux (ϕ_{th}), the mass, the microscopic fission cross section of the fissionable material, and the heat transfer surface of the heater gives the heat flux:[31]

$$(q/A)_u = \frac{3.413(8.3 \times 10^{10})\,(m\sigma_u)\,\phi_n}{A_u} \quad ,$$

where

σ_u is the microscopic fission cross section of U^{235} for thermal neutrons corrected using the $1/V$ law at the MTR average temperature of 115°F.

APPENDIX IV

NOMENCLATURE

Symbol	Dimensions	Description
A	ft^2	Area
A_g	ft^2	Cross-sectional area of calorimeter rod
A_u	ft^2	Area of the uranium heater heat transfer surface
AW_u	gms/gram mol	Atomic weight of uranium
AW_{Fe}	gms/gram mol	Atomic weight of iron
B	cm^2/cm^3	Volumetric energy absorption cross section of iron for 7.6 Mev gammas = 0.189 cm^{-1}
C_l	Btu/watt-hr	Conversion factor
C_2, C_3	°F	Constants determined by boundary conditions, inner and outer diameters of heater
c_p	Btu/lb-°F	Specific heat
D	ft	Diameter
D_g	ft	Diameter of the calorimeter rod = 0.0208 ft
D_{gs}	ft	Inner diameter of the sheath enclosing the calorimeter rod = 0.0358 ft
D_{ir}	ft	Inner diameter of the test heater = 0.0286 ft
D_{is}	ft	Inner diameter of the stainless steel tube in in the uranium heater = 0.0382 ft
D_{iu}	ft	Inner diameter of the uranium in the uranium heater = 0.0181 ft
D_{or}	ft	Outer diameter of the test heater = 0.0311 ft
D_{os}	ft	Outer diameter of the stainless steel tube in the in-pile heater = 0.0521 ft
D_{ou}	ft	Outer diameter of the uranium in the uranium heater = 0.0334 ft

Symbol	Dimensions	Description
F	$\frac{(\text{watt-hr})_a}{\text{gm-40(Mwh)}_o}$	Energy absorption rate in polyphenyl due to fast neutron moderation
G_f	$\frac{(\text{watt-hr})_a}{\text{gm-40(Mwh)}_o}$	Heat generation rate in calorimeter rod due to n-gamma reactions in the iron of the calorimeter rod
G_N	$\frac{(\text{watt-hr})_a}{\text{gm-40(Mwh)}_o}$	Net gamma energy absorption rate in polyphenyl, i.e., gamma energy absorption exclusive of n-gamma reactions in calorimeter rod
G_t	$\frac{(\text{watt-hr})_a}{\text{gm-40(Mwh)}_o}$	Total heat generation rate in calorimeter rod
h	Btu/hr-ft^2-°F	Heat transfer coefficient
HBR	lbs	High boiler residue
h_N	Btu/hr-ft^2-°F	Heat transfer coefficient of the nitrogen annulus surrounding the calorimeter rod at 600°F
h_t	Btu/hr-ft^2-°F	Heat transfer coefficient, test heater
h_u	Btu/hr-ft^2-°F	Heat transfer coefficient, uranium heater
I	amperes	Current
I_t	amperes	Total current to the test heater
k	Btu/hr-ft-°F	Thermal conductivity
k_f	Btu/hr-ft-°F	Thermal conductivity of the iron calorimeter rod at 600°F = 24.7 Btu/hr-ft-°F
k_N	Btu/hr-ft-°F	Thermal conductivity of nitrogen at 600°F = 0.026 Btu/hr-ft-°F
k_{NaK}	Btu/hr-ft-°F	Thermal conductivity of NaK at 875°F = 15.6 Btu/hr-ft-°F
k_{ss}	Btu/hr-ft-°F	Thermal conductivity of Type 321 stainless steel at 800°F = 12.05 Btu/hr-ft-°F
k_u	Btu/hr-ft-°F	Thermal conductivity of uranium at 900°F = 19.3 Btu/hr-ft-°F

Symbol	Dimensions	Description
L_L	ft	Heated length of the lower half of the test heater = 0.417 ft
L_u	ft	Length of the uranium in the uranium heater = 0.417 ft
m	grams	Mass of fissionable material
M	$(ft)^{-1}$	$(h_N \pi D_g / k_F A_g)^{1/4}$
$(Mwh)_o$	megawatt hours	Energy delivered by the Materials Testing Reactor.
$(Mwh)_a$	megawatt hours	Energy absorbed by the coolant.
N_o	atoms/gm mol	Avogadro's number = 6.023×10^{23} atoms/gm mol
q	Btu/hr	Rate of heat flow
q_{Lr}	Btu/hr	Rate of heat flow in lower half of test heater
q_t	Btu/hr	Total rate of heat flow from upper part of test heater and half of lower half of heater
q_u	Btu/hr	Rate of heat generation in the uranium heater
q_{up}	Btu/hr	Rate of heat flow in upper half of test heater
q/A	$Btu/hr\text{-}ft^2$	Heat flux
$(q/A)_L$	$Btu/hr\text{-}ft^2$	Heat flux, lower half of test heater
$(q/A)_u$	$Btu/hr\text{-}ft^2$	Heat flux, uranium heater
q/V	$Btu/hr\text{-}ft^3$	Volumetric heat strength
$(q/V)_g$	$Btu/hr\text{-}ft^3$	Total volumetric heat strength, calorimeter rod
$(q/V)_L$	$Btu/hr\text{-}ft^3$	Volumetric heat strength, lower half of test heater
R	ohms	Resistance

Symbol	Dimensions	Description
R_L	ohms	Resistance in lower half of test heater
t	°F	Bulk temperature
t_{av}	°F	Average test heater wall temperature
t_b	°F	Fluid bulk temperature at test heater station where heat transfer coefficient is measured
t_{bu}	°F	Fluid bulk temperature at uranium heater station where heat transfer coefficient is measured
t_{bi}	°F	Inlet bulk temperature, test heater
t_{bo}	°F	Outlet bulk temperature, test heater
t_i	°F	Inner wall temperature of test heater at station where heat transfer coefficient is measured
t_{iu}	°F	Temperature on the inside of the uranium tube
t_o	°F	Outer wall temperature of test heater at station where heat transfer coefficient is measured
t_{os}	°F	Outer wall temperature of uranium heater at station where heat transfer coefficient is measured
t_{ou}	°F	Temperature on the outside of the uranium tube
t_w	°F	Wall temperature
T	$\frac{(\text{Mwh})_a}{(\text{Mwh})_o}$	Total energy absorption rate in polyphenyl
V	ft^3	Volume
V_L	ft^3	Volume of the lower half of the test heater
V_u	ft^3	Volume of the uranium in the uranium heater
x	ft	Length of the calorimeter
w	lb/hr	Mass rate of flow

Symbol	Dimensions	Description
Δt	°F	Temperature difference across the nitrogen annulus.
Δt_b	°F	Temperature difference between the base of the gamma calorimeter and its surroundings
Δt_r	°F	Temperature rise of polyphenyl from test heater inlet to station where heat transfer coefficient is measured
Δt_t	°F	Temperature difference between the top of the gamma calorimeter and its surroundings
ρ_{av}	gm/cm^3	Average density of the in-pile polyphenyl
ρ_f	gm/cm^3	Density of iron at 600°F = 7.87 gm/cm^3
σ	cm^2/nucleus	Microscopic thermal neutron capture cross section of iron for neutrons having energies at reactor temperature of 319°K
σ_u	cm^2/atom	Thermal neutron fission cross section of U^{235} at 319°K
Σ_f	cm^{-1}	Macroscopic thermal neutron capture cross section of iron at 319°K
ϕ_f	neutrons/cm^2-sec	Fast neutron flux as measured by the nickel monitor wire for neutron energies greater than 1 Mev
ϕ_{th}	neutrons/cm^2-sec	Thermal neutron flux
Σ_H	cm^{-1}	Macroscopic scattering cross section for hydrogen = 0.109 cm^{-1}
Σ_C	cm^{-1}	Macroscopic scattering cross section for carbon = 0.08 cm^{-1}

REFERENCES

1. E. L. Colichman and R. H. J. Gercke, "Radiation Stability of Polyphenyls," Nucleonics 14 No. 7, 50-54 (1956)

2. R. O. Bolt et al., "Organics as Reactor Moderator - Coolants; Some Aspects of Their Thermal and Radiation Stabilities," Proceedings of the International Conference on the Peaceful Uses of Atomic Energy (Geneva, August 1955) (New York: United Nations, 1956), VII, 546-555

3. E. L. Colichman and R. F. Fish, "Resistance of Terphenyls to Heat and Radiation," Nucleonics 15 No. 2, 72-74 (1957)

4. S. Nakazato and R. H. J. Gercke, "Organic In-Pile Loop," NAA-SR-1592, July 1956

5. M. McEwen, "Preliminary Engineering Study of Organic Nuclear Reactor Coolant - Moderators," Montsanto R & E CR 964, March 31, 1956

6. C. A. Trilling, Nucleonics 14 No. 8, 42 (1956)

7. C. A. Trilling, "OMRE Reactor Description," Proceedings of the SRE-OMRE Forum (Los Angeles, November 1956), TID-7525 (NAA-SR-1804), January 15, 1957

8. R. J. Nertney, "Calculated Surface Temperatures for Nuclear Systems and Analysis of Their Uncertainties," IDO 16343, June 1, 1957, p. 63

9. C. F. Leyse, "Facilities for Irradiations Within the MTR Reactor Tank," IDO 16048, June 5, 1953

10. M. McEwen, op. cit., p. 23

11. Ibid., p. 7

12. M. Silberberg and D. A. Huber, "Heat Transfer Characteristics of Polyphenyl Coolants," NAA-SR-2314, November 1957

13. G. M. Dusenberre, Numerical Analysis of Heat Flow (New York: McGraw-Hill Book Co., 1949)

14. H. E. Kline, N. J. Gioseffi, and W. N. Bley, "Dynamic Corrosion in Polyphenyls Under Irradiation," NAA-SR-2046, May 1958

15. R. H. J. Gercke, "OMRE Research and Development Program," Proceedings of the SRE-OMRE Forum (Los Angeles, February 1958), TID-7553 (NAA-SR-2600), May 1958

16. H. O. Forrest, W. Brugman, and L. W. T. Cumings, Ind. Engr. Chem. 23 (1931)

17. M. Jakob, Heat Transfer (New York: John Wiley and Sons Inc., 1949), p. 246

18. E. R. G. Eckert, Introduction to the Transfer of Heat and Mass (New York: McGraw - Hill Book Co., 1950), p. 23

19. J. H. Berry, Chemical Engineer's Handbook (New York: McGraw - Hill Book Co., 1950), p. 456

20. W. H. McAdams, Heat Transmission (3rd Ed.; New York: McGraw - Hill Book Co., 1954), p. 458

21. R. Stephenson, Introduction to Nuclear Engineering (New York: McGraw - Hill Book Co., 1954), p. 31-36

22. Ibid., p. 211

23. W. Primak, "An Elementary Treatment of Gamma Ray Heating and Gamma Ray Dosage in Inhomogeneous Reactors," ANL 4762, 1952, p. 36

24. R. Stephenson, op. cit., p. 380

25. S. Nakazato and R. H. J. Gercke, op. cit., p. 30

26. W. H. McAdams, op. cit., p. 5

27. S. Glasstone, Principles of Nuclear Reactor Engineering (Princeton: D. Van Nostrand and Co. Inc, 1955), p. 662

28. Stainless Steel Handbook (Pittsburgh: Allegheny Ludlum Steel Corporation, 1951), p. 2

29. G. M. Inman, "Sodium Graphite Reactor Quarterly Progress Report, June - August, 1953," NAA-SR-878, January 20, 1954 (Declassified March 4, 1957), p. 65

30. Liquid Metals Handbook, TID-5277, July 1955, p. 41

31. S. Glasstone, op. cit., p. 110